Investigating the Surface Energy and Bond Performance of Compression Densified Wood

Jessica D. Jennings

Thesis submitted to the Faculty of Virginia Polytechnic Institute and State University in partial fulfillment of the requirements for the degree of

MASTER OF SCIENCE
in

Wood Science and Forest Products

Approved by:

Dr. Audrey Zink-Sharp, Chair

Dr. Charles E. Frazier

Dr. Frederick A. Kamke

February 25, 2003
Blacksburg, Virginia

Keywords: Densified Wood, Surface Energy, Bond Durability, Fracture Mechanics

Investigating the Surface Energy and Bond Performance of Compression Densified Wood

Jessica Jennings

(ABSTRACT)

The bond performance and surface energy of hygro-thermal compression densified wood were studied using comparisons to hygro-thermally treated and control yellow-poplar (*Liriodendron tulipifera*).

Bond performance was studied using opening mode double cantilever beam fracture testing and cyclic boiling of one half of all fracture samples. Phenol formaldehyde film (PF-film) and polymeric diphenylmethane diisocyanate (pMDI) were the two different adhesives used to bond fracture samples. Hygro-thermal samples bonded with PF-film had significantly higher fracture toughness than control samples, while no difference was found for densified samples. Densified samples bonded with pMDI had significantly higher fracture toughness than control samples while no change was seen for hygro-thermal samples. Boil cycling reduced fracture toughness of hygro-thermal fracture samples only, irrespective of adhesive type.

Surface energy was studied using sessile drop contact angle measurement and the Chang model of acid-base, surface energy component calculation. Water, glycerol, formamide, ethylene glycol, and α-Bromonapthalene were used as probe liquids. Densified and hygro-thermally treated yellow-poplar had significantly higher contact angles than control samples. The contact angle trends for densified and hygro-thermally treated wood were found to be the same. Total surface energy as well as the polar and acid components of surface energy decreased with hygro-thermal treatment. The dispersive and base components of surface energy increased with hygro-thermal treatment.

Acknowledgements

I would like to take this opportunity to thank the many people whose help and support I have greatly appreciated throughout this process. I would like to thank my committee members, Dr. Charles Frazier and Dr. Fred Kamke, whose knowledge and support has been immeasurable. I would especially like to thank my committee chair, Dr. Audrey Zink-Sharp, whose encouragement and guidance made it all possible.

I would like to thank the graduate students of the Virginia Tech Wood Science department for their invaluable friendship and help, throughout the process. I would like to thank Linda Caudill, Kenneth Albert, Rick Caudill, and Harrison Sizemore for their assistance along the way. I would like to thank the Wood-Based Composites Center for logistical support, and Keun Pyo Kim of the Virginia Tech Statistical Consulting Center for data analysis support.

A special thanks goes to God and family. Their bottomless well of support have made anything I tried possible. Thanks to my husband, Ken, for his unswerving belief, patience, encouragement, and sanity amidst the chaos. Thanks to my mom for reminding me that "I can't" isn't in my vocabulary. Thanks to my dad for the unending supply of "Atta girl" and "stop whining". They have always believed in me even when I have not. Thanks to my brother, grandmother, grandfather, and newly acquired family for the constant support. Thanks also go to my friends (you know who you are) for their patience, even after not hearing from me for months on end.

Table of Contents

List of Tables

List of Figures

Chapter 1
Introduction

1.1 Defining the Problem

The forest products industry is currently operating in a demanding and dynamic marketplace worldwide. Consumer demand is increasing for higher quality and environmentally friendly products. The industry is dealing with a decrease in raw material sources, competition from non-wood products, and an increasingly global market. The decrease in raw material sources is partially due to the significant influence of environmentally conscious citizens and environmental non-government organizations. These citizens have had particular influence in the United States. Increasing amounts of land are being removed from the raw material base due to endangered species issues, the demand for roadless areas, and concern about water quality. Endangered species and water quality issues also make it increasingly complicated for private landowners to sell timber. The decrease in natural material supply is only partially offset by the introduction of new sources, due to increasing technology, global economies, and plantation growth.

Industry response to the current market place has been to continue developing and increasing the number of engineered wood products. Engineered products increase the efficiency of production by reducing waste and increasing the range of usable raw material. Product properties are generally better than those of traditional products, which has allowed engineered wood products to be competitive with non-wood products.

Hygro-thermally compressed, densified wood is a unique material in the field of wood science that falls into the realm of engineered products. High temperature, moisture, and compression are utilized to make a wood product with higher strength properties than natural wood. Compressed densified wood has not become a common wood product, due to the instability of the compressed form in the presence of moisture. A review of the literature shows

that research has fundamentally solved this problem by refining the densification process.

The next step is to develop products made from compressed wood. Industry will not invest in converting recently developed densification processes into manufacturing processes unless viable product ideas exist. Interest has been expressed in developing a composite product from densified wood. A limited amount of research on densified wood has focused on material properties. The majority of this research deals with mechanical properties. Little research exists on bonding densified wood, which leaves a large gap in understanding the material. Filling this gap is a critical step in determining if a composite product from densified wood is feasible.

Almost any material can be bonded using today's technology. Research shows that densified wood is not an exception to this rule. However, several important questions remain unanswered. The overall goal of this research project is to further the understanding of the surface free energy and bond performance of densified wood.

1.2 Technical Objectives

The specific objectives of the study follow directly from the justification and overall goal. Objective one is to determine the surface energy of hygro-thermally compressed densified wood and bond performance when using phenol formaldehyde (PF) film or polymeric diphenylmethane diisocyanate (pMDI) adhesives. Objective two is to differentiate between the influence of hygro-thermal treatment and compression treatment on surface energy and bond performance. Meeting these objectives will be a small step in determining the viability of a new densified wood product.

Chapter 2
Literature Review for Densification

Section 2.1 Introduction

In order to place the current research and results into proper perspective an understanding of the research leading to the densification process used, as well as definitions and forms of the densification process must exist. This literature review contains a history of densification, theories behind densification, and some properties of densified wood.

Section 2.2 History

The concept of wood densification dates back to the early 1900's [1]. Densification is the process by which wood density is increased by compression of the wood, impregnation of cell lumens with a fluid substance, or a combination of compression and impregnation [1]. Wood compression is the process of applying force to deflect cell walls, which results in decreased lumen volume. Impregnation is the process of using pressure to force liquid phase polymers or metals into the cell lumen, then solidifying the liquid [1]. All forms of densification result in wood that has a lower volume of air space, which increases the overall density.

Patents on compressed wood in the United States date back to a patent by Sears in 1900 [1]. Production of compressed wood and laminated compressed wood dates back to the 1930's in Germany. Wood densified by compression will be referred to as densified wood throughout the remainder of this paper. Wood densified by impregnation also originated in the early 1900's [1]. Densification by impregnation will not be discussed further because it is beyond the scope of this research project.

Section 2.3 Related Theory

Wood densified using compression has a tendency to spring-back, or recover, when placed in moisture rich environments, which induce swelling. Spring-back is the recovery of the original cell shapes and can be complete or partial, depending on environmental and processing conditions. The tendency to recover the original shape limits the usefulness of compressed products. The majority of past research has focused on applying the theory of viscoelasticity in determining process conditions required to minimize spring-back after compression. Research has also been done on the chemical fixation of compression, but is beyond the scope of this project.

The behavior of wood during and after the densification process can be related back to basic composition. Wood is primarily a composite of 3 polymers, which are cellulose, hemicelluloses, and lignin. Cellulose and hemicelluloses are semi-crystalline polymers, with cellulose having a high degree of crystallinity. Hemicelluloses are amorphous *in situ* with a glass transition temperature (point of softening) around 180ºC [2]. Lignin is an amorphous polymer with a glass transition temperature (Tg) around 150ºC [2]. Like all polymeric materials, wood is viscoelastic. Viscoelasticity is the exhibition of both plastic and elastic characteristics depending on time, temperature, and the presence of platicizers. Plasticity is increased flexibility, and decreased stiffness and brittleness, due to the introduction of a softening (plasticizing) agent, an increase in temperature, or the presence of a sustained load (as in creep). Water is a known plasticizer for wood causing decreases in the Tg of lignin, hemicelluloses, and amorphous regions of cellulose [2]. The Tg of lignin was reported to decrease to 80-100ºC for water saturated Norway spruce (*Picea abies*) [3]. Increased softness of wood in the presence of water was also proven by decreases in molding process time [2].

Understanding the viscoelastic behavior of wood led researchers to studying the effects of temperature, time, and moisture on springback. A 1996 study [4] found decreased springback as compression time and temperature increased. Increasing temperature also decreased stress in radially compressed

wet wood [5]. Another study reported decreases in yield stress of wet wood as temperature was raised from 0 to 200°C [6]. Decreases observed in stress indicate decreased springback. Steam pretreatment was also shown to influence springback. A 1988 study [7] reported reduced thickness swelling with steam pretreatment. The effects of pre-steam time and temperature were also studied. Shape recovery was found to decrease as time and temperature of pre-steaming were increased [8]. A more recent study also reported that increasing the temperature of particle steam pretreatment caused a decrease in shape recovery, as well as an increase in compressibility [9].

Several different densification conditions were shown to produce densified wood with compression set. A 1993 study [10] found compression set was achieved by steaming solely during compression. More recent studies focus on using steam pre-treatment to obtain compression set. Compression was reported to be fixed after steaming for 10 minutes at 210-220°C in a 1996 study [8]. A second study showed that steaming at temperatures >180°C provides compression set [9]. A 1998 study reported that thermo-hygro-mechanically compressed (compression in the presence of increased temperature and moisture) wood had no significant shape memory [11]. Apart from steam treatments, it was also found that heating wood to 180-200°C using high frequencies during hot pressing resulted in compression set while not drying the wood [12].

Several studies have focused on the mechanisms leading to compressive set found for different temperature and moisture combinations used in densification. A 1996 study [13] found that steaming at 180°C relaxed stresses in microfibrils and increased cellulose crystallinity. The rearrangement of cellulose sections was also shown to reduce stresses in wood compressed with three minutes of saturated steaming at 200°C [14]. A second stress relaxation method was proposed in a 2000 study [15]. Nonpermanent cohesive structures, formed within the wall before cooling, were found to occur for wood compressed with steam between 120°C and 180°C [15]. Two studies support the theory that stress relaxation is induced mainly by increased temperature. Increasing

temperature, from 100 to 140°C, was shown to decrease internal stress by 40% for wood compressed with steam at 210-220ºC for 10 minutes [16]. The greatest decreases in stress were found at temperatures >160°C [16]. A different study found that temperature was more important than moisture in increasing stress relaxation, and that the greatest stress relaxation was observed at temperatures above the Tg of lignin [17].

Section 2.4 Processes

Several processes for wood densification have been identified by researchers. The first complete process for making stabilized compressed wood (Staypak) was published in 1948 [18]. Veneers were glued, then compressed at 165-174°C and 30-50% relative humidity [18]. An improved densification method, published in 1998 [19], listed the following process. Wood was softened using steam at 150°C for three minutes, compressed, then steamed for two minutes at 200°C to give shape fixation [19]. Two different densification processes were published in 2000. The first process required softening wood for 10 minutes at 150°C prior to compression [20]. Wood was then compressed in steam saturated conditions [20]. The second process listed the following steps. Wood was steam soften at 140°C for 10 minutes, compressed to a set pressure at 140°C, held at pressure with no steaming for a designated time, then steamed for either two minutes at 200°C or 60 minutes at 160°C [21]. Each process contains various combinations of moisture and temperature to obtain stable compressed wood.

Section 2.5 Mechanical Properties

The motivation for compression of wood is to provide an increase in the mechanical strength properties. In the majority of available research, mechanical properties were shown to have been improved by the compression process. A 1998 study found that wood compressed using a thermo-hygro-mechanical process showed increased shear strength parallel to grain and

increased surface hardness [11]. Similar results were reported in a 2000 study [20]. A 1999 study [22] reported that ultimate tensile stress and tensile modulus increased with densification. A second study published in 2000 [21] showed an increased bending strength, in addition to verifying previous results for increased tensile modulus and surface hardness [21]. One study was found to contradict the previously cited research. Perkitny and Jablonski [23] reported densified wood to be weaker than natural wood, when tested in bending and compression. Another mechanical property shown to be affected by densification is thermal conductivity. The “effective thermal conductivity” of Japanese cedars was reported to increase after radial compression [24].

One factor affecting the degree of improvement in properties is the amount of thermal degradation induced by the compression process. Thermal degradation causes weight loss in wood, which can influence mechanical strength properties. Increases in modulus of elasticity (MOE) and modulus of rupture (MOR) in compressed wood were found to decrease as weight loss increased [4]. Prolonged exposure to high temperatures is the proven cause of weight loss. A 1998 study [16] found that weight loss increased slowly as temperature was increased up to 140°C, while temperature increases above 160°C caused weight loss to increase rapidly. A second 1998 study [6] found significant thermal degradation between 150-200°C. Thermal degradation at high temperatures is proven to occur even in the presence of moisture. A study found that steaming for 10 minutes between 210-220°C caused an approximate weight loss of 7.5% [8]. One study suggested that thermal degradation could be limited by starting the densification process with wood close to the fiber saturation point [5].

Section 2.6 Anatomical & Physical Properties

Several studies of compression densified wood have attempted to describe the anatomical aspects of compressed wood. Earlywood cells were found to deform easier than latewood cells, which results in a zone of compressed cells beside a zone of uncompressed cells seen as wave-like

patterns [25]. A 1999 study [22] also showed wave-like patterns of compressed and uncompressed cell zones in densified wood. A 2001 study [26] showed that moisture uptake by compressed wood during shape recovery began between previously identified compressed and uncompressed cell zones.

Study has determined that the conditions used during densification dictated how cells deformed. A 1996 study [8] found brittle fracture of cells after wood was steamed at temperatures >180°C. A 1999 study [22] expands on the previous research by using three different combinations of temperature and moisture in densification to determine how these parameters influence cell deformation. Wood compressed at 140°C and 62% relative humidity showed elastic/plastic yielding of cells [22]. Wood compressed at 200°C and 6.5% relative humidity showed brittle fracture of cells [22]. Wood compressed at 90°C and 95% relative humidity showed cell separation and brittle fracture [22].

One study was found on the physical properties of compressed wood. Obvious cupping of water soaked compressed wood samples was observed [27]. Edge restraint during compression was reported as a method to reduce subsequent cupping [27].

Section 2.7 Bonding

Little research has been done in the area of bonding densified wood. A 1993 study [28] investigated the lap shear tension strengths of densified yellow-poplar as affected by resin type. Densified veneers bonded with either urea formaldehyde (UF) or phenol formaldehyde (PF) showed the same strengths as nondensified veneers [28]. Densified veneers bonded with polyvinyl acetate (PVAc) had higher strengths than control samples [28]. These results give an early indication that densified wood can be bonded successfully.

Section 2.8 Summary

Densification processes have been developed to make stable densified wood. Temperatures are raised above the glass transition temperatures of lignin

and some hemicelluloses during densification. This allows cell walls to deform upon compression and polymer constituents to flow. High moisture content during densification increases the plasticity of the cell walls. The correct combination of temperature and moisture allows plastic yielding of cells with minimal weight loss due to thermal degradation. The plastic yielding of cell walls reduces internal stresses thought to cause springback. Cellulose crystallinity is increased during the process.

The densification process results in wood with increased mechanical strength properties. In theory, the increased strength of densified wood make it an excellent candidate for making a structural composite. One study on bonding densified wood suggests that densified wood can be bonded to form a composite product.

Chapter 3
Investigating Fracture Toughness

3.1 Introduction

Bond performance data are important to making informed decisions on bonding any material. The bond performance of differently treated yellow-poplar (*Liriodendron tulipifera*) was investigated using the opening mode, double cantilever beam fracture toughness test. Treatment groups were: a control, hygro-thermal treatment, and hygro-thermal densification. Bonds were constructed using a phenol formaldehyde film (PF-film) adhesive and a polymeric diphenylmethane diisocyanate (pMDI) adhesive.

3.2 Background

Understanding bond performance of wood is an important issue within the wood products industry. This fact is especially true for many engineered wood products and all composite products. Composites are formed by bonding smaller pieces of wood together with adhesive to create a larger product. The strength and durability of the adhesive bond between wood components is critical to the product quality and market success.

Several standard tests exist to analyze the bond performance of wood samples. The most commonly used tests are the ASTM D-905 compression shear block test, the ASTM D-906 tensile shear test for laminates [29], and the ASTM D-1037 internal bond test for strand or fiber composite panels [30]. ASTM D-3433-99 [29] has recently been modified and adopted for use in testing wood bonded in the double cantilever beam (DCB) geometry. Only ASTM D-905 and the opening mode DCB fracture test are applicable to this study. ASTM D-906 and ASTM D-1037 would be used to test a product made from densified wood, but do not address the basic question of how well two panels bond.

A fracture test method recently published [31] and later refined [32] was chosen as the test method for this study. ASTM D-905 (see Figure 3.1) relies on measurement of ultimate failure load and an estimate of percent wood failure to quantify bond performance [29].

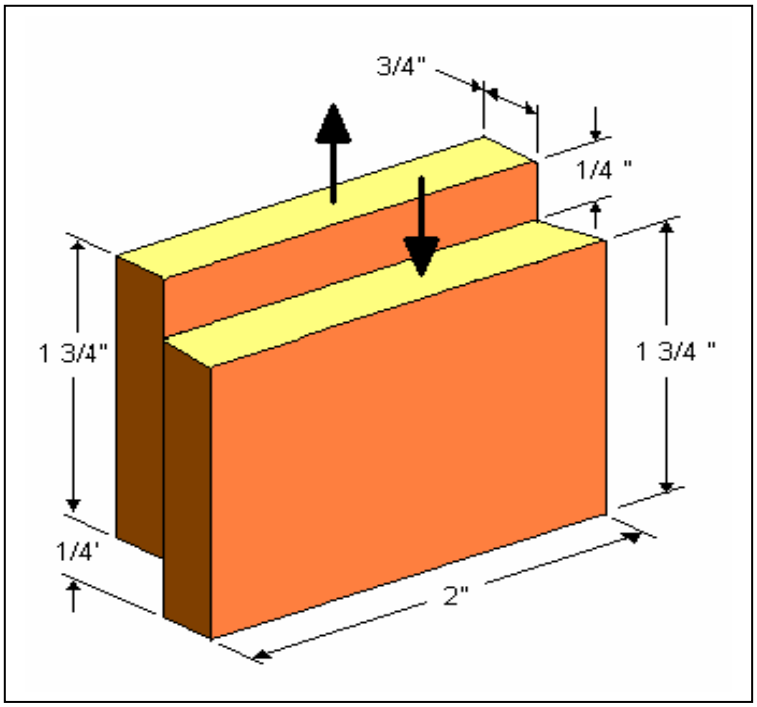

Figure 3.1: Illustration of an ASTM D- 905 test sample.

This method results in average bond strength and, more importantly, is highly dependent on wood strength. Opening mode fracture tests (see Figure 3.2) measure the energy required to initiate a crack in the bond-line and the energy associated with crack arrest [32].

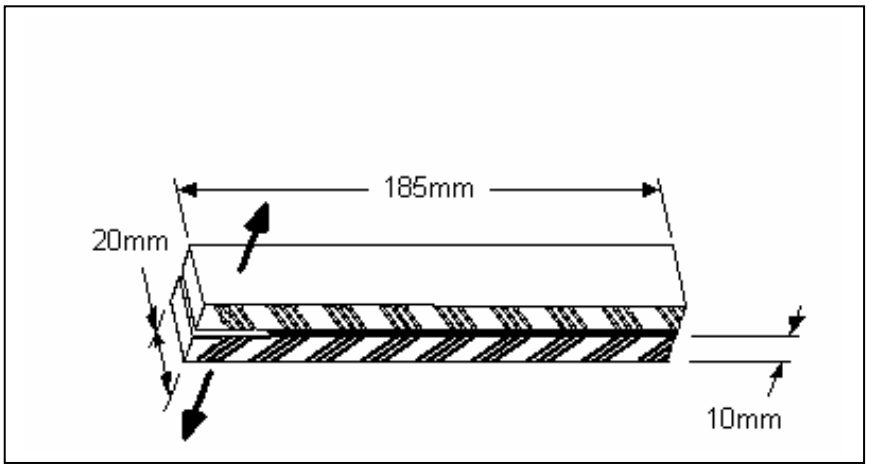

Figure 3.2: Simple illustration of a double cantilever beam fracture sample.

The energy required to propagate a crack (G_{max}) and energy at crack arrest (G_{arr}) can then be calculated from the test data. These values are known as the strain energy release rate (SERR) or fracture toughness. Strain energy release rate is a material property of the adhesive, giving a clearer picture of the bond performance. Several advantages exist to the fracture test method. Fracture testing results in material properties that could be used to design products for future use. Fracture testing is also sensitive to changes in surface energy [33]. Failed fracture samples can yield information on whether failure was cohesive (within the adhesive), adhesive (between the wood and resin), substrate (within wood), or a mixture of failure modes.

3.3 Materials and Methods

Fracture toughness of bonded yellow-poplar samples from three different wood treatment groups was studied. Treatment group one (control) consisted of clear sapwood yellow-poplar, and was chosen for basic comparison to the remaining treatment groups. Treatment group two (hygro-thermal) consisted of clear sapwood yellow-poplar subjected to a hygro-thermal treatment. The third treatment group (densified) consisted of clear sapwood yellow-poplar densified using a hygro-thermal compression method. Yellow-poplar was chosen as a raw material for two main reasons. Wide availability and relatively low density make

this species a good candidate for making densified wood products, and previous research exists on the properties of densified yellow-poplar. Table 3.1 shows the basic experimental design.

Table 3.1: The number of samples to be tested for each treatment/adhesive combination.

Adhesive used in bonding	Control	Hygro-thermal conditioning	Densification
phenol formaldehyde film	6	6	6
polymeric diphenylmethane diisocyanate	6	6	6

Two very different commercially available adhesives were chosen to bond samples in each treatment group. A phenol formaldehyde (PF) film adhesive was chosen to provide a controlled bond-line thickness, which has been shown to effect fracture test results [34]. Polymeric diphenylmethane diisocyanate (pMDI) adhesive was chosen for its low viscosity, proven bond performance, and ability to penetrate wood cell walls and lumens. Adhesive penetration into wood influences the overall bond quality and will be more difficult with the reduced lumen volume in densified wood.

3.3.1 Wood Machining

Preparation of fracture samples for this study began with machining of wood panels from rough-cut, flat-sawn, green, sapwood, yellow-poplar lumber. Lumber was obtained from a local sawmill with the approximate dimensions of 8/4-inches thick by eight inches wide by 10-feet long. The lumber was then machined according to a process found in the literature [31,32].

Rough lumber was machined using the following process. Tangential faces (width) of each rough board were planed to obtain parallel surfaces. Planed boards were then cut into 1.5-foot lengths using a radial arm saw. A

jointer was used to smooth and square the radial faces (thickness) of each 1.5-foot lumber length. Each length was then squared and cut to 14-15/16-inches (373-mm) long with a table saw. Saw blade angle was adjusted, using a handheld wood square, to ensure a 90-degree angle with table prior to cutting. All boards were then ripped to 3 1/16-inches (75-mm) wide.

Adjusting the existing grain angle was the next step in machining wood panels. The angle between the wood grain and the longitudinal axis of the lumber must be adjusted to three degrees. Angle adjustment helps to ensure that the crack propagates through the bond-line during fracture testing. Grain angle was found to affect wood fracture testing by enabling crack propagation away from the bondline [34].

Grain angle of the lumber was adjusted using the following process. Natural grain angle of each ~2 x 3 x 15-inch board was measured. Measurement of the grain angle was taken on the radial face using a SPI 0-180 degree protractor. Long edges of the radial face were assumed to be parallel to each other and perpendicular to the thickness edge for calculations. Refer to Figure 3.3 for a diagram of the radial surface and natural grain angle measurement.

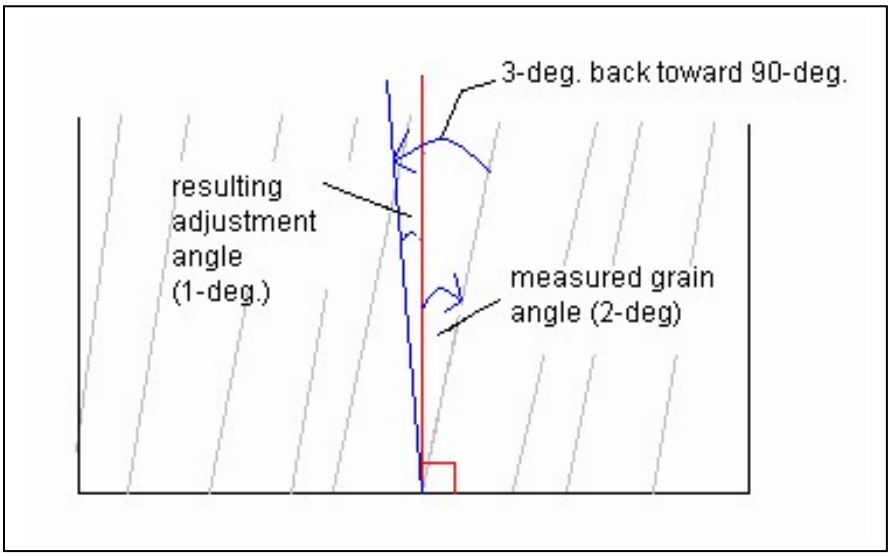

Figure 3.3: Illustration of measuring natural grain angle and the resulting adjustment angle.

Measurement of the natural grain angle was then adjusted three degrees back toward a 90-degree reference line. The resulting angle of difference from perpendicular was the adjustment angle. Figure 3.3 also illustrates angle adjustment on the radial surface. The adjustment angle was then used to draw guidelines along the length of the radial face to aid in slicing panels. Lines 11/16-inches (17-mm) apart and parallel to the adjustment line were then drawn on the radial face to further assist in slicing. Figure 3.4 illustrates the parallel guidelines drawn on the radial face.

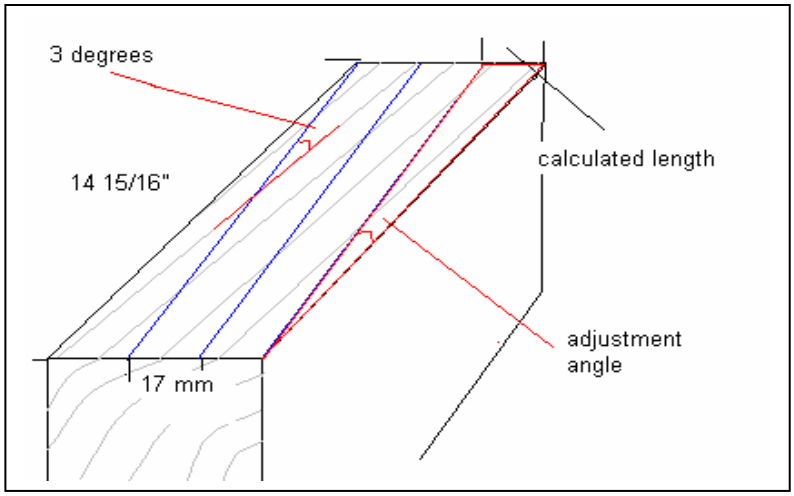

Figure 3.4: Three-dimensional view of parallel guidelines, the adjustment triangle, and adjusted grain angle on the radial face.

Basic trigonometric functions were used to ensure a three-degree angle was maintained the full length of the board when drawing parallel guidelines. Figure 3.5 illustrates the use of the adjustment triangle.

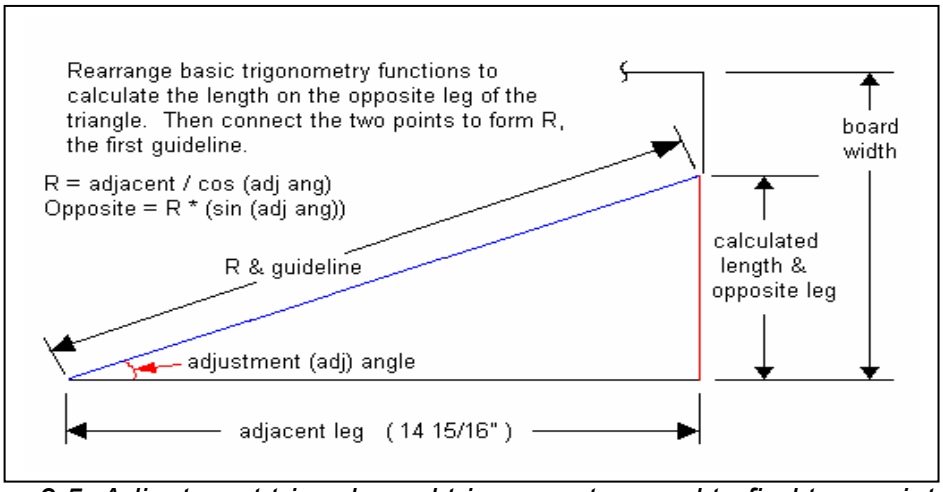

Figure 3.5: Adjustment triangle and trigonometry used to find two points that were connected to draw the first guideline.

Each board was then cut into two or three separate boards, depending on natural grain angle, by slicing through the thickness. A band saw equipped with a 2-inch band was used to cut through the thickness along the longitudinal axis following the guidelines on the radial face. The resulting board dimensions were 11/16 (17-mm) x 3 1/16 (75-mm) x 14 15/16-inches (373-mm).

All boards were randomly divided into one of the three treatment groups. Boards assigned to the control group were placed in a conditioning chamber set to 20°C and 65% relative humidity to obtain equilibrium moisture content (EMC) of 12 ± 2%. The remaining panels, assigned to the hygro-thermal treatment group and the densified treatment group were conditioned at 21.1°C and 89% relative humidity to achieve 23% ± 2% EMC. Panels were conditioned to 23% EMC to speed the heating process during densification [5]. All samples were conditioned to constant weight before further processing.

3.3.2 Wood Treatment

Treatment of boards in groups two and three was the next step in wood preparation. Careful review of the literature resulted in the identification of a densification process to be used in treating boards from group three (densified). The environmental conditions associated with densification were then utilized, without compression, to treat boards from group two (hygro-thermally treated). Densification conditions were chosen to maximize compression set while minimizing weight loss due to thermal degradation.

A 2000 publication was the basis for treatments used in this research [21]. Equipment capability dictated modification of the originally planned treatments. The published process called for: steaming at 140°C for 10 minutes, compression at 140°C with steam, maintaining compression without steam for a designated time, then steaming for 2 minutes at 200°C or 60 minutes at 160°C [21]. A pressure vessel (see Figure 3.6) designed by Lenth [35] was used to treat all wood for this project.

Figure 3.6: Pressure vessel used for wood treatment.

A 4 x 4-inch hydraulic press was placed inside the vessel to compress and/or hold samples. Heating coils around and under the enclosed chamber regulated internal temperature of the vessel. Live steam was injected into the vessel to increase temperature and relative humidity only at the beginning of each densification run due to equipment limitations. Existing temperature regulation methods for the pressure vessel dictated the choice of a single temperature to be used throughout the process. A temperature of 160°C was chosen based on previous research [16,21].

Further modification to the treatment process was made following preliminary densification runs. The preliminary chosen process called for: sealing wood in the pressure vessel, simultaneously heating to 160°C and increasing

relative humidity to 100% using steam and water, compressing to 1200-psi over 5 minutes, holding all conditions for 60 minutes, releasing the internal atmosphere, releasing compression and removal. Preliminary treatment resulted in wood that flowed off press platens and was severely cracked. Adjustments to compression force and wood thickness did not eliminate the problems. Limited heat transfer was discovered to be the cause. Stainless steel plates, used to increase the size and number of wood panels densified during each densification run, were limiting heat transfer into wood. The process was modified to compensate for slower heat transfer by adding a 2 hour hold.

Boards from group three were prepared using the following process. Two boards were removed from the conditioning chamber and planed to a 10-mm thickness. These boards were then cut to make four panels 7 ¼ x 2 ¼ -inches. Panels were then paired so that grain angles on the radial faces formed a 'V' (see Figure 3.7).

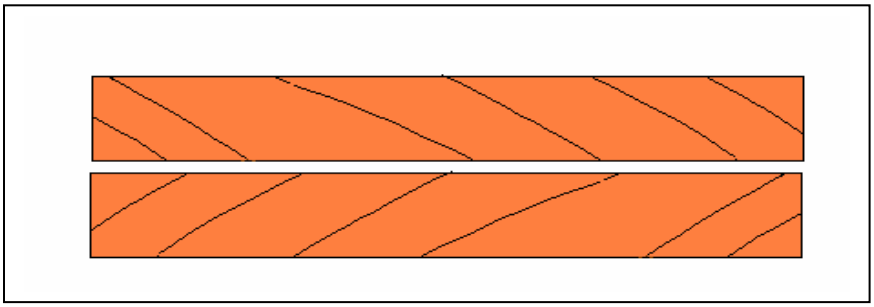

Figure 3.7: Grain angle alignment during panel pairing.

Panel sides were then labeled to identify panel orientation and future bond faces. Labeling was critical for future identification when bonding fracture samples. Measurements of panel dimensions were taken (see Appendix A). Panels were stacked between stainless steel plates. An aluminum frame was placed around each wood panel. Figure 3.8 shows a diagram of this arrangement for one panel.

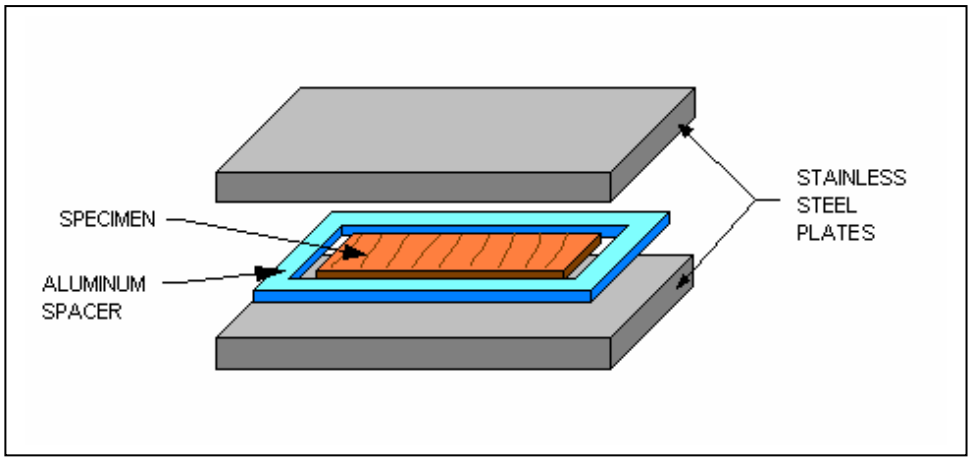

Figure 3.8: Stainless steel plate, aluminum frame, and wood arrangement for one panel in a stack.

Aluminum frames were used to limit densified thickness to 4-mm and increase heat transfer rate between steel plates. A stack of five stainless steel plates and four wood panels with aluminum frames was placed into the press.

The following process was used to treat group three panels. The press was lowered into the pressure vessel and the vessel sealed. Internal conditions were changed to 160°C with 100% relative humidity using steam, heating coils, and water over approximately one hour. Resulting saturated water vapor pressure was 90-psi (608-kPa). Steady state conditions were held constant for approximately 2 hours to allow equilibration. A 600-psi compressive load was applied using the hydraulic press over the course of 5 minutes. All conditions were maintained for one hour after the five-minute compression ramp-up. Internal humidity and temperature were then vented outside the vessel. Compressive load was released and panels removed when internal temperature dropped to approximately 45ºC.

Four panels were treated in each densification run. Densification runs were performed until all panels were treated. Dimensions of each panel were measured after treatment (see Appendix A). All panels started the run 10-mm thick and came out ~4-mm thick. Panels were secured so that the faces placed together were the faces that would later be bonded together. This was done in an attempt to prevent the bond face from aging during conditioning. Panels were

then placed in a conditioning chamber set to 12 ± 2% EMC. All panels were conditioned to constant weight before further use.

Boards from treatment group two were subjected to the same process as those from group three, with one modification. Compression load was 0-psi for group two panels. All other steps remained the same. All panels went into the press 10-mm thick, but came out ~8-10-mm thick (Appendix A). A compressive load of 0-psi should have resulted in no thickness change. One possible explanation for the unexpected thickness change was the cumulative weight of the stainless steel plates combined with increased temperature and moisture.

Stainless steel plates and aluminum frames were cleaned with the following method before and after each run. Each metal piece was rinsed three times, front and back, with hexane, methylene chloride, methanol, and acetone successively. Rinse chemicals were chosen to remove the largest range of organic contaminants from the plate surface. Rinsing plates was an attempt to control the surfaces in contact with wood over a number of treatment runs. Extractive contamination of metal was visually evident despite continuous rinsing. Contamination buildup necessitated the scrubbing of all metal with a stainless steel wire brush in acetone. Scrubbing was done approximately half way through the entire wood treatment process. All panels within each treatment group were then randomized and re-paired prior to fracture sample preparation.

3.3.3 Fracture Sample Preparation

Three major steps remained in making fracture samples. Panels were first bonded together to form a billet. Fracture samples were then cut from the billets and pin-holes drilled in each sample. Samples cut from group two and group three billets required the addition of two small wooden blocks before pin holes could be drilled, due to the reduced sample thickness.

3.3.3.1 Preparing Billets

Each pair of panels was bonded with adhesive to form a billet. One half of the billets from each treatment group were to be bonded with phenol formaldehyde film adhesive (PF-film) supplied by Dyno Overlays, Inc. Film adhesive was .127-mm thick with a 60% resin content. Remaining billets were to be bonded with polymeric diphenylmethane diisocyanate (pMDI) adhesive. The pMDI adhesive was supplied by Dow Chemical Company with a viscosity of 187-cps and was stored under nitrogen to prevent polymerization. A coverage of .0116-g/cm^2 per bond face was used [36]. Liquid pMDI adhesive was applied using a rubber roller. Panels were weighed before and after adhesive application to ensure proper coverage. PF-film was applied by cutting a sheet to match the size of the billet and then placing this sheet between the two panels.

Six preformed billets from each treatment group were prepared for bonding. Panels for billets from the control group were machined just prior to bond preparation. Six boards from group one were removed from the conditioning chamber and planed to 10-mm thick. Each board was then cut to 7 ¼ (185-mm) x 3-inches (75-mm). Panels were then paired so that grain angle on the radial face formed a 'V'. Newly paired panels were sealed in bags to maintain moisture content. Panel pairs from treatment groups two and three were removed from the conditioning chamber and sealed in bags to maintain moisture content. Billets were removed from bags as necessary during preparation. Figure 3.9 illustrates the layout of two panels into a billet.

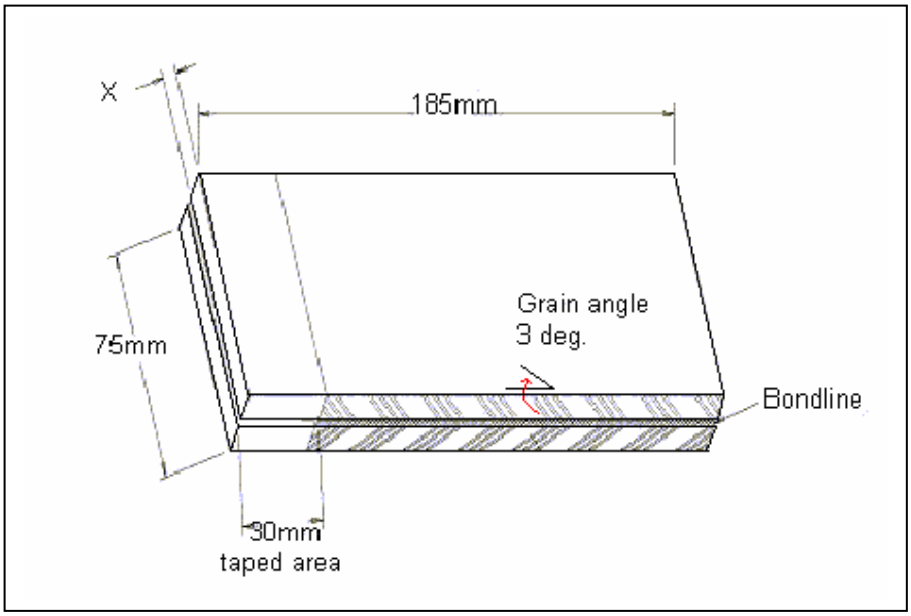

Figure 3.9: Illustration of a billet.

Tape was applied to the first 30-mm of every panel, to prevent the adhesive from bonding the panels in this region. This section formed the pre-crack of fracture samples and was located at the opening of the grain angle 'V' (see Figure 3.9). Three billets were prepared at one time according to treatment group and adhesive type. Adhesive was applied and billets wrapped in aluminum foil within 5 minutes of beginning preparation. These three billets were then pressed side by side at 200°C using 100-psi of force. A 12-inch square press with electrically heated platens was used. Billets were sandwiched between two thin metal plates to equally distribute the applied force. Temperature of both platens was monitored using two J-type thermocouples with a two-channel handheld digital thermocouple thermometer. Billets from treatment groups one (control) and two (hygro-thermal treatment), bonded with PF-film, were pressed for 37 minutes. Billets from treatment group three (densified), bonded with PF-film, were pressed for 27 minutes. Billets from groups one and two bonded with pMDI were pressed for 20 minutes. Billets from group three which had been bonded with pMDI were pressed for 11 minutes. Dielectric analysis was used to determine press time (see Section 3.3.3.2).

One problem was observed while pressing densified billets bonded with pMDI. One of the three billets de-bonded when the pressure (100-psi) was released. Excessive internal vapor pressure was one possible cause of de-bonding, but no direct evidence existed to explain this event. One side of the billet appeared to be swollen. This swelling could have been due to actual compression recovery in the wood, or to fiber separation during "blow-out". Any prior weakness in the wood material could also have made de-bonding more likely. Fracture samples cut from this billet were not used in final testing.

All billets were placed in a fume hood to cool following pressing. Billets were then unwrapped, placed back into the conditioning chamber (set to 12 ± 2% EMC) and conditioned to constant weight before further machining. Billets made from densified wood did not reach 12% moisture content, but stabilized at ~10% moisture content.

3.3.3.2 Dielectric analysis

Press time for each adhesive was determined using dielectric analysis prior to bonding billets. Two different press times were identified for each adhesive type. One press time was for billets made from 8-10-mm thick panels, and the second time was for billets made from 4-mm thick densified panels.

One billet was tested for each adhesive thickness combination. Billets were prepared using the method described in section 3.3.3.1. A Micromet IDEX sensor was placed in the bond-line beside a K-type thermocouple wire. A Eumetric System III dielectric analyzer was used to record conductivity measurements every 5 seconds at frequencies of 1, 10, 100, 1k, and 100k Hz. Figure 3.10 graphically shows the data collected during dielectric analysis.

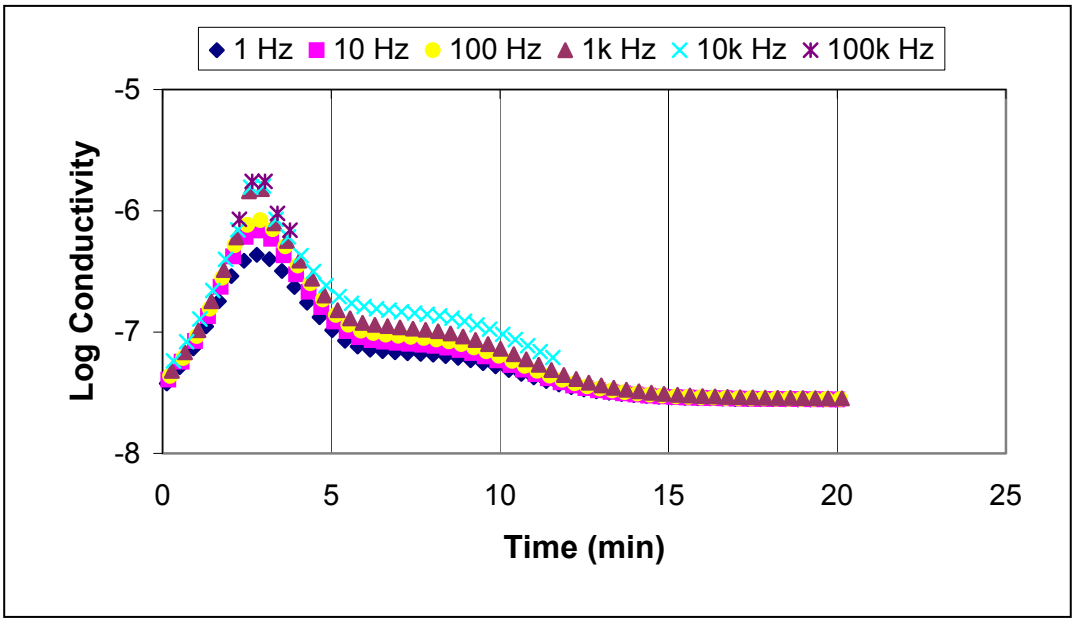

Figure 3.10: Log conductivity versus time at 6 frequencies for 8 - 10mm thick panels bonded with pMDI.

The data curve from the 100-Hz frequency was then analyzed to find a time corresponding with full cure. This frequency was chosen as the representative midpoint of all data collected. Full cure was defined as the point where the slope of the line reaches zero. The slope of the 100-Hz line was calculated at every point. The point at which the slope rose above -.015 was designated as full cure for this study. Time was read from the line graph at this point to determine similar cure points. Figure 3.11 is a graphic representation of determining the designated cure point.

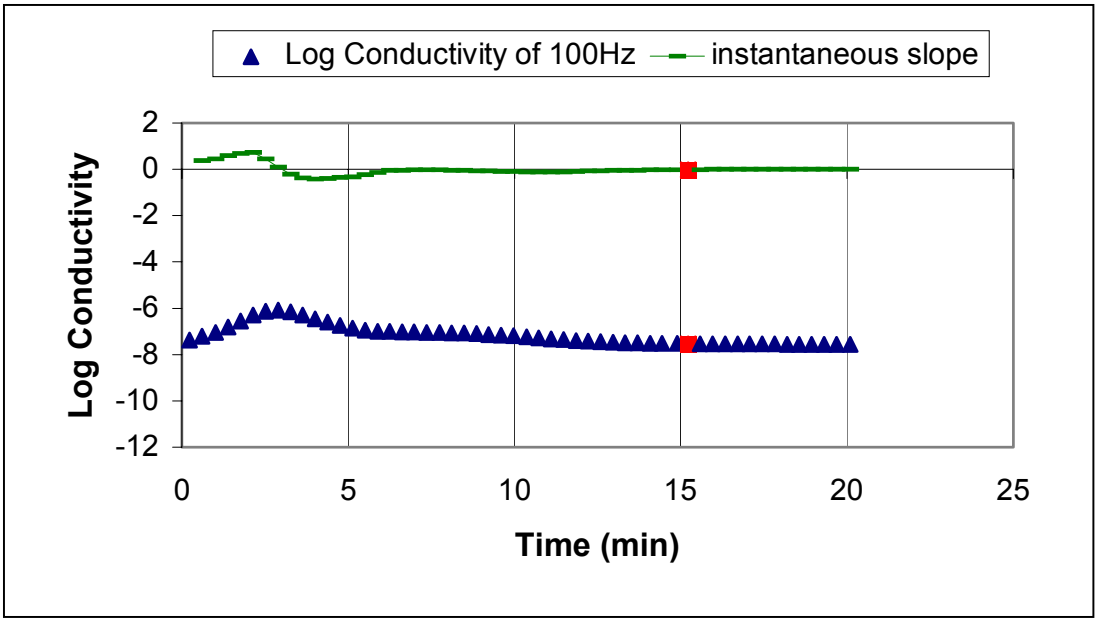

Figure 3.11: Cure time determination using 100-Hz log conductivity curve and the instantaneous slope of the curve for 8 - 10-mm thick panels bonded with pMDI.

Vitrification is defined as the point where the instantaneous slope is zero plus five minutes. Five minutes were added to the designated time to ensure full cure without over curing. Determining press time in this manner allowed each adhesive/ wood thickness combination to be pressed to similar cure points. Log conductivity and time determination graphs for the remaining three data sets can be found in Appendix B.

3.3.3.3 Preparing samples

Machining fracture samples was the final step before testing. Each billet from groups two and three produced two 20-mm wide fracture specimens. Each billet from group one produced three 20-mm wide specimens. Extra specimens from group one were treated as real samples during preparation, but were used as practice samples for fracture testing.

The following machining process was used. Each billet was cut into 20-mm wide strips using a hand-made jig placed on a table-saw. Figure 3.12 illustrates a single fracture sample.

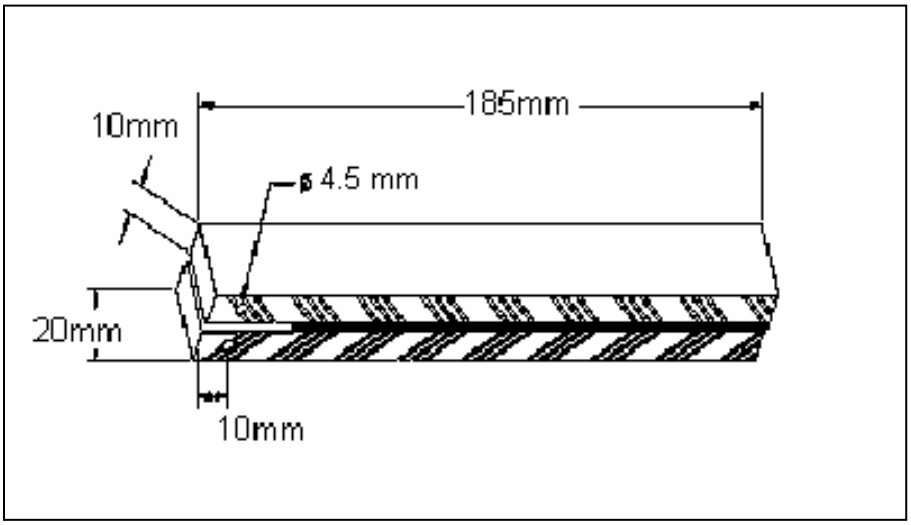

Figure 3.12: Diagram of a fracture sample with pinholes.

Each sample was measured to ensure proper width. Width was adjusted using a jointer, as necessary. All samples from groups two and three had two 1/2-inch X 20-mm X 30-mm red oak blocks bonded to the 30-mm taped end [37]. Blocks were added so that sample thickness was sufficient to drill pin holes into the sample. Figure 3.13 illustrates the placement of these blocks. Oak blocks were bonded to samples using Devcon clear, 1,500-psi rated, five-minute, all purpose epoxy.

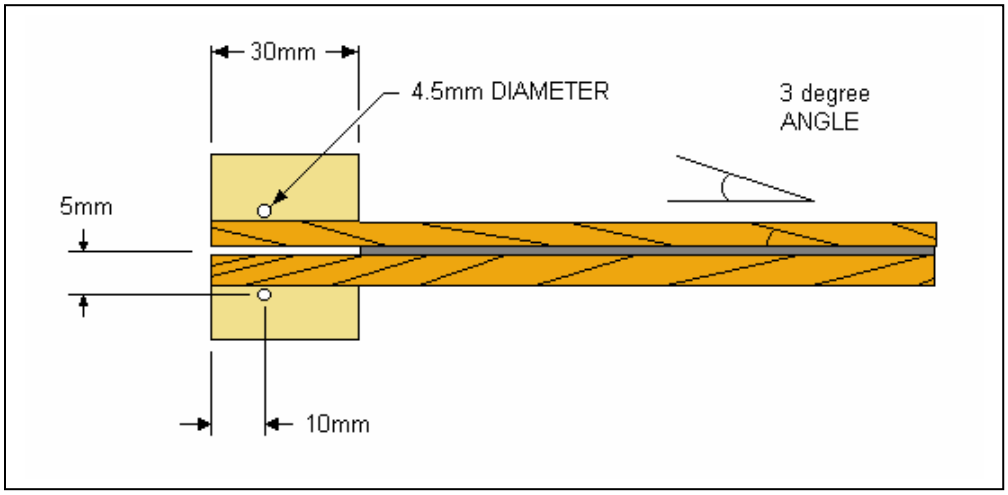

Figure 3.13: Illustration of fracture sample with 30mm long oak block additions and 4.5 mm pinholes.

The taped end of each specimen was marked using a small wood square. Excess wood was removed using a coarse grit sanding-drum attached to a hand-held rotary-tool (Dremel). Taped ends were then squared to the mark by holding the sample against a small sanding-disc, mounted on a 2/3 horsepower tabletop belt/disc sander. A drill press and a #18 (∅0.169") drill bit were used to drill two holes, one on either side of the bond-line, 10-mm from the front on the taped end and 5-mm from the bond-line, as shown in Figure 3.13.

A single-edge razor blade was used to ensure that the 30mm pre-crack, formed by the tape, was open on all samples. Finally, the bond-line was painted with white typewriter correction fluid and a metric ruler was glued to the sample. Correction fluid and the ruler were applied three days prior to testing to allow drying time. Figure 3.14 shows a fracture sample during testing.

Figure 3.14: A fracture sample in testing which illustrates the use of white correction fluid and a ruler.

White correction fluid makes the crack more visible during testing. The correction fluid cracks very easily which increases the visibility of the actual crack tip. The white color also enhances the view of the crack. The ruler allows measurement of the crack length, and is placed under the bond-line with zero centered in the lower pin-hole. Samples were then ready for testing.

3.3.4 Sample Testing

Opening-mode fracture testing was used to obtain information about bond performance. Six samples were tested for each treatment group / adhesive combination. Each sample resulted in numerous test cycles.

The test method used in this study was found in the published literature [32]. A 200-pound load cell was attached to an MTS load frame. A stationary metal grip was attached to the MTS base while a second metal grip was attached to the load cell. A sample was attached to the grips using two hardened, steel, ∅ 4-mm pins run through the grips and pin holes in the sample (see Figure 3.15). A stationary metal rod was placed under the free end of the sample to hold it steady and level.

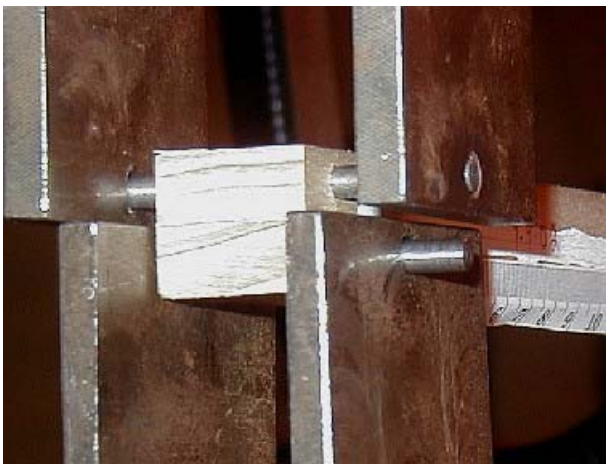

Figure 3.15: Close-up view of loading a fracture sample into the MTS load frame grips.

A CCD video camera module was mounted on a rolling track in front of the sample. The rolling camera mount allowed the operator to follow and measure crack growth during testing. A Cosmicar television lens with a 10-mm adapter ring was attached to the camera. Camera images were viewed using a Panasonic color video monitor. Figure 3.16 shows the testing setup, without the monitor.

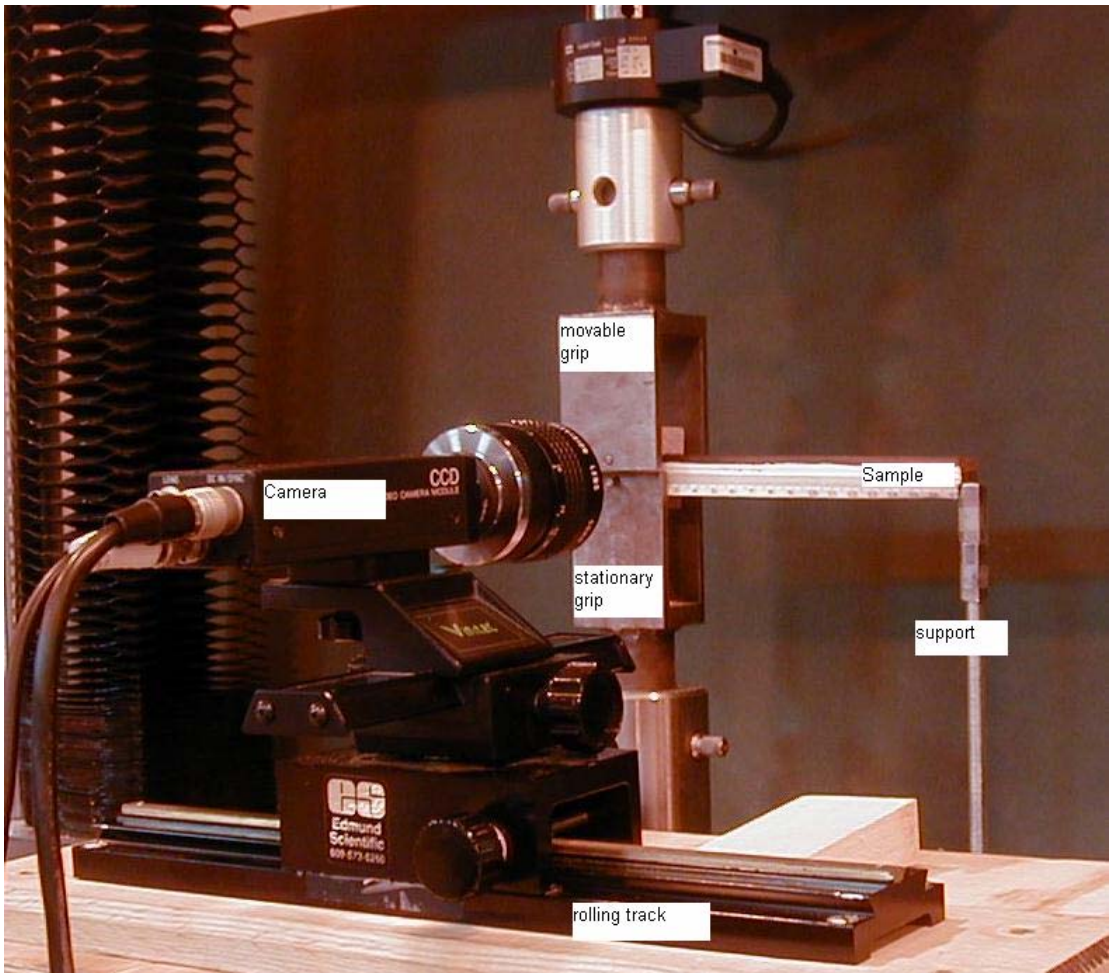

Figure 3.16: Fracture testing set-up.

Testing was controlled and data collected using "Testworks" version 3.09 software. The sample was loaded to 10-N using hand-held machine controls. Cross-head displacement was then set to zero. Crosshead displacement was the distance between the grips. Next, testing began with an initial crosshead displacement rate of 1 mm/min., in the upward direction. Crack initiation should occur at close to 1 minute [32]. The software was set up to detect crack initiation in the sample with a $\geq$ 3% drop below the maximum applied load. Crosshead movement was stopped upon crack initiation and a 45-second arrest (hold-time) started. The maximum applied force and force at the end of arrest time were recorded. Crosshead displacement was recorded during the first few seconds of

arrest. The length of the crack in the bond-line was observed and recorded during the last few seconds of arrest. The crosshead then returned to 0 displacement and a second cycle started. The displacement measured at the beginning of the previous arrest period was entered as the new crosshead displacement rate. Changing the crosshead rate with each successive test cycle keeps crack initiation around one minute [32]. Test cycles continue until the operator stops the program. Cycling is stopped when a crack visually leaves the bond-line and enters wood, or a point less than 50-mm from the sample end is reached. The same testing method was used for all samples.

3.3.5 Data Analysis

Data analysis consisted of three main steps. Strain energy release rates (G) were calculated and then data were scanned for outlying points. The last step was to analyze data using Statistical Analysis Software.

3.3.5.1 Calculating Strain Energy Release Rate (SERR)

Each fracture sample resulted in an average of 20 cycles. Figure 3.17 shows a representative set of cycles for one sample.

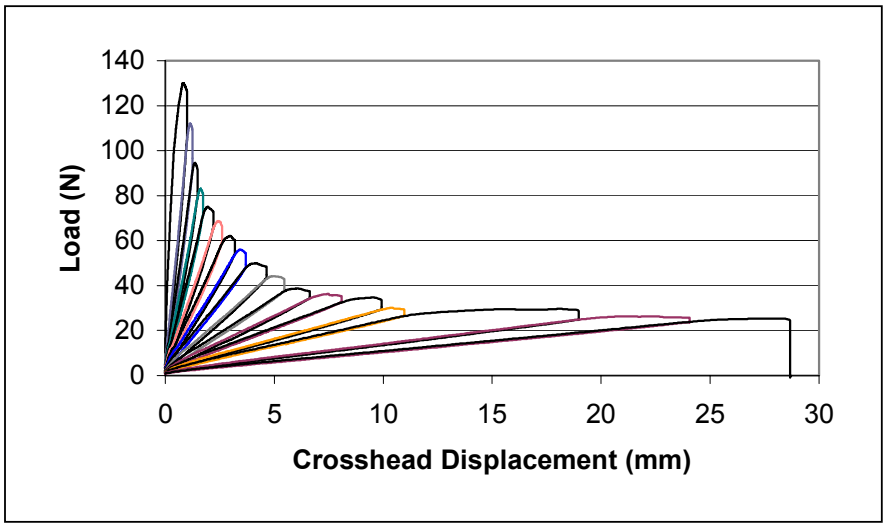

Figure 3.17: Representative set of fracture test cycles for one fracture sample.

Crack extension, maximum load, slope, and arrest load (see Section 3.3.4) were recorded for each cycle. Data from cycles with crack extension values that fall within the first and last 50-mm of the sample were discarded. These data points were deleted because they are subject to more than one failure mode [32].

Several steps were required to calculate strain energy release rate (SERR) values from the raw data. The corrected compliance method was used for all calculations [32]. This method is described below.

Crack extension values were first converted from millimeters to meters. Compliance was then calculated for each cycle from the respective slope (see Equation 3.1).

Compliance [m/N] = 1 / slope / 1000 *Equation 3.1*

The third step was to take the cube-root of compliance and plot versus crack extension. Figure 3.18 shows a representative compliance plot with a linear trend and equation.

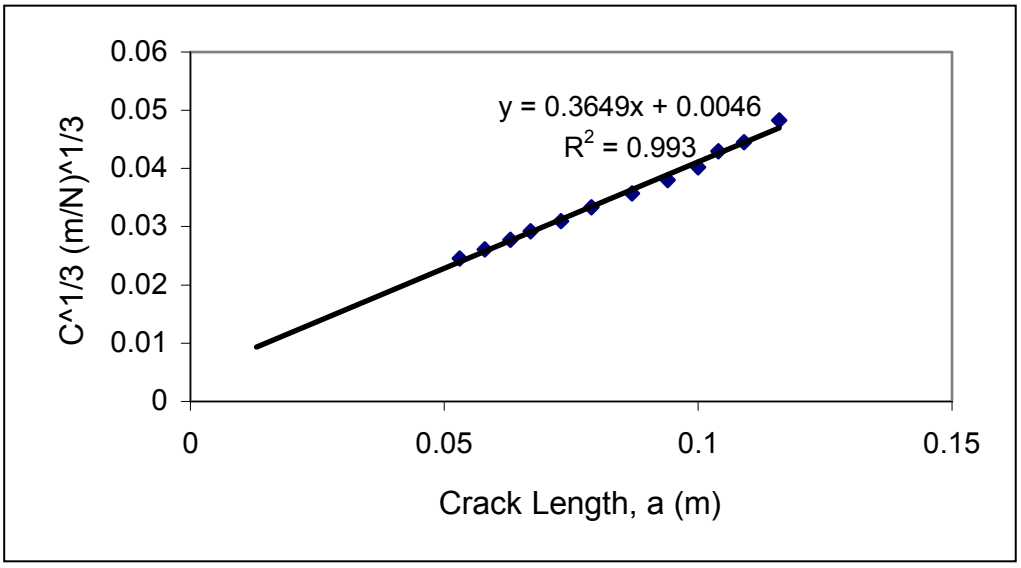

Figure 3.18: Cube root of compliance ([m/N] $^{1/3}$) versus crack length (m) for all valid cycles from one sample.

The slope (*m*) and y-intercept (*b*) were then read from the equation and used to calculate a shear correction factor (*x*). Equation 3.2 gives the equation used to find "*x*".

$$x = b / m$$

Equation 3.2

The effective modulus of elasticity multiplied by the moment of inertia (EI_{eff}) for each sample was also calculated (Equation 3.3) using the graph shown in Figure 3.18

$$EI_{eff} = \frac{2/3}{m^3}$$

Equation 3.3

The maximum and arrest SERR (G) values for each cycle were then calculated using equations 3.4 and 3.5.

$$G_{\max} = \frac{(Maxload)^2 (ext + x)^2}{(.02)(EI_{eff})} (J / m^2)$$

Equation 3.4

$$G_{arr} = \frac{(Arrestload)^2 (ext + x)^2}{(.02)(EI_{eff})} (J / m^2)$$

Equation 3.5

Example data with calculated values for two cycles of a fracture sample is in Table 3.2.

Table 3.2: Example data for the first two cycles of a fracture sample.

Specimen Cycle End	**Ext** mm	**Ext** m	**Slope** N/mm	**Comp** m/N	**Max Ld** N	**Arr Ld** N	**C^1/3** (m/N)^1/3	**G-max** J/m^2	**G-arr** J/m^2
1	52	0.052	66.5	1.5E-05	131.9	124.1	0.024683	274.7	243.2
2	56	0.056	57.8	1.7E-05	130.1	121.2	0.025864	299.6	260

All maximum (G_{max}) and arrest (G_{arr}) SERR values were then plotted against crack length. Figure 3.19 shows a typical plot.

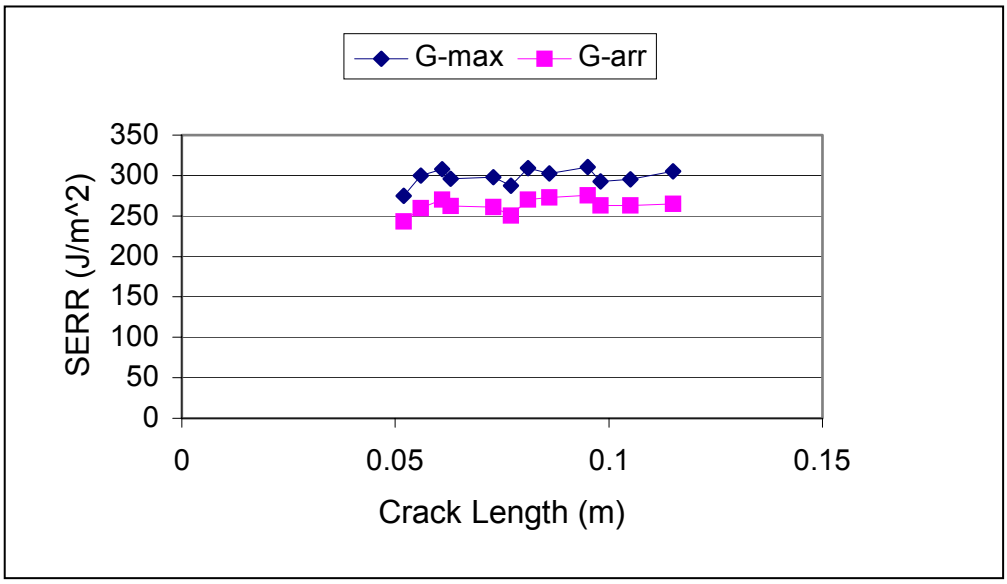

Figure 3.19: Crack length versus maximum and arrest SERR (J/m²).

Each sample within a treatment group resulted in a characteristic SERR plot. Data were then ready for further evaluation.

3.3.5.2 Data Evaluation

The strain energy release rate (SERR) plot for each sample was carefully examined for outlying points. Individual data points near the first and last 50-mm cut-off points which were observed to be obviously out of line with the overall trend were deleted. These data points were deleted because of the greater probability that they were affected by mixed failure modes [32]. Figure 3.20 illustrates a data set where outlying data were deleted.

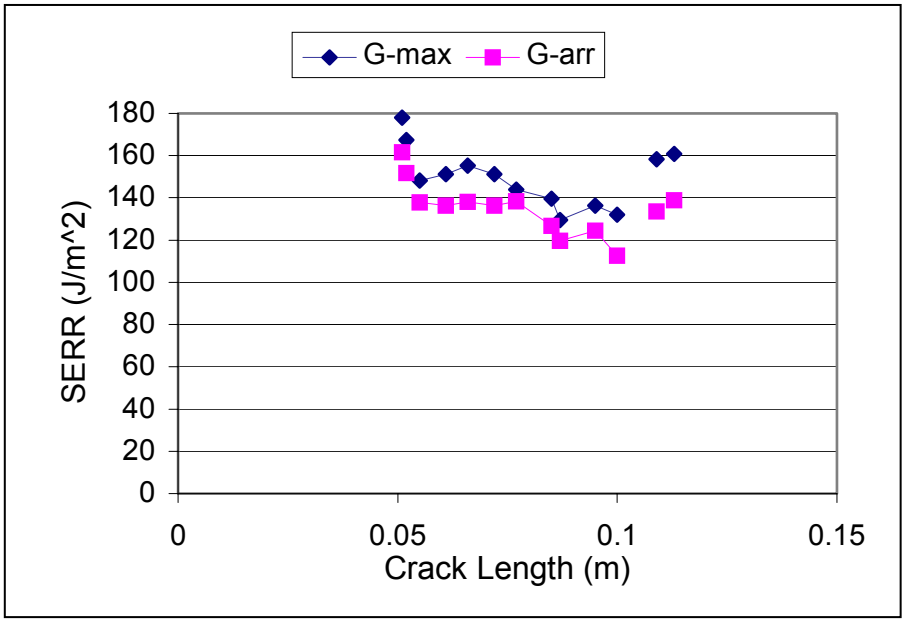

Figure 3.20: Illustration of a data set with outlying points.

A few samples were completely deleted from the final data set because they exhibited improper crack propagation. The crack ran off the bondline into the wood. Two samples of hygro-thermally treated wood bonded with PF-film adhesive and two samples of densified wood bonded with PF-film were deleted. One densified sample bonded with pMDI was deleted due to improper bonding (see Section 3.3.3.1).

Section 3.3.5.3 Statistical Analysis

Raw data were collected for two types of fracture samples during this research project. Regular non-boiled fracture samples are the topic of Chapter 3 (see Appendix C for raw data). Boiled fracture samples are the topic of Chapter 4 (see Appendix D for raw data). All data were statistically analyzed at one time for future comparison purposes. Results for the two types of fracture samples were then divided into separate chapters. The statistical method used to analyze all data is described below.

Maximum and arrest SERR values were analyzed using Statistical Analysis Software (SAS) version 8.0. A 3x2 factorial design was used for this study. Wood was first treated with one of three treatments; control, hygro-thermal, or densification. Fracture samples were then subjected to one of two weathering treatments; none, or boil cycling (see Section 4.3.2).

A mixed general linear model code was created by the Virginia Tech Statistical Consulting Center. Three class variables with multiple levels were used in this model. A third variable was added to account for having a number of specimens in each treatment group. Adhesive type and SERR type were accounted for by repeating the model for separate types. Appendix E shows all SAS output.

An interaction between treatment types was found to be significant at a 95% confidence level ($p<.05$) in all cases. Interaction between two factors is defined as; "[When] the difference in mean responses for the two levels of one factor is not constant across levels of the second factor." [38]. Interaction results are listed in Table 3.3.

Table 3.3: Results for statistical test of interaction between main treatment groups. "Treat1" represents weathering type and "Treat2" represents wood treatment type.

Sample Group Tested	Effect	Num Degrees of Freedom	F-value	Pr > F
PF-film Gmax	Treat1*Treat2	2	7.96	0.0021
PF-film Garr	Treat1*Treat2	2	8.22	0.0018
pMDI Gmax	Treat1*Treat2	2	4.53	0.0219
pMDI Garr	Treat1*Treat2	2	4.55	0.0216

A test of each treatment level significance was then run because significant interactions were found. Table 3.4 shows a representative treatment level analysis. A 95% confidence level ($p<.05$) was used to determine significance in all cases.

Table 3.4: Example results for a test of treatment level significance. Treat1 represents the levels of weathering; boiled (b), and non-boiled (n). Treat2 represents the levels of wood treatment; control (c), densified (d), and hygro-thermal treatment (t).

Effect	Treat1	Treat2	Num Degrees of Freedom	F Value	Pr > F
Treat1*Treat2	b		2	2.47	0.105
Treat1*Treat2	n		2	27.63	<.0001
Treat1*Treat2		c	1	1.02	0.3215
Treat1*Treat2		d	1	0.05	0.8228
Treat1*Treat2		t	1	16.97	0.0004

Summary results containing average values and standard errors for SERR were printed for all results. Individual results were then divided and are discussed in the appropriate chapters.

3.4 Results and Discussion

Strain energy release rate data were obtained from samples of wood bonded with either PF-film or pMDI adhesive. Raw data are given in Appendix C. Results for each wood treatment type were compared for each adhesive. An adhesive comparison was then made.

3.4.1 PF-film Adhesive

Summary results of maximum and arrest strain energy release rates were obtained for samples bonded with PF-film. Maximum SERRs were compared to arrest SERRs. Maximum SERRs for each wood treatment type were then compared.

3.4.1.1 Results

Maximum and arrest SERR results are summarized in Table 3.5.

Table 3.5: Average maximum (G_{max}) and arrest (G_{arr}) strain energy release rate (J/m²) and standard errors for samples bonded with PF-film.

	Gmax (J/m²)		Garr (J/m²)	
	average	**std. error**	**average**	**std. error**
Control	229.69	21.06	200.28	19.76
Densified	281.26	25.93	264.07	24.33
Hygro-thermal Treated	472.67	25.86	439.48	24.26

G_{arr} was found to be the same as G_{max}. Results are graphically displayed in Figure 3.21.

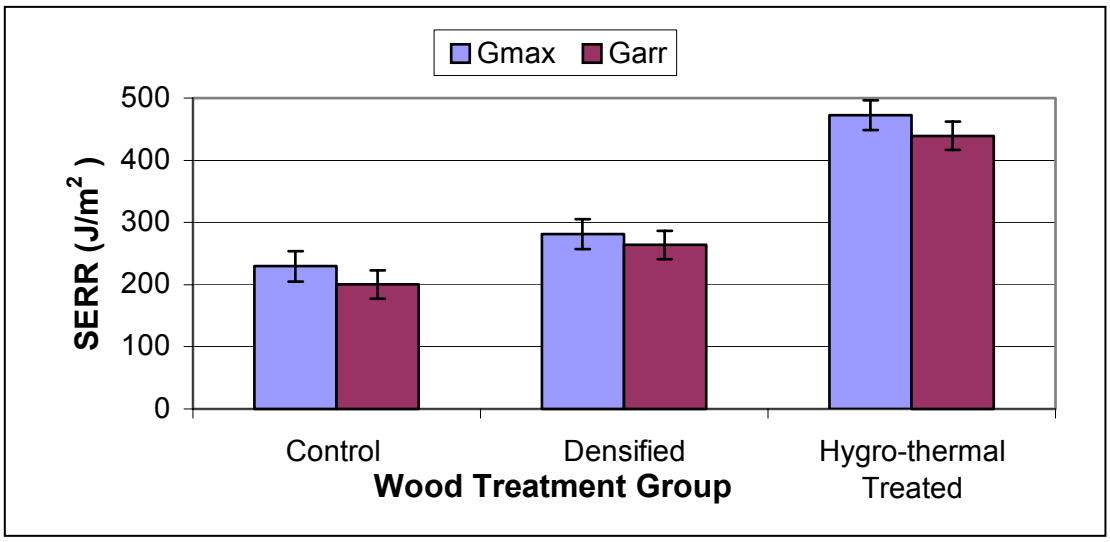

Figure 3.21: Comparison of average maximum and arrest SERR (J/m²) values for samples bonded with PF-film adhesive.

A test of treatment effect was run, and at least one wood treatment type was found to be significantly different than the others. A 95% confidence level was used and a p-value of <.001 was found. Figure 3.21 clearly shows that hygro-thermal treatment of yellow-poplar significantly increased maximum fracture toughness from 229.7 J/m² for control samples and 281.3 J/m² for densified samples to 472.7 J/m². Densified (281.3 J/m²) and control (229.7 J/m²) samples had the same SERRs (p-value= .266).

3.4.1.2 Discussion

Several important observations were made during testing that should be included when considering the results. The first set of observations deals with the mechanics and location of crack propagation, while the second set deals with adherend properties.Two significant differences in crack propagation were observed for control samples versus treated wood samples. Crack propagation for control samples was
straight and relatively smooth. Hygro-thermally treated and densified wood exhibited a type of zig-zag crack propagation. The degree of zig-zag varied with each sample. Figure 3.22 illustrates this difference in crack propagations.

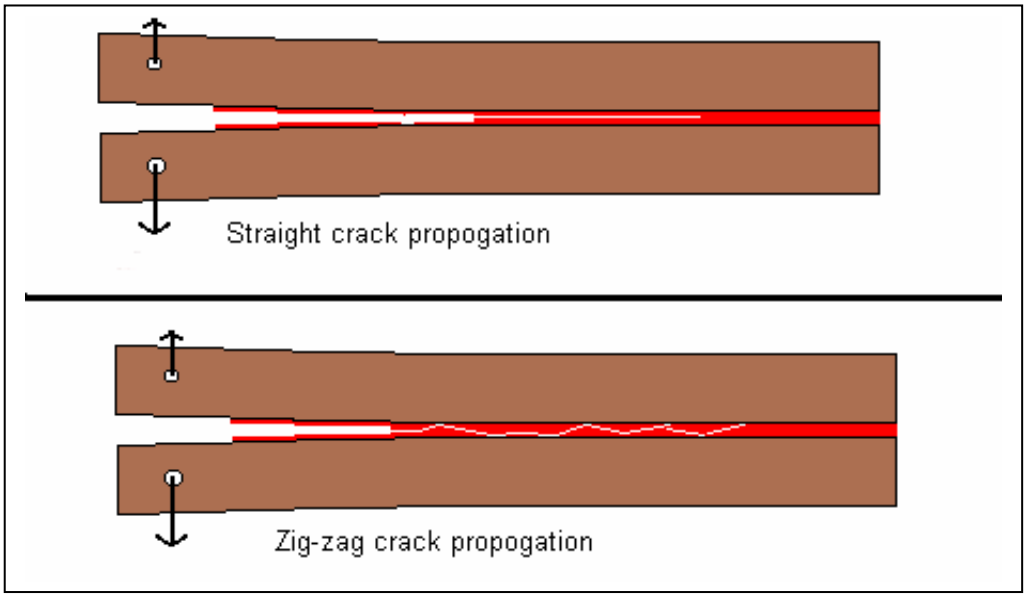

Figure 3.22: Observed patterns of crack propagation: top- straight, bottom- zig-zag.

Densified samples also exhibited 'tying' of adherends during testing. Tying is defined here as when a fiber (thin wood strand) is attached to both adherends even after crack propagation continues. Figure 3.23 illustrates this concept.

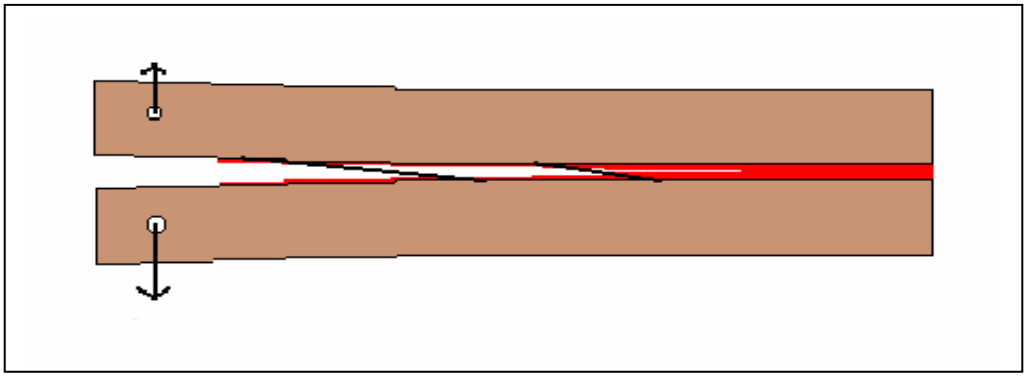

Figure 3.23: illustration of the tying of two adherends together with wood fibers after and during crack propagation.

A change in bondline failure location was also noted for control samples versus treated wood samples. All observations were made visually with no chemical analysis performed. Control samples appeared to show mixed cohesive and substrate failure with smooth discolored surfaces on both failed faces. Cohesive failure occurred over the majority of the surface. Hygro-thermally treated wood samples showed a distinctly different failure pattern. The apparent failure location followed directly beneath the adhesive layer. The location would occasionally shift from one side of the bondline to the other as the crack extended. Distinct layers of wood with adhesive in between were visible. The adhesive was visible as bands of film outlining the changes between bondline sides. Reflected light microscopy with a simple UV filter was performed to help clarify the visual observations. Figure 3.24 clearly shows a section of a film paper band observed at the transition of failure between bondline sides.

Figure 3.24: Reflected light microscope image (taken @ 5 x, 1626 x 1235 μm field of view) of a failed bondline for a hygro-thermally treated fracture sample bonded with PF-film.

Substrate failure was predominant on both failed surfaces of the sample. Figure 3.25 shows the wood surface visible over the majority of the failed bond surface.

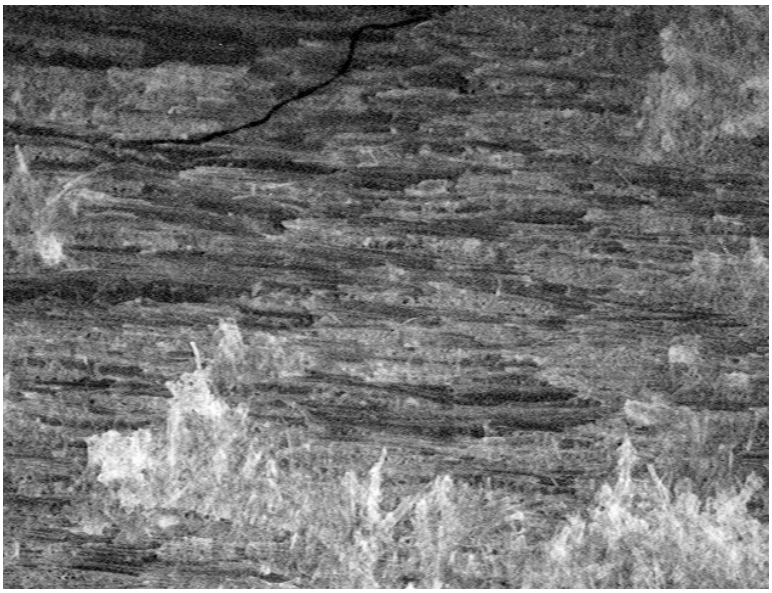

Figure 3.25: Reflected light microscope image (taken @ 2.5 x, 3258 x 2474 μm field of view) of a failed bondline surface for a hygro-thermal fracture sample bonded with PF-film.

Densified samples exhibited a failure pattern very similar to the pattern seen for hygro-thermal samples with one notable difference. Failure location remained on one side of the bondline for the majority of the length. Transition between bondline sides was usually limited to once per sample. Figure 3.26 shows a crack transition between bondline sides for a densified fracture sample.

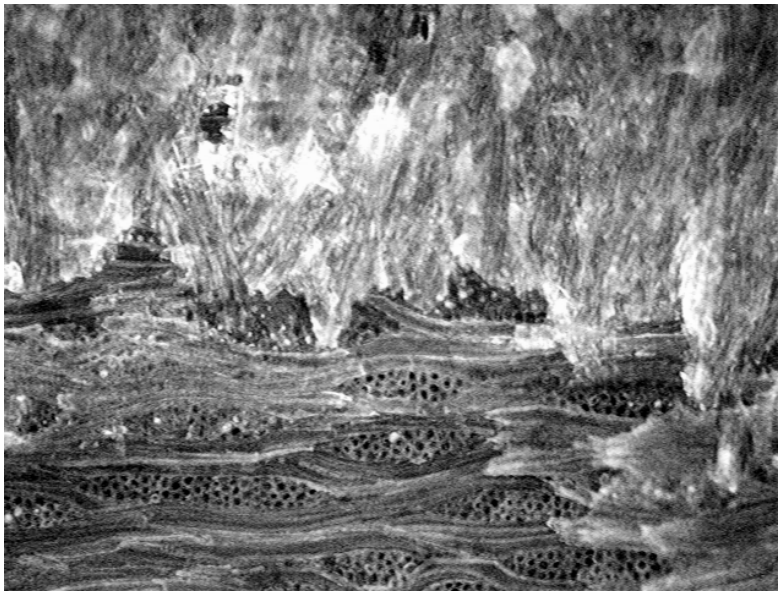

Figure 3.26: Reflected light microscope image (taken @ 5 x, 1626 x 1235 μm field of view) of a failed bondline for a densified fracture sample bonded with PF-film.

Figure 3.27 shows the surface visible over the majority of the bondline of a densified sample.

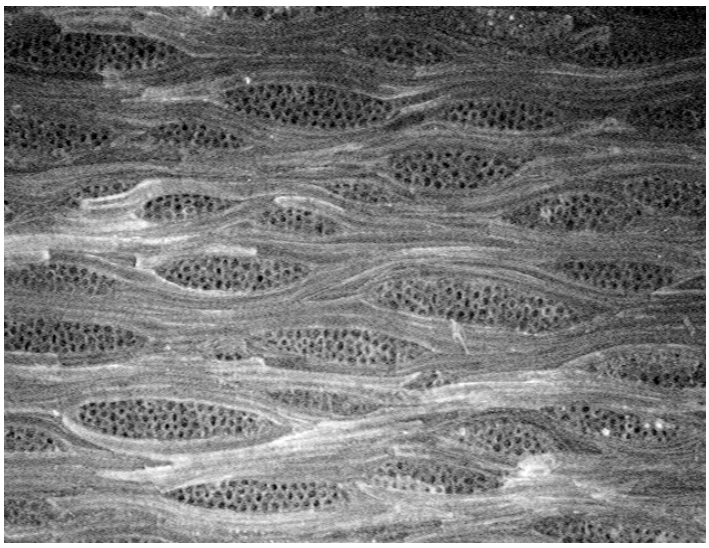

Figure 3.27: Reflected light microscope image (taken @ 5 x, 1626 x 1235 μm field of view) of a failed bondline surface for a densified fracture sample bonded with PF-film.

Additional reflected light microscope images taken of different failed bondline surfaces can be found in Appendix F. Images of a clean surface for each wood treatment type are included in Appendix F for comparison purposes. The observed differences in failure location suggest that caution should be used when forming conclusions from the observed results.

Two factors could have contributed to the failure patterns seen for treated wood groups. The first factor is the use of PF-film as an adhesive. The paper delivery system used in film adhesives could have influenced the failure location by creating a barrier and increasing the complexity of the bondline. The second factor is the probable damage to surface cells during treatment. Cell walls can either yield in an elastic/plastic manner, show brittle failure, or exhibit a combination of the two [22]. Responses are directly related to moisture and temperature combinations chosen for the densification process [22]. Surface cells are subjected to greater damage than bulk cells, which could make surface cells weaker. Weaker surface cells would fail more easily, and therefore contribute to the observed failure location. Small thickness changes observed during wood treatment for hygro-thermally treated samples (see Section 3.3.2) make this theory possibly applicable to both wood treatment groups.

Differences in adherend thicknesses should be considered in a discussion of the results. The fracture test method assumes that the top and bottom adherends have the same dimensions. This assumption was suspect for densified and hygro-thermal treated samples. The adherends of densified samples had only slightly different thicknesses, while those for hygro-thermal samples had greater variability. Adherend thicknesses are listed in Appendix A. Differences in adherend thickness would increase the variability in the results.

3.4.2 pMDI Adhesive

Summary maximum (Gmax) and arrest (Garr) strain energy release rates were obtained and compared for samples bonded with pMDI. Maximum SERRs were then compared for each wood treatment type. One significant difference was found between wood treatment groups.

3.4.2.1 Results

Fracture toughness results are summarized in Table 3.6 for samples bonded with pMDI.

Table 3.6: Average maximum (Gmax) and arrest (Garr) SERR (J/m²) and standard errors for samples bonded with pMDI.

	Gmax (J/m²)		Garr (J/m²)	
	average	**std. error**	**average**	**std. error**
Control	187.35	17.62	162.33	16.47
Densified	303.41	21.67	282.14	20.25
Hygro-thermal Treated	170.67	17.67	156.39	16.51

No significant difference was found between Gmax and Garr. At least one wood treatment type was found to have a significantly different Gmax than the others at a 95% confidence level. A test of treatment effect resulted in a p-value of .0002. Figure 3.28 graphically shows the differences between wood treatment types.

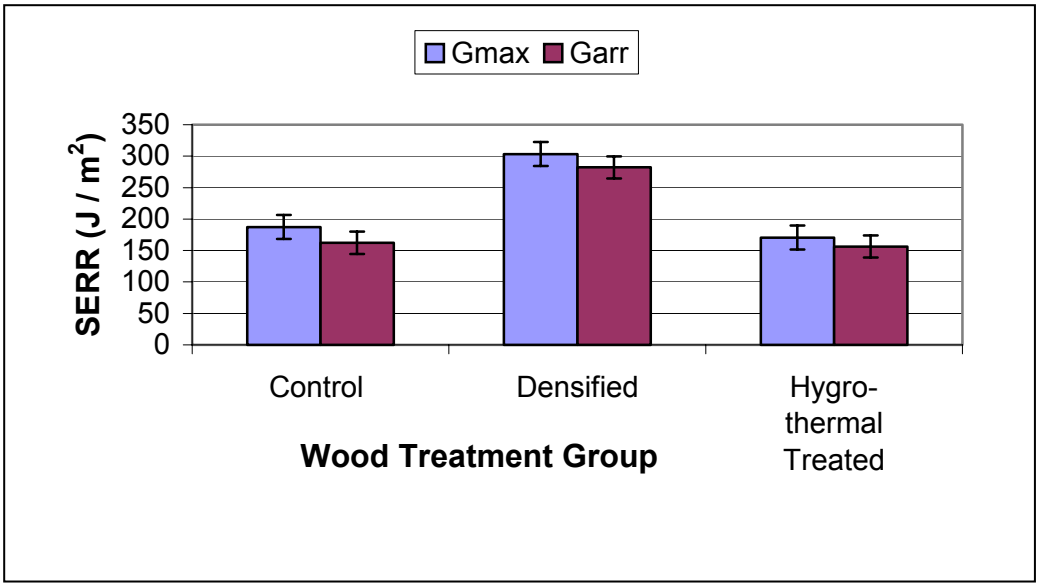

Figure 3.28: Comparison of average maximum and arrest SERR (J/m²) values for samples bonded with pMDI adhesive

Densification was found to significantly increase Gmax from 187.4 J/m² for control samples and 170.7 J/m² for hygro-thermal samples to 303.4 J/m². Hygro-thermal treatment of yellow-poplar did not significantly change the fracture toughness when compared to control samples (p-value= .219).

3.4.2.2 Discussion

Microscope analysis of failed bond surfaces showed little difference in the location of failure. All samples appeared to have a mixture of cohesive and substrate failure, but chemical analysis would be necessary to determine the exact location of bond failure. Figure 3.29 is an image from a failed surface of a control sample bonded with pMDI.

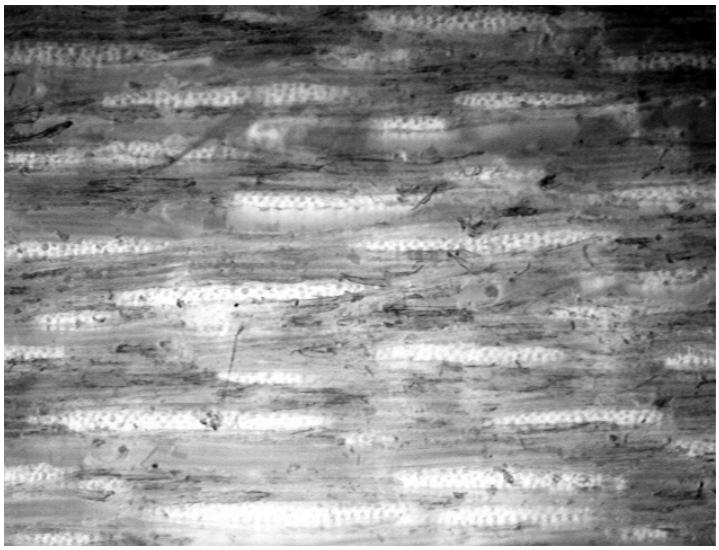

Figure 3.29: Reflected light microscope image (taken @ 5 x, 1626 x 1235 μm field of view) of a failed bondline surface of a control fracture sample bonded with pMDI.

Failed bond surfaces of control samples were slightly discolored with minimal fiber pullout. Failed surfaces of hygro-thermal samples were similar to surfaces seen for control samples but had increased roughness. Figure 3.30 is an image from a hygro-thermal bondline surface.

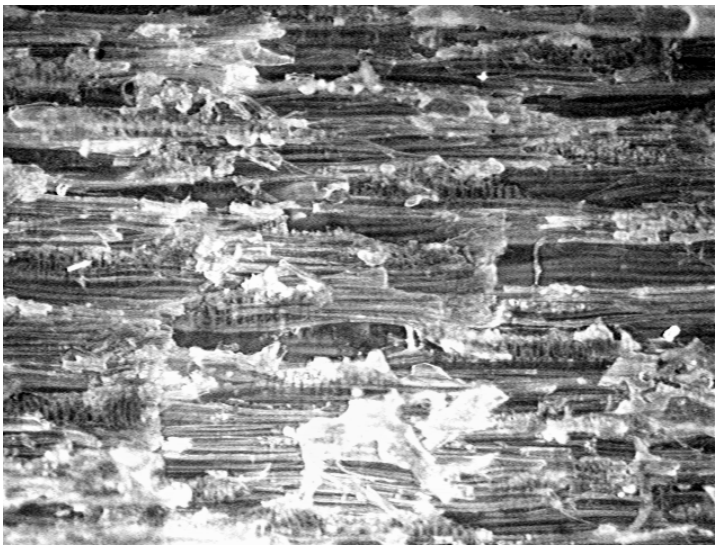

Figure 3.30: Reflected light microscope image (taken @ 5 x, 1626 x 1235 μm field of view) of a failed bondline surface for a hygro-thermal fracture sample bonded with pMDI.

One difference was noted for failed surfaces of densified fracture samples. Figure 3.31 is an image of a densified sample failed surface.

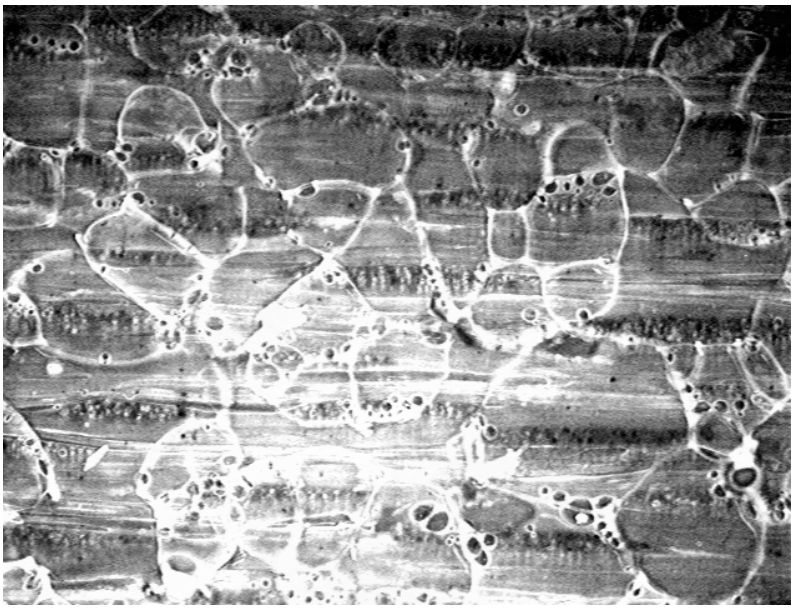

Figure 3.31: Reflected light microscope image (taken @ 5 x, 1626 x 1235 μm field of view) of a failed bondline surface for a densified fracture sample bonded with pMDI.

Densified samples showed bright rings in patches across the bonded surface. One possible explanation is that gas bubbles formed and broke during the bonding process. This correlates with difficulties experienced during the bonding of densified wood with pMDI (see Section 3.3.3.1). Additional reflected light microscope images can be found in Appendix G.

Several additional observations should be considered. Observations made during testing showed that crack propagation for densified fracture samples was not straight. The zig-zag path of the crack tip discussed and illustrated (see Figure 3.22) in Section 3.4.1.2 was observed. The tying of adherends was also observed (see Section 3.4.1.2, Figure 3.23). Tying could be an energy dissipation mechanism. The zig-zag crack pattern could have implications on crack length measurement, but affects could average out over the width of the bondline. The last observation deals with different adhesive coverage for densified samples. Excess squeeze out of adhesive was noted

during the bonding of densified billets. This leads to the speculation that coverage was less for densified samples. Decreased adhesive coverage for densified samples could lead to differences in bondline thickness and increased variance in the results.

3.4.3 Adhesive Comparison

A comparison of average maximum SERR results was made based on adhesive type. Only fracture toughness of hygro-thermally treated wood seemed to be impacted by adhesive type. A graphic comparison is seen in Figure 3.32.

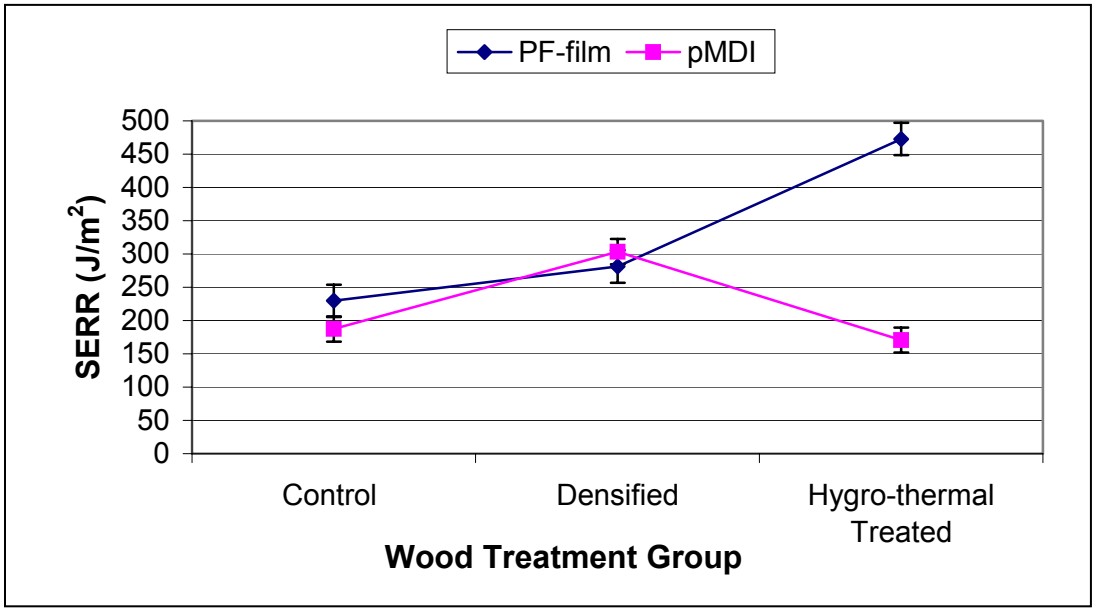

Figure 3.32: Comparison of average maximum SERR (J/m²) values for samples bonded with PF-film and pMDI adhesives.

Gmax for hygro-thermal samples bonded with PF-film was 472.7 J/m² while Gmax was 170.7 J/m² when pMDI was used. No difference based on adhesive type was seen for densified and control wood treatments.

This comparison is for theoretical discussion purposes only. Significant differences between the adhesives make a true comparison invalid. The pMDI adhesive is a low viscosity liquid that penetrates easily and rapidly into cell

lumens and walls. Rapid penetration usually results in a thinner bondline. Bondline thickness significantly impacts fracture results [34]. The pMDI adhesive also has a 100% solids content and a different cure mechanism than phenol formaldehyde. PMDI cures by chemically reacting with water, while PF polymerizes. To complicate matters, a PF-film adhesive was used instead of a liquid PF adhesive. The impregnated paper delivery system changes the bondline dynamics. Any comparisons should be made very cautiously.

3.5 Conclusions

The affect of yellow-poplar wood treatment type on fracture toughness was found to differ based on adhesive type. Fracture toughness was significantly improved by hygro-thermal treatment when PF-film was used to bond samples, while densification showed no statistical difference from control samples. Results were reversed for samples bonded with pMDI. Densification significantly increased the strain energy release rate while hygro-thermal treatment caused no significant change. No clear conclusions could be drawn about the different effects of the hygro-thermal treatment and compression components of densification on the resultant fracture toughness.

Chapter 4
Investigating Bond Durability

4.1 Introduction

Simple moisture cycling, consisting of boiling and drying, was used to investigate fracture sample bond durability. Fracture samples were made from yellow-poplar taken from three different treatment groups (control, hygro-thermal, densified) and bonded with two different adhesives (PF-film, pMDI). Test results were compared to study treatment effect. Bond durability was investigated by comparing fracture results from boiled samples to results from non-boiled samples (see Section 3.4).

4.2 Background

Bond durability is an important and complicated issue in wood products. A variety of factors can affect the durability of a wood bond. Age, insects, UV rays, and moisture have all been shown to change the expected longevity of bonds. Moisture is generally perceived to be the more serious factor affecting bond durability in wood science. Durability is defined here as the ability to maintain the fracture toughness of the bond over time in the presence of moisture.

Moisture affects wood bonds in several different ways. Anisotropic properties of wood cause uneven shrinkage and swelling as relative humidity and moisture content change. Uneven changes in dimensions can cause internal bond stresses. Moisture also softens wood, degrades some adhesives, and can degrade the actual wood/adhesive bond.

The negative affects of moisture on bonded wood make this an important area of study. One standard accelerated aging procedure for adhesively bonded wood is found in ASTM D 1037-99. This process calls for six steps per cycle. Cycle steps are: immersion in water at 49 ± 2^{o}C for 1 hour, subjection to steam and water vapor at 93 ± 3^{o}C for 3 hours, storage at -12 ± 3^{o}C for 20 hours,

heating at 99 ± 2°C in dry air for 3 hours, subjection to steam and water vapor at 93 ± 3°C for 3 hours, and heating in dry air at 99 ± 2°C for 18 hours [30]. This cycle is repeated six times for a total of 288 hours of cycling [30].

An alternative to ASTM D 1037-99 was found in the literature [39]. Two simple moisture cycles were shown to have property results similar to those seen after ASTM D 1037 cycling. The first short cycle consisted of four steps: water soaking at 120°F for 2 hours, heating in dry air at 210°F for 4 hours, water soaking at 120°F for 2 hours, and heating in dry air at 210°F for 16 hours [39]. The second short cycle consisted of two steps: water soaking at 120°F for 8 hours, and dry air heating at 210°F for 16 hours. Each cycle variation was to be repeated four times [39].

A two step moisture cycle, similar to but more severe than the ones published by McNatt and McDonald [39], was used by another researcher [36]. The method consists of boiling in water for 2 hours followed by dry air heating at 103°C for 22 hours. This cycle was repeated four times [36].

4.3 Materials and Methods

Bond durability was investigated by subjecting DCB fracture samples to moisture cycling and then completing opening mode fracture testing. Clear sapwood yellow-poplar panels taken from three different treatment groups were bonded with phenol formaldehyde film (PF-film) or polymeric diphenylmethane diisocyanate (pMDI) to form fracture samples. Treatment groups were: control, hygro-thermal conditioning, and densification. Explanations of adhesive, wood species, and treatment group choices are given in Section 3.3. The overall design of bond durability testing, including the number of samples tested for each treatment /adhesive combination, is outlined in Table 4.1.

Table 4.1: Testing design for bond durability with the number of samples per treatment group.

Adhesive used in bonding	Control	Hygro-thermal conditioning	Densification
phenol formaldehyde film	6	6	6
polymeric diphenylmethane diisocyanate	6	6	6

4.3.1 Preparing Samples

Three major processing steps are required to prepare fracture samples from clear sapwood yellow-poplar. First, rough lumber must be cut into wood panels for treatment. Next, panels from groups two and three must be treated. Lastly wood panels are bonded into billets and cut into fracture samples.

Rough lumber was first cut into 11/16 (17-mm) x 3 1/16 (75mm) x 14 15/16-inch (373mm) panels with a 3 degree grain angle using the process described in Section 3.3.1. Panels were then divided into three different treatment groups and conditioned in preparation for treatment. Group two and three panels were conditioned to 23 ± 2% EMC (89% relative humidity, 21.1ºC). Group one panels were conditioned to 12 ± 2% EMC (21ºC, 65% relative humidity).

Panels from groups two and three were treated following the process described in Section 3.3.2. Group two panels were subjected to hygro-thermal treatment. Group three panels were densified. All panels were conditioned to 12% EMC following treatment.

Fracture samples were then made from wood panels using the process described in Section 3.3.3. Panels were first paired and bonded to form billets (see Section 3.3.3.1). Billets were then cut into 20-mm wide strips. Final preparation of samples (see Section 3.3.3.3) was done following moisture cycling of the 20-mm wide strips. Six samples per adhesive/treatment group combination were made for all combinations except densified wood bonded with pMDI. Two samples (one billet) from this group were lost during billet pressing.

One of the three billets which were bonded delaminated at the end of the pressing cycle. This issue was discussed in detail in Section 3.3.3.1.

4.3.2 Sample Moisture Cycling

Unfinished fracture samples were subjected to five cycles of boiling and drying as published in the literature [36]. Dimensions of each sample were recorded prior to cycling (see Appendix H). Two gallons of distilled water were placed into a three gallon, stainless steel stockpot. The container was placed on a heat source and the water brought to a boil. All samples were dropped into the boiling water, weighted to keep submersed, and boiled for two hours. Samples were removed from the water and blotted dry with paper towels at the end of the two hours. Within five minutes the samples were placed into a convection oven set to 103^{o}C. Samples were dried for 22 hours. This cycle was repeated for a total of five cycles. Drying time at the end of the fifth cycle was shortened to give a higher moisture content and speed final conditioning at 12% EMC. Samples were conditioned to constant weight at 12% EMC prior to further machining. Sample Dimensions were measured and recorded after conditioning and prior to final sample preparation (see Appendix H).

Several important observations were made during and after boil cycling of samples. Samples made from control yellow-poplar were relatively unaffected by boiling. Most samples had only minor end splitting after the last cycle. One sample bonded with pMDI and one bonded with PF-film had begun to delaminate at the bondline. Samples made from hygro-thermally treated wood were the most severely damaged. Two samples bonded with pMDI and one sample bonded with PF-film showed delamination along the bondline. Almost all samples showed uneven swelling of the adherends (see Figure 4.1).

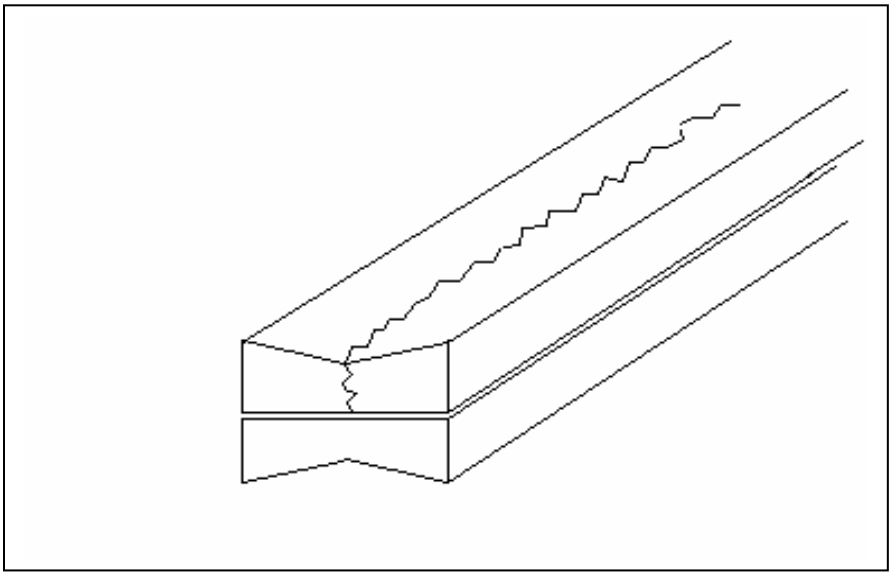

Figure 4.1: Illustration of uneven swelling and breaking found in hygro-thermally treated samples after boil cycling.

This uneven swelling caused cracking down the center of the adherend in seven samples, irrespective of adhesive type (see Figure 4.1). Samples made from densified wood were also affected by boiling. Most samples were either twisted or cupped. Wood splitting along the grain was also commonly observed (see Figure 4.2).

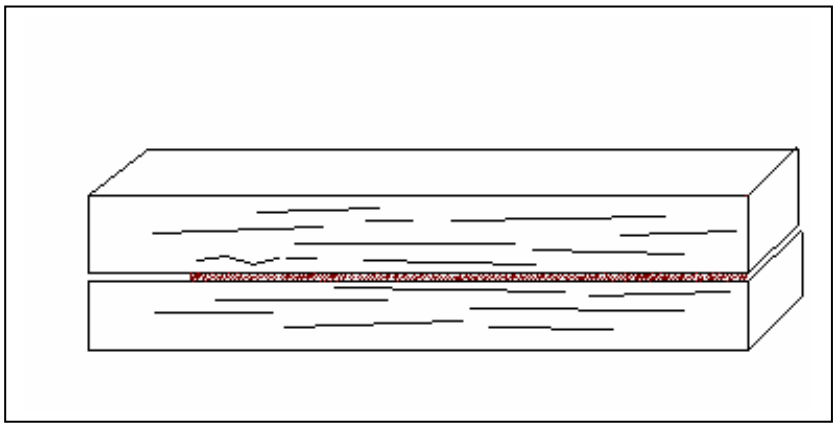

Figure 4.2: Example of splitting along the grain that was seen in some boiled samples.

Two samples bonded with pMDI showed slight delamination of the bondline. Densified samples also exhibited slight thickness swell. Samples bonded with PF-film exhibited an average thickness increase of .4-mm. Samples bonded with pMDI exhibited an average thickness increase of .9-mm (see Appendix H). These measurements could have been influenced by twisting and cupping observed in densified samples.

4.3.3 Sample Testing

Fracture samples were tested using the method described in Section 3.3.4.

4.3.4 Data Analysis

Strain energy release rate was calculated from the raw data collected during testing. Calculations were made following the process detailed in Section 3.3.5.1.

Calculated values were evaluated using the criteria described in Section 3.3.5.2. Data from five samples were deleted in this step. One sample from the treated group bonded with PF-film and one bonded with pMDI were deleted because crack extension was unmeasureable due to damage incurred during boiling. Three samples from the densified group bonded with pMDI were deleted. Two samples were unusable due to delamination after billet formation. The remaining sample was deleted due to crack propagation though the wood.

Data were then analyzed as described in Section 3.3.5.3. Raw data are given in Appendix D. Statistical analysis output is given in Appendix E.

4.4 Results and Discussion

Boiled fracture toughness samples were tested and analyzed for differences between wood treatment groups. Results were also compared to results found in Section 3.4 to determine bond durability. Samples bonded with pMDI are discussed separately from samples bonded with PF-film.

4.4.1 PF-film Adhesive

Fracture toughness (G) and bond durability of boiled samples bonded with PF-film were analyzed. Results are given and discussed in the following sections according to adhesive type.

Section 4.4.1.1 Results

Maximum (Gmax) and arrest (Garr) strain energy release rates (SERR) were calculated. Table 4.2 lists summary results with standard errors.

Table 4.2: Average maximum (Gmax) and arrest (Garr) SERRs (J/m²) with standard errors for boiled samples bonded with PF-film.

	Gmax (J/m²)		Garr (J/m²)	
	average	**std. error**	**average**	**std. error**
Control	259.83	21.08	233.53	19.77
Densified	288.84	21.17	262.49	19.86
Hygro-thermal Treated	329.49	23.22	303.68	21.79

A test of treatment effect showed no significant differences between wood treatment types at a 95% confidence level. A p-value of .1050 was found. Figure 4.3 shows the graphed results.

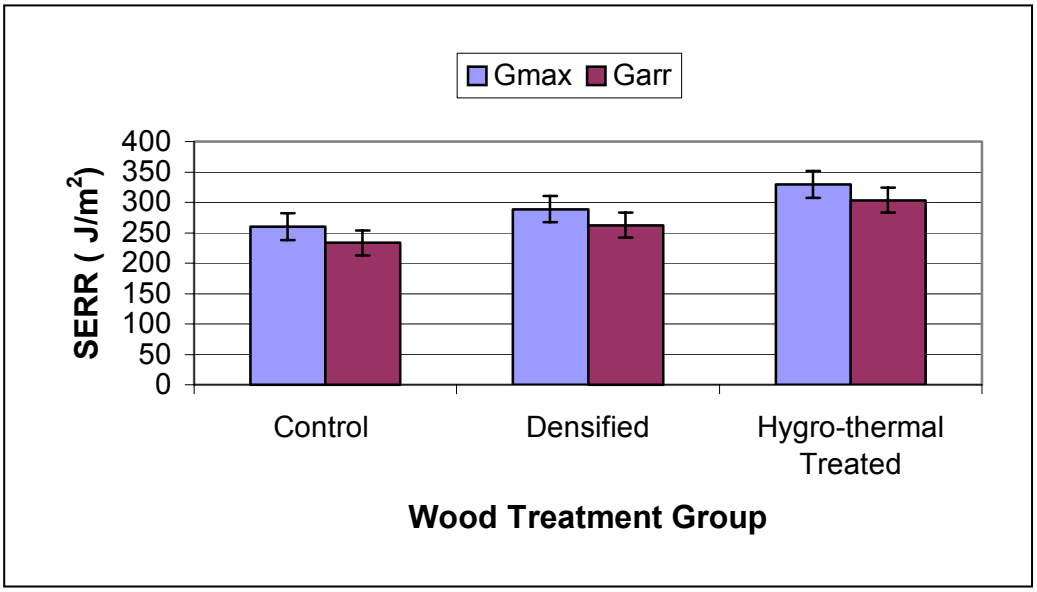

Figure 4.3: Comparing average maximum (Gmax) and arrest (Garr) SERR (J/m²) values for boiled samples bonded with PF-film adhesive.

Fracture toughness results for boiled samples were compared to the results for non-boiled samples (see Section 3.4.1) bonded with PF-film. Figure 4.4 shows this comparison.

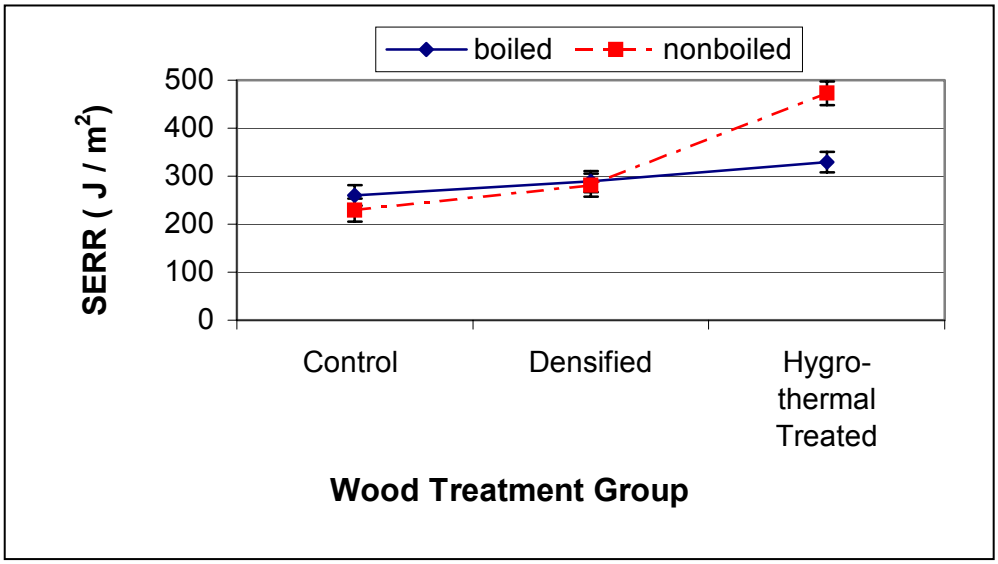

Figure 4.4: Comparison of average maximum SERR (J/m²) for boiled and non-boiled fracture samples bonded with PF-film.

Fracture toughness for hygro-thermal samples was significantly reduced by boiling of samples. A test of treatment effect showed a significant difference with a p-value of .0004. Fracture toughness for hygro-thermal samples was reduced from 472.7-J/m² to 329.5-J/m². Fracture toughnesses for control and hygro-thermal samples were not significantly effected.

Section 4.4.1.2 Discussion

The results show that only fracture toughness of samples made from hygro-thermally treated wood was significantly reduced by boiling. These results clearly point back to damage incurred during boil cycling. Hygro-thermal samples exhibited serious uneven shrinkage and swelling that caused some samples to partially break (see Section 4.3.2). Uneven swelling would have induced greater internal bond stresses. Breaks in the sample also increased the total area of the bondline directly contacted by water during boiling.

Several other facts could have contributed to the bond durability results. The different thicknesses seen for hygro-thermal sample adherends (see Appendix A) could cause increased internal bond stresses created in cycling. Differences in press times during billet bonding for different treatment types could also influence durability results. Hygro-thermal and control samples were subjected to an additional 10-minutes at 200ºC during bonding (see Section 3.3.3). This extra thermal treatment could have allowed changes in internal wood stresses for hygro-thermally treated panels that would be less likely to occur in densified samples.

The failure location pattern found for boiled samples is similar to the pattern found for non-boiled samples (see Section 3.4.1.2). Control samples seemed to show mixed cohesive and substrate failure with smooth slightly discolored surfaces. No adhesive film paper was observed on the surface. Hygro-thermal samples showed failure directly under or over the bondline as found in Section 3.4.1.2. Fewer transitions between bondline sides were observed for boiled samples than for non-boiled samples. Figure 4.5 shows a portion of the failed bondline for a hygro-thermal sample.

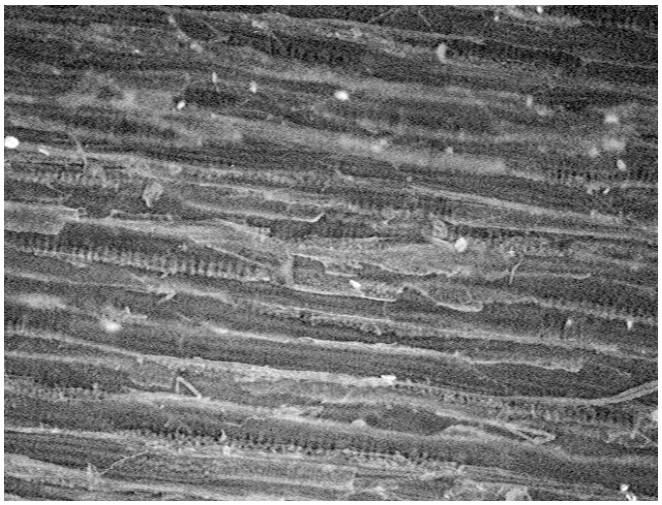

Figure 4.5: Reflected light microscope image (taken @ 5 x, 1626 x 1235 μm field of view) of a failed bondline surface of a boiled hygro-thermal fracture sample bonded with PF-film.

Densified samples exhibited a slightly different failure pattern. Failure location seemed to be closer to the bondline than in non-boiled samples. Sections of the bondline exhibited no carrier film. Figure 4.6 is an image taken of a location with no visible adhesive from a densified fracture sample.

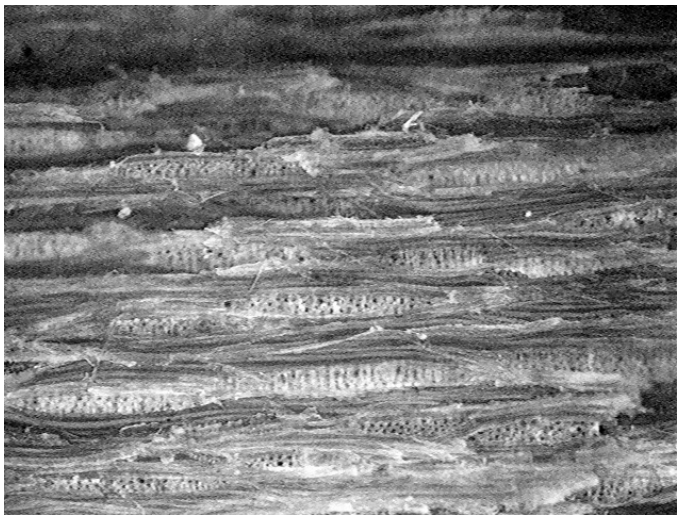

Figure 4.6: Reflected light microscope image (taken @ 5 x, 1626 x 1235 μm field of view) of a failed bondline surface of a boiled densified fracture sample bonded with PF-film.

Other sections of the failed surface exhibited greater amounts of visible film. Figure 4.7 shows the greater amount of adhesive coverage.

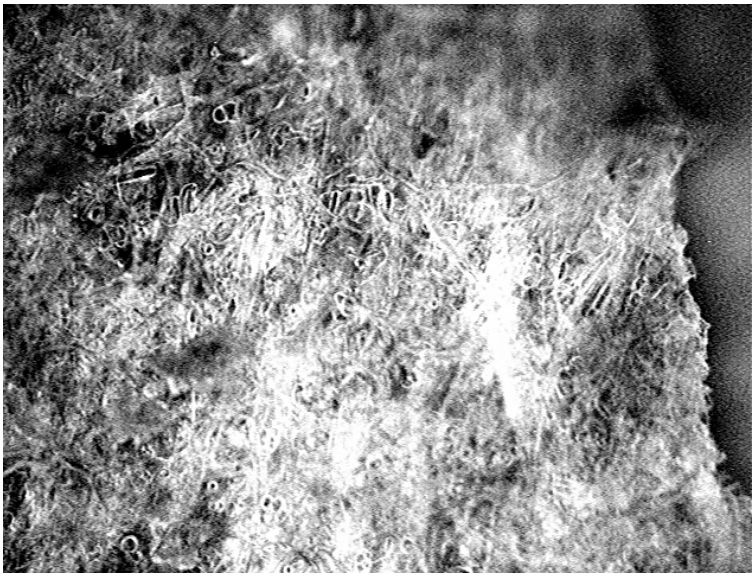

Figure 4.7: Reflected light microscope image (taken @ 5 x, 1626 x 1235 μm field of view) of a failed bondline surface of a boiled densified fracture sample bonded with PF-film.

Failed bondline surfaces were also found to be more variable than surfaces observed for non-boiled samples. Additional microscope images can be found in Appendix I.

Section 4.4.2 pMDI Adhesive

Boiled fracture samples bonded with pMDI were tested and analyzed to determine fracture toughness. Bond durability was analyzed by comparing these results with results from Section 3.4.2.

Section 4.4.2.1 Results

Maximum and arrest SERR results for boiled samples bonded with pMDI are summarized in Table 4.3.

Table 4.3: Average SERRs and standard errors for boiled samples bonded with pMDI.

	Gmax (J/m²)		Garr (J/m²)	
	average	**std. error**	**average**	**std. error**
Control	163.29	17.64	145.69	16.49
Densified	289.45	25.23	260.23	23.56
Hygro-thermal Treated	46.39	22.07	40.43	20.59

No significant difference was found between Gmax and Garr. A test of treatment effect found that at least one wood treatment type differed significantly from the others. Significance was found at the 95% confidence level with a p-value of <.0001. Figure 4.8 illustrates the results.

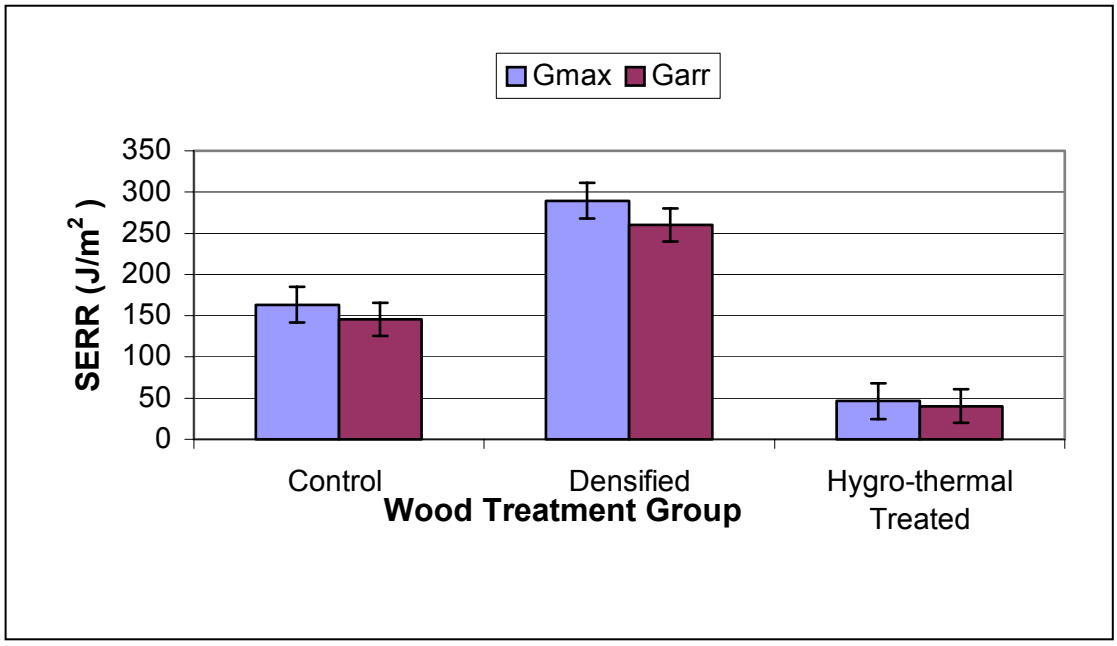

Figure 4.8: Comparing average maximum and arrest SERR (J/m^2) values for samples bonded with pMDI adhesive.

Densified samples have a significantly higher fracture toughness than both control and hygro-thermal samples. Fracture toughness for hygro-thermal samples is seen to be significantly lower than both control and densified

samples. The average maximum SERR values were found to be: 46.4-J/m² for hygro-thermal samples, 163.3-J/m² for control samples, and 289.5-J/m² for densified samples.

Average maximum SERRs for boiled samples were compared to average maximum SERRs for non-boiled (see Section 3.4.2) samples to investigate bond durability. Figure 4.9 graphically shows this comparison.

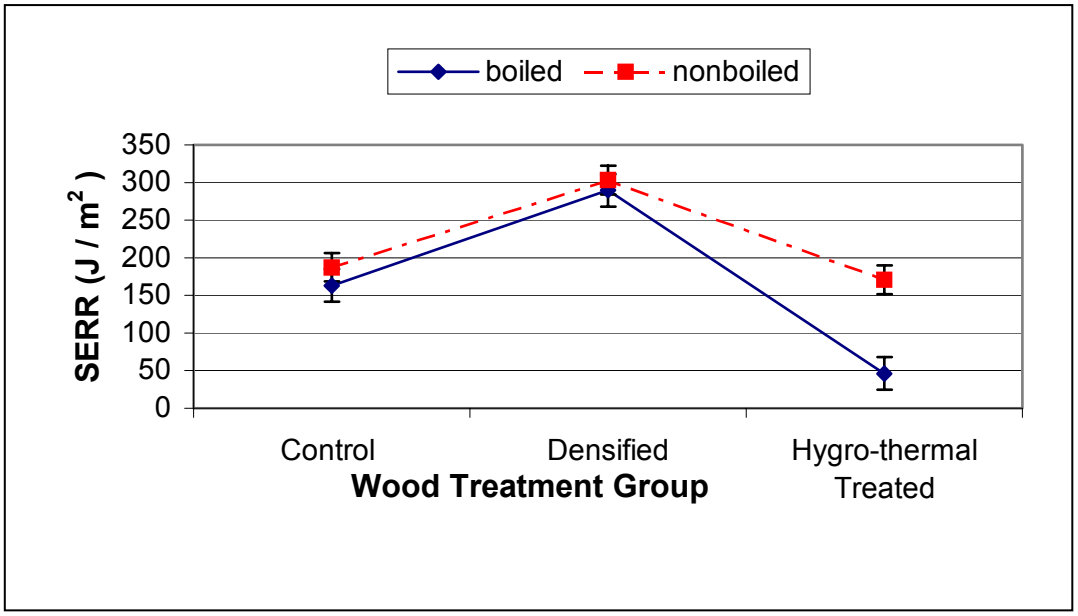

Figure 4.9: Comparing average maximum SERR (J/m²) values for boiled and non-boiled samples bonded with pMDI adhesive.

A test of treatment effect found a significant difference (p-value = .0002) between maximum fracture toughness of boiled and non-boiled hygro-thermal samples. The fracture toughness was reduced from 170.7-J/m² to 46.4-J/m².

Section 4.4.2.2 Discussion

The fracture toughness decrease for boiled hygro-thermal samples once again reflects the wood changes observed during boil cycling. The observed uneven swelling and cracking (see Section 4.3.2) probably caused internal bond stresses that weakened the bond.

The location of bond failure appeared to be similar for all wood treatment types. This pattern is the same as the pattern found earlier (see Section 3.4.2.2). Reflected light microscope images showed little differences in failed surfaces. Figure 4.10 shows a surface seen on a hygro-thermal sample.

Figure 4.10: Reflected light microscope image (taken @ 5 x, 1626 x 1235 μm field of view) of a failed bondline surface of a boiled hygro-thermal fracture sample bonded with pMDI.

This surface was similar to the surface seen for control samples, but with increased roughness. The bondline surface of densified wood differed slightly from control and hygro-thermal samples. Bright rings were visible on the surface. Figure 4.11 is an image from a densified sample.

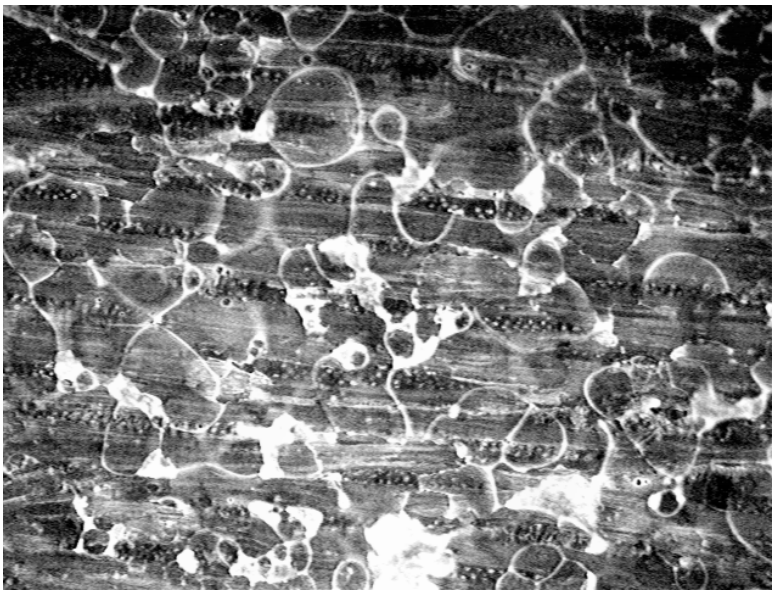

Figure 4.11: Reflected light microscope image (taken @ 5 x, 1626 x 1235 μm field of view) of a failed bondline surface of a boiled densified fracture sample bonded with pMDI.

This surface observation is the same as the observations discussed in Section 3.4.2.2. Additional microscope images can be found in Appendix J.

A note should be made that these images were not sufficient to determine the exact failure location. Chemical analysis of the surface is necessary to know the exact location.

4.5 Conclusions

Boiled fracture samples were analyzed for fracture toughness and bond durability. The hygro-thermal sample group was the only group to show a significant reduction in fracture toughness with boil cycling, regardless of adhesive type. Densified samples were found to have a significantly increased fracture toughness for pMDI bonded samples. Hygro-thermal samples were found to have significantly reduced fracture toughness for pMDI bonded samples. No clear conclusion could be made on the separate effects of hygro-thermal treatment and compression during densification of overall fracture toughness of densified samples.

Chapter 5
Investigation of Surface Energy

5.1 Introduction

Wood surface free energy plays a key role in bonding any wood surface. The surface energy of yellow-poplar from three wood treatment groups was studied using the sessile drop contact angle method. Surface energy components were then calculated from the contact angle data. Wood treatments were control, hygro-thermal treatment, and densification.

5.2 Background

The wettability and spreadability of liquids on a wood surface are greatly influenced by surface free energy. Wettability is the ability of a liquid to make intimate contact with the wood surface. Spreadability is the ability of a liquid to flow across the wood surface.

The relationship between surface energy and wettability/spreadability of a liquid is generally understood in the field of wood science. Low wood surface energy leads to liquid molecules being more attracted to other liquid molecules than to wood surface molecules. This state is generally characterized by a large contact angle of a liquid drop on a wood surface. Figure 5.1 illustrates a large contact angle.

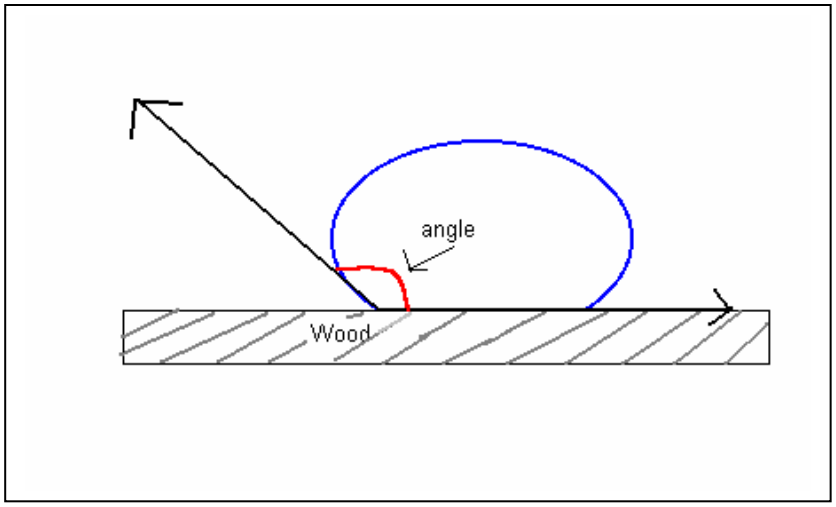

Figure 5.1: Illustration of a large liquid contact angle on wood.

A large contact angle generally indicates poor wettability/spreadability. High wood surface energy generally leads to liquid molecules being more attracted to wood surface molecules than to other liquid molecules. This state is characterized by a small contact angle. A small contact angle measurement is indicative of good wettability/spreadability. Figure 5.2 illustrates a small contact angle.

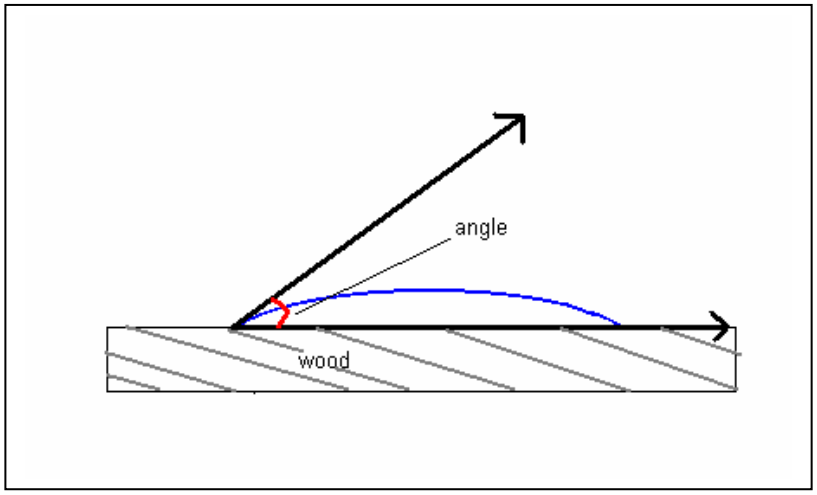

Figure 5.2: Illustration of a small liquid contact angle on wood.

Measurement of liquid contact angle on a wood surface is a currently accepted method for studying wood surface energy. Several different methods of measuring contact angle exist. The two most common methods are the sessile drop method and the Wilhelmy plate method.

The Wilhelmy method measures the contact angle of a probe liquid on a wood plank as the plank is lowered into and pulled out of the liquid. Figure 5.3 illustrates the Wilhelmy method.

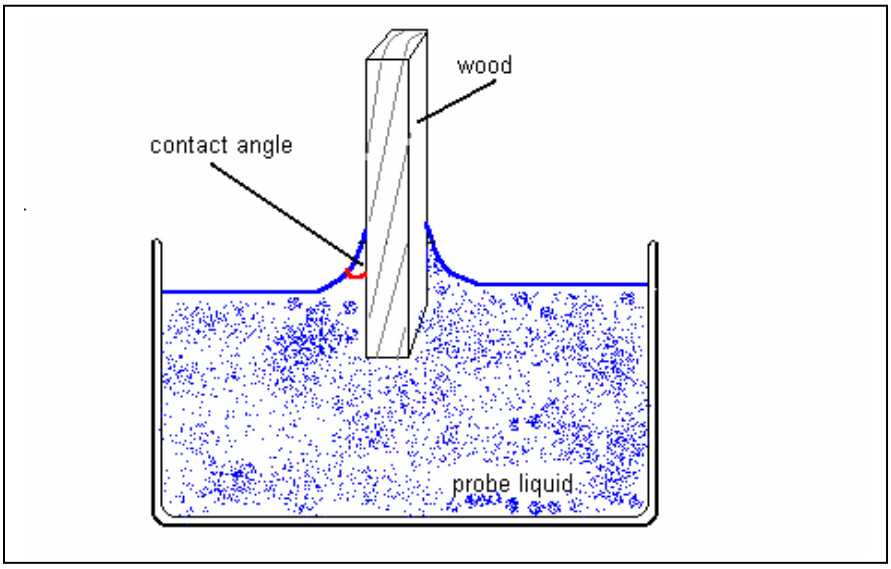

Figure 5.3: Illustration of the Wilhelmy plate method for measuring contact angle.

Determination of contact angle using the Wilhelmy method is complicated by two issues. The first complication arises from the possibility of probe liquid contamination during testing [40]. The second complication comes from the porous nature of wood. Probe liquids are wicked into the wood upon contact due to capillary structure of wood and/or chemical attraction. Wicking must be accounted for when determining contact angle [41].

The sessile drop method measures the angle between the contacted wood surface and the tangent line of the air-liquid-solid interface. Angle measurement is illustrated in Figure 5.4.

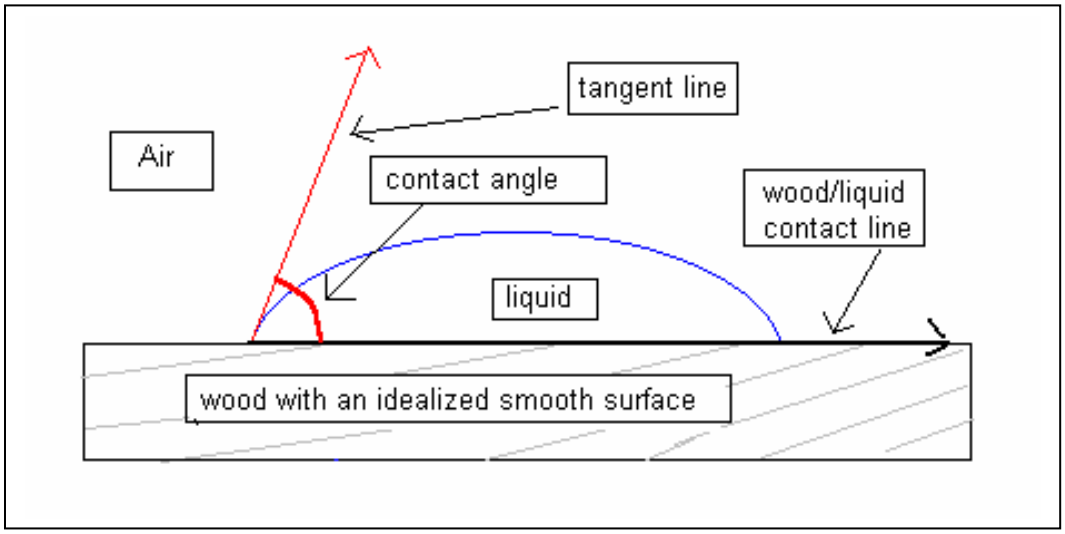

Figure 5.4: Illustration of the sessile drop method for contact angle measurement.

Contact angles are influenced by the liquid surface tension, wood surface energy, liquid viscosity, wood surface roughness and porosity, and drop orientation with respect to grain. The liquid surface tension is known and accounted for when calculating wood surface energy. Surface porosity allows the liquid to penetrate into the wood instead of equilibrating to one drop shape. Surface roughness can keep the probe liquid from completely wetting the surface for a short time.

Timing of the contact angle measurement is greatly influenced by porosity. The most common method of angle measurement is to wait until the liquid drop becomes stable on the wood surface. This method is complicated when low surface energy probe liquids are used. Low surface energy liquids tend to completely penetrate into the wood leaving no liquid drop to measure. The method is further complicated by the possibility of probe liquid contamination (as in the Wilhelmy method) and swelling of wood with the probe liquid. One published study suggest using the initial (time zero) and equilibrium contact angle to calculate a contact angle characteristic of a smooth wood surface [42]. Equilibrium contact angle is defined as the point, "when all the unevenness on

the wood surface is filled with the respective liquid and the advancing contact angle is changed to the receding one"[42].

Surface free energy values for wood are calculated using contact angle data and known probe liquid surface energies. Several methods of calculation exist using one or more probe liquids. Five of these methods were compared to each other in one study [43]. Similar surface energies were calculated using the equation of state method, the acid-base approach, and the geometric mean equation. The acid-base approach gave the most detailed results [43].

The acid-base method of calculating surface energy results in polar, non-polar, acid, and base components of the total energy. Two calculation methods of the acid-base approach, the Good-van-Oss-Chaudhury model and the Chang model, were directly compared in another study [44]. Both methods utilize known surface energy components of a series of liquids to determine the non-polar and polar components of wood surface energy. The Chang model was shown to give similar results to the Good-van-Oss-Chaudhury model, but was more robust [44].

5.3 Materials and Methods

The sessile drop method was chosen to obtain contact angles of five liquids on wood. The Chang equation method for calculating acid-base components of surface energy was used. Surface energy was investigated for sapwood yellow-poplar, densified yellow-poplar, and hygro-thermally treated yellow-poplar. Table 5.1 gives the overall contact angle test design with the number of samples per treatment group and the number of liquid drops per sample.

Table 5.1 Contact angle test design including the number of samples per wood treatment, probe liquids used, and the number of drops of liquid per sample.

		# of liquid drops per sample				
Type of wood treatment	**# of samples**	**Water**	**Glycerol**	**Ethylene Glycol**	**Formamide**	**a-Bromo-napthalene**
Control	10	3	3	3	3	3
Hygro-thermal	10	3	3	3	3	3
Densified	10	3	3	3	3	3

5.3.1 Sample Preparation

Contact angles were measured on wood from each of the three main treatment groups. Ten samples were prepared for each group. Samples from the densified and hygro-thermally treated groups were prepared using the procedures outlined in Section 3.3.1 and 3.3.2. These samples were conditioned to 12 ± 2% EMC and then cut to 2 x 7-inch dimensions prior to testing. Samples from the control group were machined using the process in Section 3.3.1. All boards were next conditioned to 12 ± 2% EMC. Seven boards (3 x 14 15/16-inches) were then planed to 10-mm thick and cut to 2x7-inch dimensions. Planing and cutting was performed immediately prior to contact angle measurement for samples from the control group.

Section 5.3.2 Probe Liquids

Contact angle measurements were made using a series of five liquids. Distilled water, glycerol, ethylene glycol, formamide, and α-Bromonapthalene were used.

Glycerol, ethylene glycol, and formamide were stored under nitrogen to prevent contamination. Twenty 1-dram vials per liquid were filled with ethylene glycol, glycerol, and formamide. Transfer was performed with a medium and large canula and nitrogen gas. Each vial was flushed with nitrogen as the cap was screwed on. Paraffin wax was used to ensure an airtight seal at the cap.

The use of small vials helped ensure that uncontaminated liquid was always used for testing.

5.3.3 Contact Angle Measurement

A series of five probe liquids were used to investigate surface energy using the sessile drop contact angle method. Surfaces of yellow-poplar, densified yellow-poplar, and hygro-thermally treated yellow-poplar were studied. Ten samples were tested per treatment group (see Table 5.1).

The following process was used to capture liquid drop images and measure contact angles. A CCD color camera was wired to a computer and used to capture drop images. Figure 5.5 illustrates the testing setup.

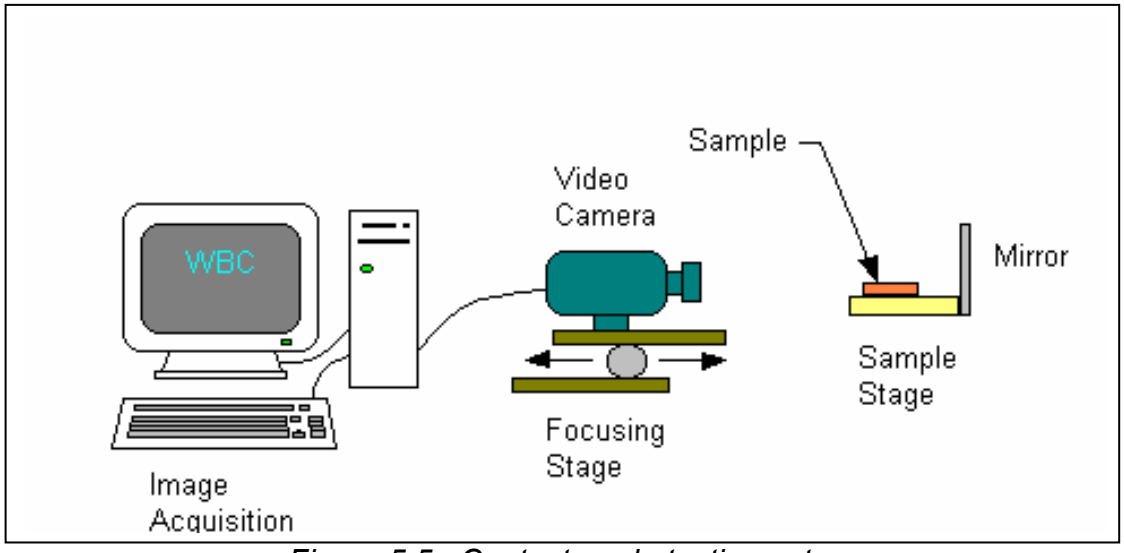

Figure 5.5: Contact angle testing setup.

Image Pro Analysis Software version 3.0 was used to analyze images. A 5-microliter drop was randomly placed on the tangential wood surface using an Eppendorf Micropipette. The drop image was captured ~1.5 seconds after contacting wood. This timing allowed the drop to settle onto the surface before the image was captured. The time also ensured that the drop was still present to

be viewed. The sample was then randomly moved and another drop image taken. Three drops were captured per liquid per sample for all five liquids.

Image analysis software was used to measure each contact angle. A base line was first drawn along the bottom of the drop at the solid-liquid interface. A tangent line from the point of the air-liquid-solid interface was then drawn. The angle between the two lines became the contact angle. Figure 5.4 illustrates drop measurement.

5.3.4 Contact Angle Analysis

Contact angle measurements were analyzed using Statistical Analysis Software (SAS) version 8.0. Raw contact angle data are listed in Appendix K.

The statistical design for this experiment was a split plot design. Each sample within a treatment group was considered to be a plot replication that was split into five treatments (liquid type). A mixed general linear model code was created by the Statistical Consulting Center of Virginia Tech to analyze the data.

Significant interactions were found between the liquid type treatment and the wood treatment (see Table 5.2).

*Table 5.2: Results for test of treatment effects during contact angle analysis for wood treatment (Treat1), liquid type (Treat2), and interactions (Treat1*Treat2).*

Type 3 Test of Fixed Effects			
Effect	**# Degrees of Freedom**	**F Value**	**Pr > F**
Treat1	2	177.85	<.0001
Treat2	4	1359.82	<.0001
Treat1*Treat2	8	30.06	<.0001

Tests of effect were then run to determine the significance of each treatment level. All SAS output is given in Appendix L. Summary results were printed and used in surface energy calculation.

5.3.5 Surface Energy Calculations

Total wood surface energy and energy components were calculated using known liquid component values and average contact angles. Liquid surface energy values were found in the published literature and are shown in Table 5.3 [44].

Table 5.3: Values for the total surface energy (γ_L), dispersion component (γ_L^d), polar component (γ_L^p), Lewis acid component (γ_L+), Lewis base component (γ_L-), Chang dispersion component (P_L^d), Chang acid component (P_L^a), and Chang base component (P_L^b) of each liquid.

	γ_L mJ/m²	γ_L^d mJ/m²	γ_L^p mJ/m²	γ_L^+ mJ/m²	γ_L^- mJ/m²	P_L^d mJ/m²	P_L^a (mJ/m²) 🗁	P_L^b (mJ/m²) 🗁
a-Bromonapthalene	44.4	44.4	0	0	0	10.5	-2.67	-3.82
Ethylene Glycol	48	29	19	1.92	47	7.5	3.69	-5.44
Formamide	58	39	19	2.28	39.6	7.3	6.92	-4.64
Glycerol	64	34	30	3.92	57.4	8	3.4	-9.3
Water	72.8	21.8	51	25.5	25.5	6.6	6.88	-7.4

Values for the probe liquid glycerol were removed from the contact angle results and the liquid surface energy data prior to any calculations because they were >90 degrees for two of the three treatment groups. Extremely low goodness of fit values for regression lines were found when glycerol was used as part of the data set.

The Chang equation model for acid-base component calculation was used [44]. Personal communication with Dr. D. Gardner resulted in the transfer of a spreadsheet to assist in calculations. The following calculation method was used within the spreadsheet.

The dispersive (non-polar) component (γ_s^d) of the solid surface energy was first determined by running a multiple linear regression based on the geometric mean equation (see Equation 5.1).

$$W_a = (1+\cos\theta)\gamma_L = 2\left(\gamma_L^d * \gamma_s^d\right)^{1/2} + 2\left(\gamma_L^p * \gamma_s^p\right)^{1/2}$$

Equation 5.1

Theta (θ) is the average contact angle for each liquid. The y-values used for the regression are calculated from Equation 5.2 using measured contact angles and the appropriate known liquid surface energies (γ_L) found in Table 5.3. Data for the entire series of four test liquids were used.

$$y = \left((1+\cos\theta) * \gamma_L\right) / 2$$

Equation 5.2

The x-values used for the regression are calculated by taking the square root of each known liquid polar (γ_L^p) component (see Table 5.3) and each known liquid dispersive (γ_L^d) component. All returned regression equations were in the form of Equation 5.3.

$$y = m_1 x_1 + m_2 x_2 + \ldots\ldots + b$$

Equation 5.3

The coefficient of the first variable (m_1) found by regression is taken to be the square root of the solid dispersive energy component. This value (m_1) is squared to obtain the solid surface energy dispersive component (γ_s^d).

Step two was to determine the acid (P_s^a) and base (P_s^b) component of solid surface energy by running a second multiple linear regression based on the Chang acid-base equation (see Equation 5.4).

Equation 5.4

$$W_a = (1+\cos\theta)\gamma_L = P_L^d P_s^d - P_L^a P_s^b - P_L^b P_s^a$$

The x-values for the regression are the known acid (P_L^a) and known base (P_L^b) components of liquid surface energy found in Table 5.3. The entire series of four liquids is again used. The y-values for the regression are calculated from Equation 5.5.

$$y = \left(P_L^d P_s^d\right) - W_a$$

Equation 5.5

All variables for Equation 5.5 are calculated using Equations 5.6, 5.7, and 5.8 based in the Chang model (see Equation 5.4). The solid surface energy dispersive component used in Equation 5.7 was calculated in step one.

$$P_L^d = \sqrt{2\gamma_L^d}$$

Equation 5.6

$$P_s^d = \sqrt{2\gamma_s^d}$$

Equation 5.7

$$W_a = (1 + \cos\theta)\gamma_L$$

Equation 5.8

The returned regression equation is again in the form of Equation 5.3. The base component of the wood surface energy for the Chang model (P_s^b) is equal to the coefficient of the first regression variable (m_1). The acid component of wood surface energy for the Chang model (P_s^a) is equal to the coefficient of the second regression variable (m_2).

Step three was to calculate the acid-base component (γ_s^p) of the solid surface energy using Equation 5.9 with acid (P_s^a) and base (P_s^b) components calculated in step two.

$$\gamma_s^p = \left(P_s^a\right)\left(P_s^b\right)$$

Equation 5.9

The last step in calculating solid surface energy components is to calculate the total wood surface energy from components found in steps one and three using Equation 5.10.

$$\gamma_s^T = \gamma_s^d + \gamma_s^p$$

Equation 5.10

This entire calculation process was done three times, once for each wood treatment group.

5.4 Results & Discussion

Surface energy of yellow-poplar, hygro-thermally treated yellow-poplar, and densified yellow-poplar was investigated by measuring contact angles of five test liquids. Average contact angle values per liquid per wood treatment group were then used to calculate surface energy components. Contact angle data are summarized in Table 5.4.

Table 5.4: Average contact angles (degrees) found for each liquid for each wood treatment.

	Control (deg)	Hygro-thermal Treated (deg)	Densified (deg)
water	41.63	82.01	85.94
glycerin	62.19	98.83	96.92
ethylene glycol	26.89	57.63	55.98
formamide	22	52.66	52.81
a-Bromonapthalene	13.33	25.87	26.55
Standard error for all average values = 1.68			

The average contact angle of at least one liquid type was found to be significantly different than other liquids for each of the three wood treatment types. A p-value of <.0001 was found in each case. Figure 5.6 illustrates differences in contact angles of each probe liquid for one wood treatment group.

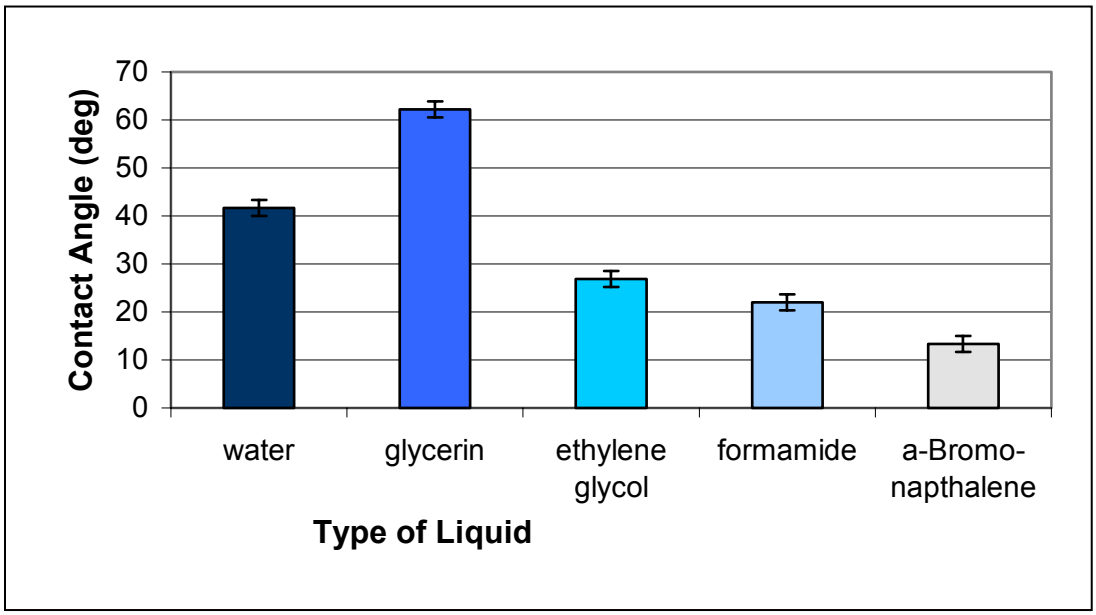

Figure 5.6: Comparing average contact angles of all liquids for control samples.

The overall trend of each liquid contact angle for a wood treatment type is the important observation for comparison. The same overall trend of contact angles was seen for hygro-thermally treated samples and densified samples. Graphs for the remaining two wood treatment groups are given in Appendix M. Contact

angle values for glycerol are noticeably higher than expected when the total surface energy for glycerol is compared to that of other liquids. An expected contact angle for glycerol would have been lower than the angle seen for water, but greater than that found for formamide. The high viscosity of glycerol may have been a factor in this since angle measurements were taken ~1.5 seconds after contact instead of at drop equilibrium.

The overall contact angle trends for each wood treatment group were compared to each other. This comparison is seen in Figure 5.7.

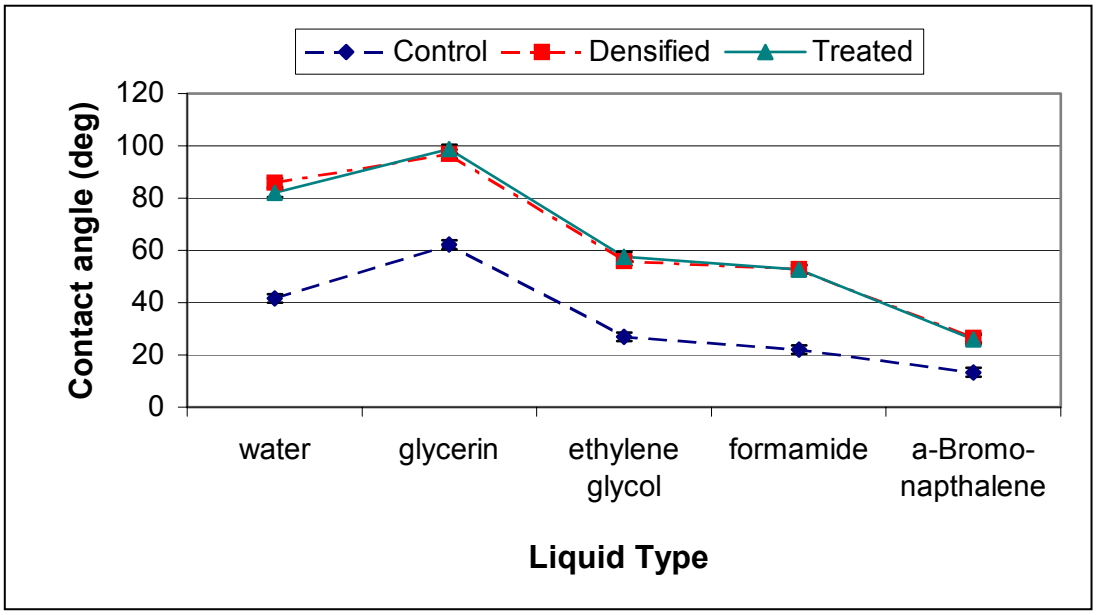

Figure 5.7: Comparing average contact angle trends for the three wood treatment groups.

The trends for densified and hygro-thermally treated wood are both significantly higher than the contact angle trend for control yellow-poplar. A test of treatment effect verifies this finding with a p-value of <.0001. There is no significant difference observed between the trends for densified and hygro-thermally treated wood.

The components of solid surface energy were calculated using the Chang model as described in Section 5.3.5. The determined surface energy components for each wood treatment group are listed in Table 5.5

Table 5.5: Surface energy component results for each wood treatment type.

	γ^{tot} (mJ/m²)	γ^{d} (mJ/m²)	γ^{p} (mJ/m²)	P^{a} $(mJ/m^2)^{1/2}$	P^{b} $(mJ/m^2)^{1/2}$
Control	53.775	37.65341	16.1216	2.850857	-5.655
Hygro-thermal Treated	38.04784	38.6543	-0.60646	-0.16104	-3.76601
Densified	37.65515	39.79142	-2.13627	-0.57267	-3.73034

The total surface energy (γ^{T}) is significantly reduced from 53.8-mJ/m² to 38.0-mJ/m² by hygro-thermal wood treatment. Total surface energy decreases slightly to 37.7-mJ/m² with densification treatment. This result is consistent with the contact angle results shown in Figure 5.7. Hygro-thermal and densification treatments deactivate the wood surface, lowering the overall surface energy. Lower surface energy leads to higher contact angles and decreased wettability and spreadability.

The dispersive (non-polar) component (γ^{d}) of the total surface energy is seen to slightly increase from 37.7-mJ/m² with each wood treatment; hygro-thermal (38.7-mJ/m²) followed by densification (39.8-mJ/m²). The total acid-base (polar) component (γ^{p}) is seen to significantly decrease from 16.1-mJ/m² to -0.606-mJ/m² with hygro-thermal treatment, and then decreases again to -2.14-mJ/m² with densification. The individual acid component (P^{a}) decreases from 2.85-mJ/m² to -.161-mJ/m² and again to -.573-mJ/m² following the same trend seen in the polar component. The basic component (P^{b}) actually increases from -5.66-mJ/m² to -3.77-mJ/m² with hygro-thermal treatment, and then slightly increases again to -3.73-mJ/m² with densification. This pattern is opposite of the pattern seen for the polar component.

The surface energy results clearly show significant changes in energy components. Total surface energy and the polar component of surface energy decrease with hygro-thermal treatment and densification. The dispersive (non-polar) component of surface energy increases with wood treatment. Control yellow-poplar exhibits an amphoteric surface. An amphoteric substance is

capable of donating either H^+ ions or OH^- ions, and is defined as having basic and acidic components with opposite signs [44]. Densified wood and hygro-thermal treated wood are shown to have basic surfaces. A basic substance donates electrons (OH^- ions), and is defined as having basic and acidic components with negative signs [44].

Additional clarification of the basic significance of surface energy results was achieved using the following process. Average contact angles were modified by adding and subtracting the standard error. The two new sets of contact angles were used to calculate surface energy components as described in Section 5.3.5. The obtained results are given in Table 5.6.

Table 5.6: Limit results for surface energy components.

		Wood Treatment Group		
Surface Energy Component	**Limits**	**Control**	**Treated**	**Densified**
γ^{tot} **(mJ/m²)**	upper	52.97	37.24	36.88
	actual	53.78	38.05	37.66
	lower	54.54	38.86	38.43
γ^{d} **(mJ/m²)**	upper	37.5	38.21	39.33
	actual	37.65	38.65	39.79
	lower	37.77	39.07	40.21
γ^{p} **(mJ/m²)**	upper	15.47	-0.97	-2.45
	actual	16.12	-0.61	-2.14
	lower	16.77	-0.21	-1.79
P^{a} **(mJ/m²)**^{½}	upper	2.76	-0.27	-0.68
	actual	2.85	-0.16	-0.57
	lower	2.94	-0.05	-0.47
P^{b} **(mJ/m²)**^{½}	upper	-5.6	-3.66	-3.62
	actual	-5.65	-3.77	-3.73
	lower	-5.71	-3.87	-3.84

Hygro-thermal treatment appears to account for the majority of changes to surface energy. Compression adds very little to the changes observed.

The observed decrease in surface energy for this study follows similar patterns found in the literature. The total surface energy found for control yellow-poplar is almost identical to the total surface energy of 54.8-mJ/m2 found in the literature [45]. A recent study of yellow-poplar surface inactivation showed that

contact angles increased as drying temperature increased [33]. The greatest contact angles were measured when drying temperatures of 200°C were applied. High drying temperatures were shown to increase the extractive and lignin content on the surface [33]. One could speculate that increased lignin and extractive content on the surface was the main cause of decreased surface energy observed in this study. The theory of increased extractives and lignin on the surface is also indicated by the increase in the non-polar component of surface energy and decrease in the polar component. Extractives and lignin are generally thought to be hydrophobic and therefore non-polar.

5.5 Conclusions

Hygro-thermal wood treatment and densification significantly reduce total surface energy and increase contact angles to a similar extent. A significant reduction of the polar (acid-base) surface energy component was found with hygro-thermal treatment and densification. The acid component decreased with wood treatment type, from control to hygro-thermal-densified, while the base component increased. A slight increase in the non-polar (dispersive) component was observed with wood treatment.

Chapter 6
Summary and Conclusions

Section 6.1 Summary

The first objective of this project was to determine the surface energy of hygro-thermally compressed densified wood and bond performance when using PF-film or pMDI adhesive. This objective was clearly met with the following results. Densified wood was found to have a SERR (281.3 J/m²) similar to control yellow-poplar (229.7 J/m²) when bonded with PF-film. Hygro-thermally treated wood bonded with PF-film had a higher SERR (472.7 J/m²) and was the only treatment group significantly impacted by weathering (329.5 J/m²). Densified wood was found to have a higher SERR (303.4 J/m²) than control samples (187.4 J/m²) when pMDI was the adhesive used in bonding. Hygro-thermal samples bonded with pMDI had a SERR (170.7 J/m²) similar to control sample, and was the only group significantly impacted by weathering (46.4 J/m²). Total surface energy of densified wood (37.7 mJ/m²) was reduced from control yellow-poplar (53.8 mJ/m²). No clear relationship was found between surface energy and bond performance. Surface energy results suggest that bond performance would decrease for densified samples, but performance was actually found to be the same as or better than performance for control yellow-poplar.

The second objective of this project was to differentiate between the influence of hygro-thermal treatment and compression treatment on surface energy and bond performance of densified wood. No clear relationship between the hygro-thermal treatment and compression treatment can be defined for bond performance. The relationship between treatment effects for surface energy can be determined. Hygro-thermal treatment significantly reduced the surface energy of yellow-poplar. Densified wood exhibits a very slight decrease in surface energy when compared to hygro-thermally treated wood. However, the average contact angles found for densified wood were not statistically different from the

angles found for hygro-thermally treated wood. This leads to the conclusion that the major cause of surface energy reduction of densified wood is due to hygro-thermal conditioning during the densification process.

Section 6.2 Conclusions

Several broad conclusions can be drawn from the results of this study.

- Densified wood bonded with PF-film has similar bond performance to control yellow-poplar.
- Densified wood bonded with pMDI has better bond performance than control yellow-poplar.
- The main cause of surface energy reduction in densified wood was hygro-thermal conditioning.
- Bond performance and surface energy results could not be related to each other.

The results found in this study lead to the broad conclusion that densified wood is a viable raw material for making a composite product.

Chapter 7
Recommendations

Several areas of interest for future research on densified wood have become apparent over the course of this study. Relatively good bond performance, found for densified yellow-poplar in comparison to untreated yellow-poplar, suggests that densified yellow-poplar is a good candidate for a structural composite product. The goal to create a new composite product coupled with the results of this study point to three key areas in need of study. A study of densified wood surface chemistry would help explain surface energy component patterns found in this study (see Section 5.4, Table 5.5). An understanding of surface chemistry could prove helpful in choosing or formulating an adhesive. Analysis of bondline failure mechanisms/location as well as bondline characteristics would improve the understanding of bond performance test results. Testing different types of small-scale composite products made from densified material would clarify what composite products could ultimately be viable. The marketability of composite densified products is another area in need of in-depth study. The last area of study recommended for future research is the transfer of small-scale densification methods to large scale manufacturing methods.

References

1. Kollman, F.P., E.W. Kuenzi, and A.J. Stamm. 1975. Principles of Wood Science and Technology. Vol. II: Wood Based Materials. Springer-Verlag, New York, Heidelberg, Berlin. Pp.139-149.

2. Back, E.L., and L. Salmen. 1982. Glass transitions of wood components hold implications for molding and pulping processes. Tappi 65(7): 107-110.

3. Salmen, L. 1984. Viscoelastic properties of *in situ* lignin under water-saturated conditions. Journal of Materials Science 19: 3090-3096.

4. Dwianto, W., M. Inoue, F. Tanaka, and M. Norimoto. 1996. The permanent fixation of compressive deformation in wood by heat treatment. *In*: Proceedings from the Third Pacific Rim Bio-Based Composites Symposium, Kyoto, Japan. Pp. 231-239.

5. Takahashi, K., T. Morooka, and M. Norimoto. 1998. Thermal softening of wet wood in the temperature range of 0 to 200°C. Wood Research No. 85. Wood Research Institute, Kyoto, Japan. Pp. 78-80.

6. Uhmeier, A., T. Morooka, and M. Norimoto. 1998. Influence of thermal softening and degradation on the radial compression behavior of wet spruce. Holzforschung 52(1): 77-81.

7. Hsu, W.E., W. Schwald, J. Schwald, and J.A. Shields. 1988. Chemical and physical changes required for producing dimensionally stable wood-based composites. Wood Science and Technology 22: 281-289.

8. Inoue, M., N. Sekino, T. Morooka, and M. Norimoto. 1996. Dimensional stabilization of wood composites by steaming I. Fixation of compressed wood by pre-steaming. *In*: Proceedings from the Third Pacific Rim Bio-Based Composites Symposium, Kyoto, Japan. Pp.240-248.

9. Sekino, N., M. Inoue, M. Irle, and T. Adcock. 1999. The mechanisms behind the improved dimensional stability of particleboards made from steam-pretreated particles. Holzforschung 53(4): 435-440.

10. Inoue, M., M. Norimoto, M. Tanahashi, and R. Rowell. 1993. Steam or heat fixation of compressed wood. Wood and Fiber Science 25(3): 224-235.

11. Tomme, F., F. Girardet, B. Gfeller, and P. Navi. 1998. Densified wood: An innovative product with highly enhanced characters. *In*: Proceedings from the World Conference on Timber Engineering, August 1998, Montreux-Lausanne, Switzerland.

12. Inoue, M., J. Kodama, Y. Yamamoto, and M. Norimoto. 1998. Dimensional stabilization of compressed wood using high-frequency heating. Mokuzai-gakkai-shi 44(6): 410-416.

13. Dwianto, W., F. Tanaka, M. Inoue, and M. Norimoto. 1996. Crystallinity changes of wood by heat or steam treatment. Wood Research No. 83, Pp. 47-49. Wood Research Institute, Kyoto Un., Kyoto, Japan.

14. Ito, Y., M. Tanahashi, M. Shigematsu, and Y. Shinoda. 1998. Compressive-molding of wood by high-pressure steam-treatment: Part 2. Mechanism of permanent fixation. Holzforschung 52(2): 217-221.

15. Higashihara, Takashi, T. Morooka, and M. Norimoto. 2000. Permanent fixation of transversely compressed wood by steaming and its mechanism. Mokuzai - gakkai-shi 46(4): 291-2.

16. Dwianto, W., T.Morooka, and M. Norimoto. 1998. The compressive stress relaxation of Albizia (*Paraserienthes falcata* Becker) wood during heat treatment. Mokuzai Gakkaishi 44(6):403-409.

17. van Houts, J.H., K. Jayaraman, and D. Bhattacharyya. 2000. Characterisation of the viscoelastic behavior of MDF using Taguchi analysis. *In*: Proceedings from the fifth Pacific Rim Bio-Based Composites Symposium, Canberra, Australia. Pp. 277-285.

18. Seborg, R.M., M.A. Millett, and A.J. Stamm. 1962. Heat-stabilized compressed wood (Staypak). FPL Report No 1580 (revised). Pp. 30.

19. Ito, Y., M. Tanahashi, M. Shigematsu, Y. Shinoda, and C. Ohta. 1998. Compressive-molding of wood by high-pressure steam-treatment: Part 1. Development of compressively molded squares from thinnings. Holzforschung 52(2): 211-216.

20. Navi, P. and F. Girardet. 2000. Effects of thermo-hydro-mechanical treatment on the structure and properties of wood. Holzforschung 54(3): 287-293.

21. Navi, P., F. Girardet, and F. Heger. 2000. Thermo-hydro-mechanical post-treatment of densified wood. *In*: Proceedings from the fifth Pacific Rim Bio-Based Composites Symposium, Canberra, Australia. Pp 439-447.

22. Kultikova, E.V. 1999. Structure and Properties Relationships of Densified Wood. Masters Thesis. Virginia Tech, Blacksburg, Virginia. Pp. 136.

23. Perkitny, Z. and W. Jablonski. 1984. On the assessment of mechanical properties of densified wood. Holz als Roh-und Werkstoff 42(3):81-84.

24. Asako, Y., H. Kamikoga, H. Nishimura and Y. Yamaguchi. 2002. Effective thermal conductivity of compressed woods. International Journal of Heat and Mass Transfer 45: 2243-2253.

25. Schrepfer, V. and F.H. Schweingruber. 1998. Anatomical structures in reshaped press-dried wood. Holzforschung 52(6): 615-622.

26. Abe, H., R. Funada, N. Kuroda, O. Furusawa, M. Shibagaki, and T. Fujii. 2001. Confocal laser scanning microscopy of water uptake during the recovery of compressed and drying-set wood. IAWA Journal 22(1): 63-72.

27. Inoue, M., K. Adachi, and K. Kanayama. 2001. Cupping of compressed wood resulting from set recovery. Mokuzai-gakkai-shi 47(3): 198-204.

28. Jennings, C.M. 1993. Bonding densified wood I. ASC/CASS Undergrad. Research Report. Center for Adhesive and Sealant Science, Virginia Tech, Blacksburg, Virginia.

29. American Society for Testing and Materials. 2000. Annual Book of ASTM Standards. Volume 15: General Products, Chemical Specialties, and End Use Products. Section 6: Adhesives. West Conshohochen, PA. Pp. 23-30.

30. American Society for Testing and Materials. 2000. Annual Book of ASTM Standards. Volume 4: Construction. Section 10: Wood. West Conshohochen, PA. Pp. 143-172.

31. Schmidt, R. G. 1998. Aspects of Wood Adhesion: Applications of ^{13}C CP/MAS NMR and Fracture Testing. Ph.D. Dissertation. Virginia Tech, Blacksburg, Virginia. Pp. 140.

32. Gagliano, J. 2001. An Improved Method for the Fracture Cleavage Testing of Adhesively-Bonded Wood. Masters Thesis. Virginia Tech, Blacksburg, Virginia. Pp. 87.

33. Sernek, M. 2002. Comparative Analysis of Inactivated Wood Surfaces. Ph.D. Dissertation, Virginia Tech, Blacksburg, Virginia. Pp.179.

34. Ebewele, R., B. River and J. Koutsky. 1979. Tapered Double Cantilever Beam Fracture Tests of Phenolic-Wood Adhesive Joints. Part 1. Development of specimen geometry; effects of bondline thickness, wood anisotropy and cure time on fracture energy. Wood and Fiber Science 11(3): 197-213.

35. Lenth, C.A. 1999. Wood Material Behavior in Severe Environments. Ph.D. Dissertation. Virginia Tech, Blacksburg, Virginia. Pp.122.

36. Scoville, C. 2001. Characterizing the Durability of PF and pMDI Adhesive Wood Composites Through Fracture Testing. Masters Thesis. Virginia Tech, Blacksburg, Virginia. Pp. 77.

37. Blackman, B., J.P. Dear, A.J. Kinloch and S. Osiyemi. 1991. The calculation of adhesive fracture energies from double-cantilever beam test specimens. Journal of Materials Science Letters 10: 253-256.

38. Ott, R.L., and M. Longnecker. 2001. An Introduction to Statistical Methods and Data Analysis. Fifth edition. Duxbury, Pacific Grove, California. Pp. 1152.

39. McNatt, J. D. and D. McDonald. 1993. Two accelerated-aging tests for wood-based panels. Forest Products Journal 43(7,8): 49-52.

40. Walinder, M. E.P. and I. Johansson. 2001. Measurement of wood wettability by the Wilhelmy method: Part 1. Contamination of probe liquids by extractives. Holzforschung 55(1): 21-32.

41. Walinder, M. E.P. and G. Strom. 2001. Measurement of wood wettability by the Wilhelmy method: Part 2. Determination of apparent contact angles. Holzforschung 55(1):33-41.

42. Liptakova E., J. Kudela and J. Sarvas. 1998. Problems concerning the equilibrium state on the wood-liquid phase boundary. *In:* Wood Structure and Properties. S. Kurjatko and J. Kudela ed. Arbora Publishers, Zvolen, Slovakia. Pp 109-114.

43. Gindl, M., G. Sinn, W. Gindl, A. Reiterer, and S. Tschegg. 2001. A comparison of different methods to calculate the surface free energy of wood using contact angle measurements. Colloids and Surfaces A: Physicochemical and Engineering Aspects 181: 279-287.

44. Gardner, D.J., S.Q. Shi, and W.T. Tze. 2000. Comparison of acid-base characterization techniques on lignocellulosic surfaces. Acid-Base Interactions 2: 363-383.

45. Carpenter, M. W. 1999. Characterizing the Chemistry of Yellow-poplar Surfaces Exposed to Different Surface Energy Environments Using DCA, DSC, and XPS. Masters Thesis. West Virginia University, Morgantown, West Virginia. Pp. 182.

Appendix A
Dimension Data for Wood Panels

Table A.1: Average panel dimensions before and after wood treatment for all panels densified at 100% relative humidity, 160°C, and 600 psi.

Treatment Run #	Billet #	Av Thickness (mm)		Av. Width (mm)		Length (mm)	
		before	after	before	after	before	after
1	1	9.88	3.95	55.5	56.8	189.0	184.0
	2	10.13	4.32	55.3	55.4	190.0	183.0
	3	10.03	4.20	55.4	57.1	188.0	182.0
2	1	9.98	4.09	57.4	54.7	185.0	184.0
	2	9.69	4.29	57.5	55.5	185.0	184.0
	3	9.78	3.99	57.4	55.3	185.0	184.0
	4	9.76	4.29	57.4	54.6	185.0	184.0
3	1	10.09	3.99	58.0	54.2	187.0	188.0
	2	10.05	4.09	58.1	54.8	188.0	187.0
	3	10.12	3.99	58.0	53.6	188.0	189.0
	4	10.09	3.98	58.1	55.1	187.0	187.0
4	1	10.21	4.15	54.0	56.2	185.0	184.0
	2	10.05	4.13	58.0	56.7	185.0	185.0
	3	10.08	4.23	57.3	56.8	185.0	185.0
	4	10.09	4.11	57.8	56.2	185.0	185.0
5	1	10.10	4.24	57.8	58.0	185.0	184.0
	2	10.11	4.25	57.3	54.6	186.0	185.0
	3	10.09	4.17	58.0	55.0	186.5	186.0
	4	10.15	4.02	57.8	54.7	185.5	189.0
6	1	10.04	4.19	58.0	56.1	186.5	186.0
	2	10.12	4.22	57.5	55.4	187.0	187.0
	3	10.20	4.15	57.3	55.5	186.5	186.0
	4	10.13	4.05	58.0	56.9	186.0	186.0
7	1	10.21	4.19	58.0	54.9	183.0	187.0
	2	10.20	4.04	58.0	55.3	183.5	187.0
	3	10.22	4.19	58.0	54.5	184.0	187.0
8	1	10.00	4.10	58.1	55.2	185.0	185.0
	2	9.94	4.25	58.1	54.1	185.0	185.0
	3	9.91	3.97	58.0	54.2	185.0	184.0
	4	9.94	4.03	58.1	56.5	185.0	184.0

Table A.2: Average panel dimensions before and after wood treatment for all panels hygro-thermally treated at 100% relative humidity, 160°C, and 0 psi.

Treatment Run #	Billet #	Av. Thickness (mm)		Av. Width (mm)		Length (mm)	
		before	after	before	after	before	after
A	1	10.05	7.83	58.0	56.3	186.0	185.0
	2	10.08	7.71	58.0	57.4	186.0	186.0
	3	10.08	8.66	58.0	54.2	185.0	185.0
	4	10.03	7.95	27.5	25.6	185.0	184.0
	5	10.07	8.36	26.5	26.9	184.0	184.0
	6	10.00	8.34	57.5	57.6	186.0	186.0
B	1	9.86	8.31	57.0	56.6	185.0	185.0
	2	9.99	8.79	57.9	56.0	184.5	185.0
	3	9.87	9.37	57.3	54.3	185.0	184.0
	4	9.92	8.47	57.7	55.3	184.0	184.0
	5	9.88	7.54	57.0	57.3	184.0	184.0
C	1	9.96	9.15	57.5	54.6	185.0	185.0
	2	9.96	9.29	57.0	54.2	184.0	184.0
	3	10.02	9.45	57.5	54.4	185.0	184.0
	4	9.96	8.77	57.5	53.3	184.0	184.0
	5	9.93	9.34	57.5	54.8	185.0	184.0
D	1	9.90	9.31	58.0	54.0	185.0	184.0
	2	9.93	8.67	58.0	55.7	185.5	185.0
	3	10.02	8.87	57.8	54.2	184.5	185.0
	4	9.93	9.12	57.5	53.8	184.5	184.0
	5	9.91	8.30	57.5	56.4	184.5	184.0
E	1	9.85	7.47	58.0	56.9	184.0	185.0
	2	9.75	8.99	57.0	54.0	184.0	183.0
	3	9.81	9.02	57.5	55.4	184.0	184.0
	4	9.87	8.96	57.3	53.6	184.0	184.0
	5	9.99	9.26	58.0	53.9	185.0	184.0
F	1	9.99	8.97	58.0	55.5	184.0	184.0
	2	10.00	9.26	58.0	53.3	182.0	182.0
	3	9.91	9.11	57.5	54.1	184.0	184.0
	4	9.97	9.33	58.0	54.2	185.0	182.0
	5	9.96	8.80	57.5	54.3	185.0	183.0

Appendix B
Dielectric Analysis Data

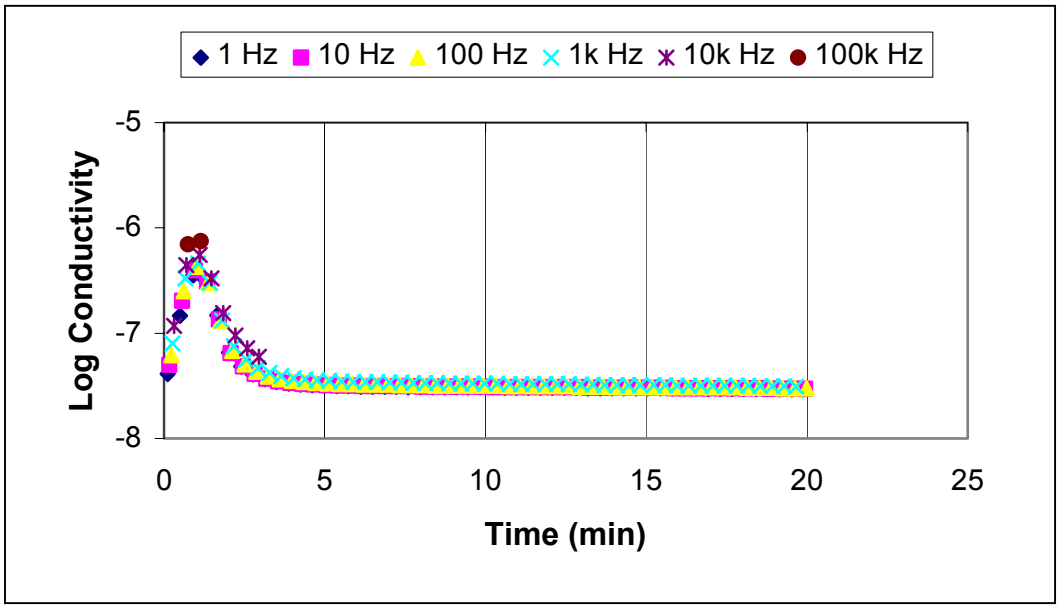

Figure B.1: Log conductivity data collected from densified wood bonded with pMDI.

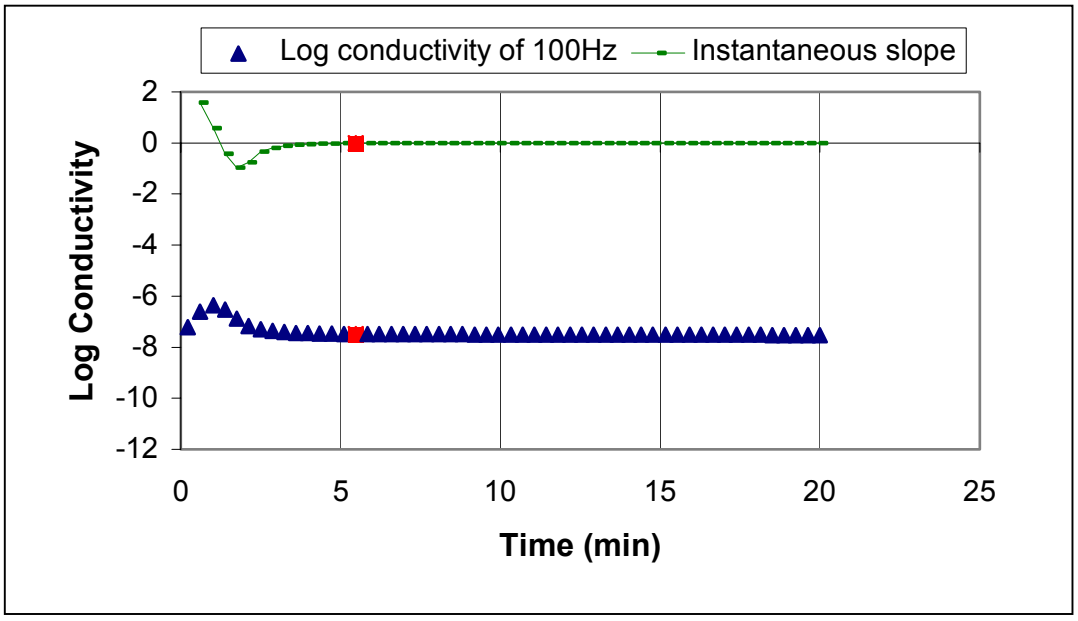

Figure B.2: Determination of press time for densified wood bonded with pMDI by using instantaneous slope of log conductivity for 100Hz.

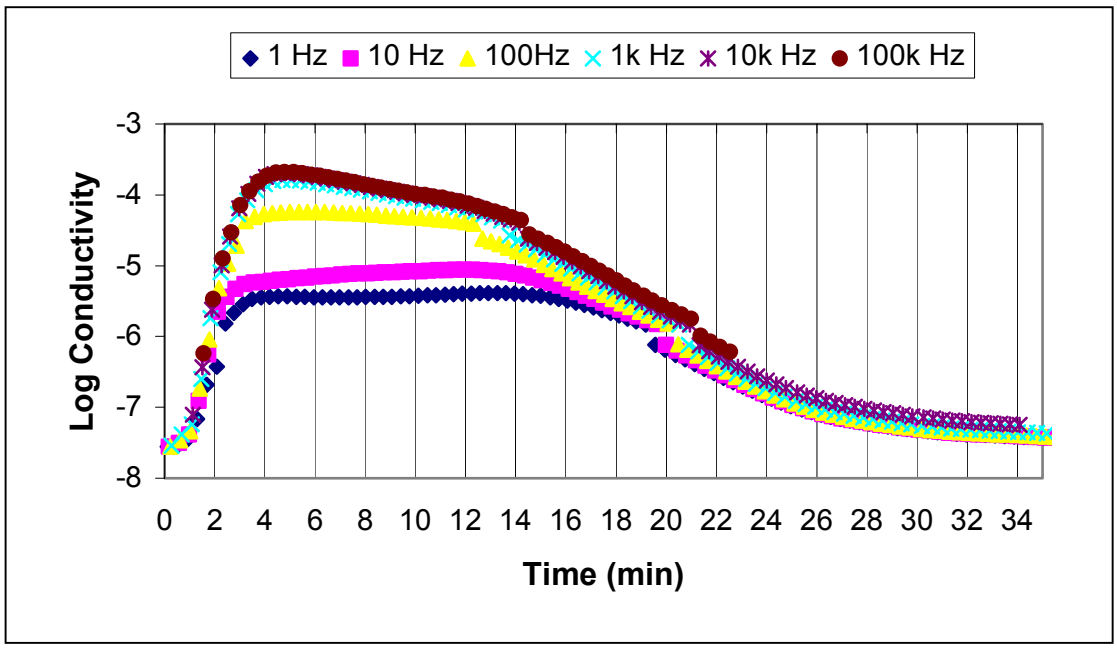

Figure B.3: Log conductivity data collected from control samples bonded with PF-film.

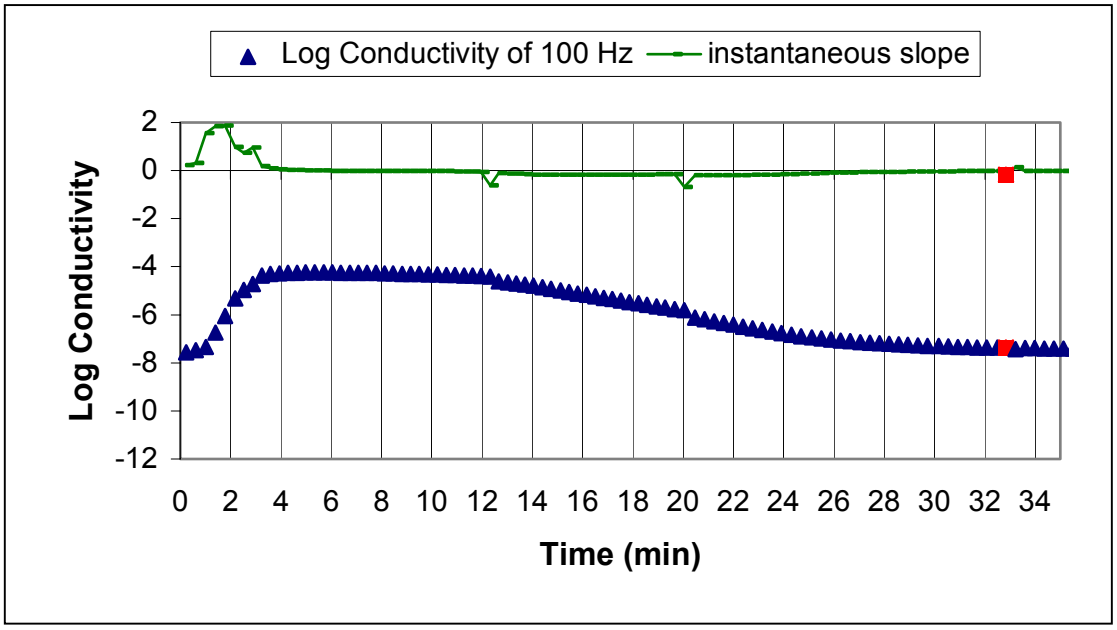

Figure B.4: Determination of press time for control samples bonded with PF-film adhesive using the instantaneous slope of log conductivity for 100Hz.

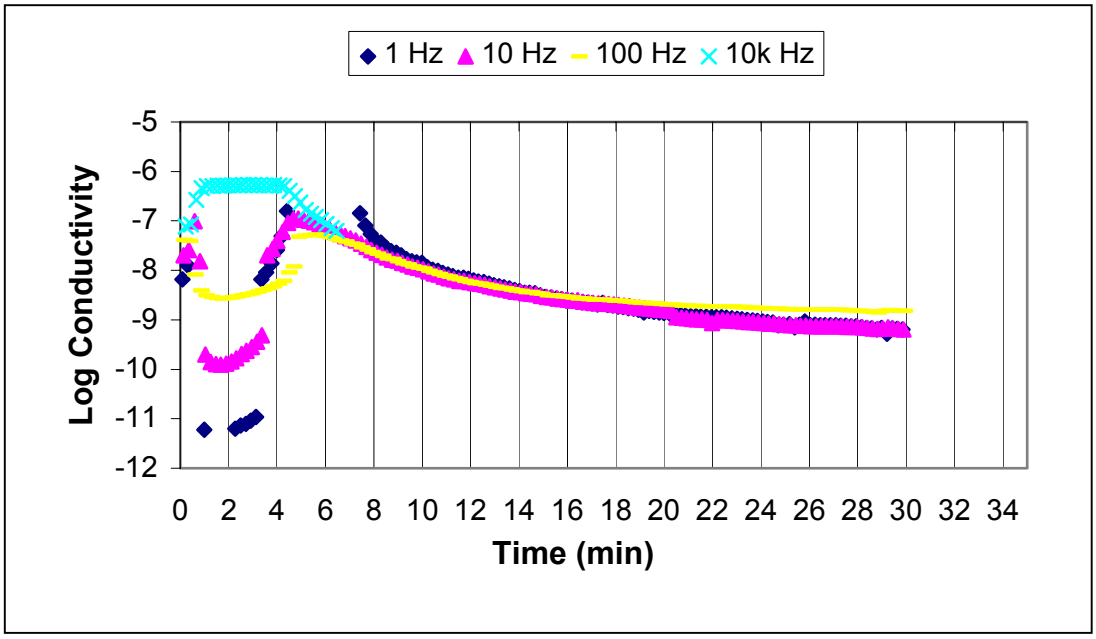

Figure B.5: Log conductivity data collected from densified samples bonded with PF-film.

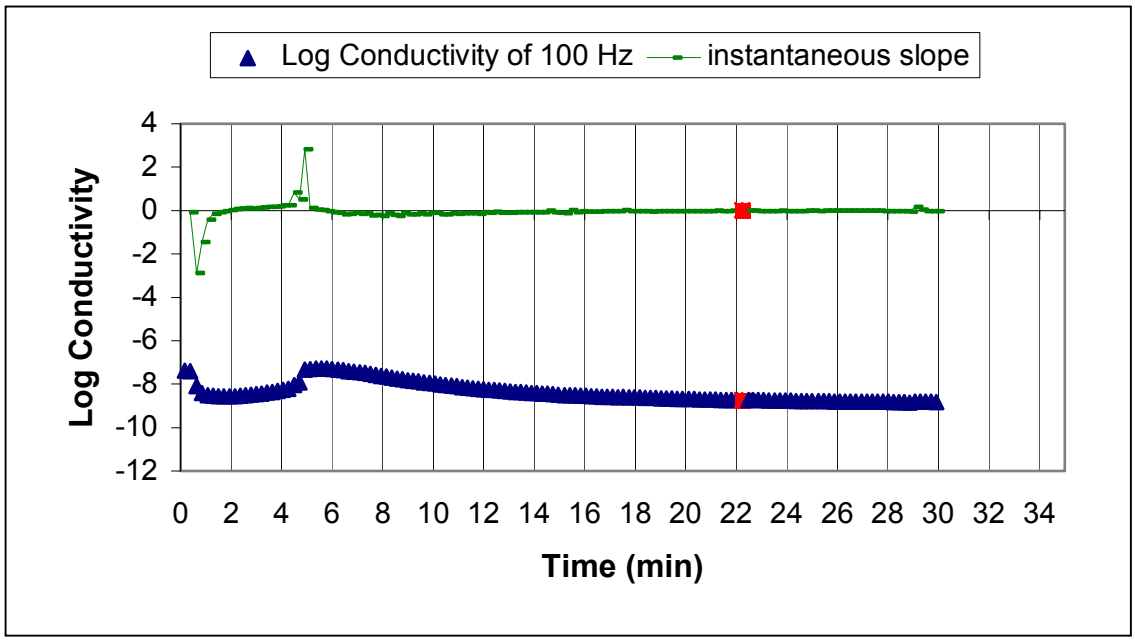

Figure B.6: Determination of press time for densified samples bonded with PF-film using instantaneous slope of log conductivity for 100Hz.

Appendix C
Fracture Toughness Data

Table C.1: SERR (J/m²) data for fracture samples bonded with PF-film.

Treatment Group	Sample #	G-max (J/m²)	G-arr (J/m²)	R² for Compliance plot
Yellow-poplar Control	1	216.7	188.5	.9978
		231.2	201.0	
		215.0	192.0	
		226.2	196.8	
		219.4	199.1	
		206.0	193.0	
		202.2	183.3	
		198.5	179.4	
		201.3	179.6	
		198.8	170.5	
		202.8	180.3	
		194.2	177.2	
		199.8	177.3	
	2	243.5	167.1	.9970
		232.5	205.9	
		224.7	192.1	
		238.2	211.9	
		225.0	196.5	
		219.0	185.6	
		217.1	192.3	
		226.6	195.4	
		216.9	195.3	
		240.8	199.6	
		258.8	213.1	
	3	245.0	223.7	.9992
		244.2	216.2	
		225.6	199.1	
		230.6	210.0	
		205.8	182.7	
		206.0	185.8	
		205.6	179.8	
		208.9	186.9	
		212.2	188.2	
		205.8	180.6	
		214.0	188.1	
		219.9	194.5	

Table C.1, cont'd: SERR (J/m²) data for fracture samples bonded with PF-film.

Treatment Group	Sample #	G-max (J/m²)	G-arr (J/m²)	R² for Compliance plot
Yellow-poplar control Continued	4	274.7	243.2	.9974
		299.6	260.0	
		307.8	270.0	
		295.7	262.5	
		298.1	260.8	
		287.6	250.4	
		309.1	270.1	
		302.6	273.2	
		310.3	275.2	
		292.5	263.0	
		295.5	262.7	
		305.3	265.3	
	5	202.7	183.0	.9983
		215.1	193.9	
		205.6	173.4	
		208.8	183.5	
		205.8	182.4	
		228.2	191.5	
		208.7	186.7	
		211.6	183.3	
		198.9	176.4	
		218.1	111.1	
		216.0	186.6	
		206.8	187.1	
		208.4	184.4	
	6	188.3	161.6	.9968
		213.0	180.9	
		217.6	183.8	
		203.5	176.3	
		216.6	185.3	
		216.1	187.4	
		219.4	196.7	
		207.4	183.6	
		204.1	181.3	
		216.0	187.1	
		208.9	186.6	
		223.5	190.7	

Table C.1, cont'd: SERR (J/m²) data for fracture samples bonded with PF-film.

Treatment Group	Sample #	G-max (J/m²)	G-arr (J/m²)	R² for Compliance plot
Hygro-thermally treated Yellow-poplar	1	518.9	489.3	.9992
		471.2	440.8	
		453.9	418.5	
		441.1	408.4	
		425.4	394.6	
		412.9	372.9	
		423.9	382.4	
		456.5	422.0	
		442.2	409.3	
		437.1	403.9	
		459.4	395.9	
	2	476.3	459.8	.9958
		480.4	448.9	
		489.3	451.2	
		474.7	445.7	
		517.7	476.5	
		495.1	461.1	
		468.9	438.0	
		401.3	377.3	
	3	450.9	429.5	.9959
		443.7	414.2	
		466.4	435.5	
		483.2	433.7	
		494.3	460.0	
		471.7	446.8	
		406.5	394.7	
		467.2	428.3	
		477.6	461.0	
		473.0	440.3	
	4	513.5	477.2	.9955
		530.4	504.1	
		479.4	467.2	
		484.6	451.6	
		500.2	459.8	
		495.3	460.5	
		474.7	453.2	
		486.2	454.1	
		510.8	443.0	
		491.5	459.3	
		560.5	498.4	

Table C.1, cont'd: SERR (J/m²) data for fracture samples bonded with PF-film.

Treatment Group	Sample #	G-max (J/m²)	G-arr (J/m²)	R² for Compliance plot
Densified Yellow-poplar	1	270.0	246.1	.9956
		248.7	234.1	
		248.4	235.2	
		252.2	234.2	
		260.0	243.7	
		229.9	218.5	
		261.7	239.0	
		260.7	247.4	
	2	222.3	206.7	.9952
		208.4	194.4	
		190.6	182.9	
		180.3	171.1	
		185.2	166.4	
		197.1	172.9	
		184.1	175.6	
	3	458.0	437.1	.9924
		450.6	427.2	
		419.9	393.8	
		392.9	363.8	
		375.1	365.2	
		320.4	312.0	
		317.6	300.6	
		323.5	301.3	
		316.8	295.8	
		311.9	289.1	
	4	328.9	310.2	.9925
		317.0	298.4	
		274.6	265.1	
		330.7	304.0	
		311.5	283.8	
		306.2	307.7	
		293.4	271.9	
		286.2	263.1	

Table C.2: SERR (J/m²) data for samples bonded with pMDI.

Treatment Group	Sample #	G-max (J/m²)	G-arr (J/m²)	R² for Compliance plot
Yellow-poplar control	1	147.1	123.4	.9961
		155.3	132.5	
		164.3	144.0	
		166.6	147.5	
		185.1	161.1	
		199.5	176.3	
		187.7	170.5	
		195.9	168.2	
		184.4	163.3	
		188.7	171.2	
		177.4	161.2	
		172.7	150.0	
		161.2	143.6	
	2	208.4	177.8	.9945
		196.2	167.2	
		199.1	165.5	
		195.8	173.6	
		199.1	175.2	
		195.7	168.9	
		190.6	177.5	
		191.6	168.7	
		169.6	154.5	
		179.7	153.2	
		169.6	152.4	
	3	228.3	189.4	.9907
		213.8	179.6	
		214.8	173.2	
		215.7	182.8	
		213.8	182.9	
		206.7	172.3	
		195.9	171.2	
		207.4	180.1	
		190.7	177.4	
		209.5	185.7	
		195.6	174.0	
	4	226.2	142.5	.9930
		204.5	183.8	
		200.0	172.7	
		176.4	158.2	
		180.8	157.8	
		177.8	161.6	
		180.5	159.5	
		182.0	161.2	
		188.7	162.8	
		200.9	168.9	
		175.6	158.0	
		172.7	155.6	

Table C.2, cont'd: SERR (J/m²) data for samples bonded with pMDI.

Treatment Group	Sample #	G-max (J/m²)	G-arr (J/m²)	R² for Compliance plot
Yellow-poplar Control Continued	5	198.5	169.8	.9883
		185.7	159.8	
		188.4	159.0	
		178.2	152.0	
		178.1	151.1	
		168.4	142.2	
		161.2	137.0	
		162.4	138.3	
		178.8	143.4	
		161.7	149.3	
		149.5	111.6	
		157.4	133.1	
		172.6	141.1	
	6	199.5	174.1	.9977
		194.6	169.3	
		187.4	165.9	
		182.9	160.7	
		190.1	159.8	
		189.4	167.4	
		173.8	155.4	
		181.3	155.7	
		197.0	172.5	
		184.4	167.5	
		184.3	167.7	
		194.9	180.9	

Table C.2, cont'd: SERR (J/m²) data for samples bonded with pMDI.

Treatment Group	Sample #	G-max (J/m²)	G-arr (J/m²)	R² for Compliance plot
Hygro-thermally treated Yellow-poplar	1	232.4	225.3	.9976
		219.7	203.0	
		203.6	194.3	
		196.8	160.3	
		181.4	178.9	
		185.7	170.5	
		184.1	172.2	
		192.4	170.2	
	2	206.9	186.2	.9927
		194.2	172.2	
		185.1	158.9	
		167.6	152.4	
		152.7	143.3	
		140.2	134.1	
		140.6	128.1	
		122.7	117.6	
		129.3	117.5	
		139.4	129.8	
		140.5	127.9	
	3	186.7	175.0	.9973
		208.7	182.0	
		188.0	171.8	
		184.7	174.2	
		166.8	153.5	
		172.7	157.1	
		179.7	158.1	
		184.1	171.4	
		189.8	174.4	
		197.5	180.3	
		207.5	186.8	
	4	148.4	135.7	.9992
		146.9	137.7	
		163.1	147.2	
		159.6	151.1	
		156.3	144.5	
		147.9	138.6	
		153.1	139.4	
		163.5	147.4	
		166.2	152.6	
		186.3	166.7	

Table C.2, cont'd: SERR (J/m²) data for samples bonded with pMDI.

Treatment Group	Sample #	G-max (J/m²)	G-arr (J/m²)	R² for Compliance plot
Hygro-thermally treated Yellow-poplar continued	5	192.0	180.0	.9956
		199.0	181.6	
		191.7	172.5	
		195.0	167.3	
		204.2	191.0	
		185.4	169.2	
		190.6	175.9	
		204.1	192.3	
		175.8	150.1	
	6	135.7	123.1	.9966
		137.6	130.7	
		135.1	127.4	
		124.7	113.6	
		117.5	112.6	
		123.1	110.7	
		121.1	110.8	
		130.0	120.2	
		137.2	123.2	
		122.6	115.2	

Table C.2, cont'd: SERR (J/m²) data for samples bonded with pMDI.

Treatment Group	Sample #	G-max (J/m²)	G-arr (J/m²)	R² for Compliance plot
Densified Yellow-poplar	1	246.7	231.3	.9970
		286.0	267.7	
		306.0	278.3	
		336.1	313.8	
		318.9	303.4	
		333.8	314.6	
		302.7	284.5	
		271.5	249.7	
		293.4	258.2	
	2	204.3	194.9	.9971
		192.9	181.2	
		216.4	194.6	
		256.6	225.6	
		301.5	278.9	
		308.1	282.7	
		257.7	261.0	
	3	349.2	312.5	.9984
		340.0	313.5	
		351.7	336.7	
		346.6	325.7	
		345.9	322.2	
		355.4	330.4	
		347.3	319.8	
		315.7	299.5	
		344.7	314.9	
		353.4	325.0	
		374.2	333.9	
		368.1	339.4	
	4	332.2	324.3	.9971
		308.8	292.7	
		310.6	287.9	
		325.0	294.4	
		328.3	298.9	
		336.4	313.5	
		314.6	305.3	
		291.6	263.6	
		294.4	282.2	

Appendix D
Bond Durability Data

Table D.1: SERR (J/m²) data for boiled samples bonded with PF-film.

Treatment Group	Sample #	G-max (J/m²)	G-arr (J/m²)	R² for Compliance plot
Yellow-poplar control	1	405.0	379.9	.9976
		398.9	362.5	
		387.2	359.1	
		397.7	348.7	
		389.1	351.3	
		309.4	282.0	
		303.2	271.3	
		318.6	281.0	
		334.3	305.8	
		323.0	295.2	
		312.5	265.1	
	2	241.5	220.2	.9965
		240.5	215.2	
		254.6	232.9	
		223.5	201.9	
		219.7	202.7	
		226.2	199.2	
		246.2	212.5	
		267.7	231.3	
		234.7	214.9	
		233.8	207.8	
		222.4	201.2	
	3	262.9	237.3	.9956
		254.0	237.5	
		262.3	233.4	
		254.6	224.1	
		269.9	242.6	
		260.8	234.0	
		253.5	223.5	
		247.4	222.5	
		254.6	228.7	
		277.8	244.1	
		265.2	233.6	
		274.9	247.8	
	4	229.5	200.9	.9984
		218.3	207.8	
		212.4	192.6	
		204.5	187.3	
		217.4	183.8	
		251.7	230.6	
		249.2	222.1	
		230.5	194.7	
		214.9	191.0	
		204.5	190.4	

Table D.1, cont'd: SERR (J/m²) data for boiled samples bonded with PF-film.

Treatment Group	Sample #	G-max (J/m²)	G-arr (J/m²)	R² for Compliance plot
Yellow-poplar control Continued	5	275.2	243.6	.9886
		229.7	217.1	
		222.5	197.4	
		254.6	226.2	
		244.1	222.3	
		234.0	210.8	
		247.7	222.3	
		251.9	227.9	
		266.4	239.0	
		256.1	227.5	
		216.9	196.7	
		226.8	200.5	
	6	238.0	217.2	.9930
		239.2	220.4	
		235.5	214.7	
		243.2	213.8	
		244.6	221.1	
		244.9	222.4	
		247.7	222.1	
		253.0	225.9	
		256.9	225.5	
		231.5	211.0	
		224.5	202.8	
		226.0	202.3	

Table D.1, cont'd: SERR (J/m²) data for boiled samples bonded with PF-film.

Treatment Group	Sample #	G-max (J/m²)	G-arr (J/m²)	R² for Compliance plot
Hygro-thermally treated Yellow-poplar	1	429.0	394.6	.9748
		380.7	370.3	
		331.4	314.1	
		339.8	300.3	
		349.5	328.3	
		334.1	298.3	
		377.1	334.7	
		382.3	357.4	
		383.1	348.5	
	2	360.4	331.7	.9904
		401.1	379.9	
		391.2	353.8	
		413.9	365.1	
		407.5	380.9	
		367.7	330.7	
		362.4	341.8	
	3	293.8	286.4	.9916
		265.7	263.3	
		246.6	226.4	
		239.0	220.3	
		300.2	272.2	
		272.8	258.4	
		299.6	255.6	
	4	255.8	239.1	.9920
		255.2	236.7	
		228.2	212.7	
		223.2	207.4	
		203.1	182.3	
		227.6	196.2	
		244.9	208.9	
		241.4	222.8	
	5	389.3	364.8	.9848
		437.5	402.3	
		419.6	388.2	
		392.0	369.4	
		369.6	334.0	
		325.3	304.6	
		361.1	337.7	

Table D.1, cont'd: SERR (J/m²) data for boiled samples bonded with PF-film.

Treatment Group	Sample #	G-max (J/m²)	G-arr (J/m²)	R² for Compliance plot
Densified Yellow-poplar	1	232.9	215.2	.9957
		248.1	230.5	
		266.6	255.6	
		248.8	239.8	
		234.0	220.7	
		213.8	205.6	
		236.5	210.0	
		246.7	204.9	
	2	305.5	292.5	.9796
		266.2	247.3	
		277.1	248.5	
		244.2	242.1	
		270.0	240.1	
		282.2	254.1	
		333.0	284.1	
		324.9	312.7	
		321.8	283.5	
	3	401.7	372.6	.9138
		390.9	349.3	
		350.0	330.9	
		321.4	309.0	
		291.4	262.5	
		301.3	260.5	
		319.8	286.6	
		403.3	356.5	
		414.4	407.7	
	4	223.7	216.2	.9986
		233.5	210.6	
		225.4	205.0	
		256.6	232.1	
		264.0	238.5	
		275.0	247.8	
		257.8	245.8	
		266.8	230.5	
		277.7	258.0	
	5	173.7	149.9	.9940
		201.3	172.9	
		226.2	198.2	
		266.8	219.6	
		307.1	283.5	
		313.8	272.9	

Table D.1, cont'd: SERR (J/m²) data for boiled samples bonded with PF-film.

Treatment Group	Sample #	G-max (J/m²)	G-arr (J/m²)	R² for Compliance plot
Densified Yellow-poplar continued	6	336.6	305.3	.9746
		298.5	275.9	
		290.4	266.2	
		342.6	297.0	
		388.0	359.9	
		408.2	375.4	
		338.2	306.7	
		341.0	308.7	
		367.8	313.4	
		319.8	291.4	

Table D.2: SERR (J/m²) data for boiled samples bonded with pMDI.

Treatment Group	Sample #	G-max (J/m²)	G-arr (J/m²)	R² for Compliance plot
Yellow-poplar control	1	182.1	163.4	.9900
		167.2	148.7	
		184.1	159.6	
		183.0	167.9	
		190.9	167.6	
		178.8	159.0	
		200.0	171.7	
		199.6	176.0	
		202.0	175.3	
		187.0	172.2	
	2	214.4	191.8	.9944
		187.7	167.5	
		203.6	176.0	
		189.0	172.1	
		176.9	158.9	
		168.5	151.7	
		179.6	161.6	
		174.5	165.8	
		180.4	162.4	
		184.6	168.9	
		152.9	141.1	
	3	105.5	86.6	.9922
		107.1	93.3	
		120.9	99.7	
		112.0	96.7	
		111.5	97.4	
		111.5	98.2	
		96.8	90.7	
		81.3	77.3	
		85.6	72.6	
		89.3	74.5	
	4	214.9	187.6	.9976
		206.1	180.1	
		192.4	178.4	
		206.9	183.6	
		196.9	177.6	
		200.6	184.8	
		199.2	176.0	
		196.5	176.9	
		197.3	178.6	
		190.3	178.3	
		196.1	170.8	

Table D.2, cont'd: SERR (J/m²) data for boiled samples bonded with pMDI.

Treatment Group	Sample #	G-max (J/m²)	G-arr (J/m²)	R² for Compliance plot
Yellow-poplar control Continued	5	177.9	161.7	.9958
		167.3	151.8	
		148.2	137.9	
		151.3	136.3	
		155.1	138.2	
		151.2	136.3	
		143.9	138.4	
		139.6	126.6	
		129.5	119.6	
		136.4	124.4	
		132.1	112.7	
		158.3	133.6	
		160.8	138.9	
	6	179.7	166.9	.9986
		164.2	148.6	
		155.2	143.0	
		150.9	135.2	
		152.4	135.0	
		152.6	133.5	
		146.1	121.7	
		148.7	132.6	
		156.6	131.8	
		162.1	145.0	
		161.6	142.2	

Table D.2, cont'd: SERR (J/m²) data for boiled samples bonded with pMDI.

Treatment Group	Sample #	G-max (J/m²)	G-arr (J/m²)	R² for Compliance plot
Hygro-thermally treated Yellow-poplar	1	67.3	41.3	.9915
		52.8	46.8	
		57.9	44.8	
	2	42.7	41.6	.9760
		43.0	40.1	
		39.4	37.1	
		29.5	27.9	
		26.5	24.3	
	3	12.8	11.9	.9602
		13.4	12.4	
		11.8	10.6	
		12.0	10.5	
	4	79.1	72.9	.9877
		79.5	73.7	
		83.7	80.8	
		68.4	66.2	
		76.8	64.5	
Treatment Group	**Sample #**	**G-max**	**G-arr**	**R² for Compliance plot**
Densified Yellow-poplar	1	324.3	306.7	.9834
		352.0	313.4	
		299.1	286.7	
		252.9	251.5	
		260.7	240.0	
		250.4	231.6	
		274.5	234.5	
		272.6	272.6	
	2	276.0	250.7	.9924
		338.7	296.5	
		349.8	323.1	
		362.7	344.1	
		436.3	380.9	
		514.3	454.9	
		544.8	490.9	
	3	156.4	133.1	.9689
		180.1	159.4	
		169.6	156.0	
		198.0	141.5	

Appendix E
Statistics for Fracture Testing

Statistical analysis of maximum Strain Energy Release Rate (SERR) for samples bonded with PF-film adhesive

The SAS System
The Mixed Procedure
Model Information

Data Set	WORK.JESSICA
Dependent Variable	G_max
Covariance Structure	Variance Components
Estimation Method	REML
Residual Variance Method	Profile
Fixed Effects SE Method	Model-Based
Degrees of Freedom Method	Containment

Class Level Information

Class	Levels	Values
Specimen	6	1 2 3 4 5 6
Treat1	2	b n
Treat2	3	c d t

Dimensions

Covariance Parameters	2
Columns in X	12
Columns in Z	31
Subjects	1
Max Obs Per Subject	303
Observations Used	303
Observations Not Used	0
Total Observations	303

Iteration History

Iteration	Evaluations	-2 Res Log Like	Criterion
0	1	3208.81291626	
1	2	2896.33206543	0.00024875
2	1	2895.99791553	0.00001684
3	1	2895.97718313	0.00000010
4	1	2895.97706694	0.00000000

Convergence criteria met.

Covariance Parameter Estimates

Cov Parm	Estimate
Speci(Treat1*Treat2)	2605.89
Residual	685.10

Fit Statistics

-2 Res Log Likelihood	2896.0
AIC (smaller is better)	2900.0
AICC (smaller is better)	2900.0
BIC (smaller is better)	2902.8

PARMS Model Likelihood Ratio Test

DF	Chi-Square	Pr > ChiSq
1	312.84	<.0001

Type 3 Tests of Fixed Effects

Effect	Num DF	Den DF	F Value	Pr > F
Treat1	1	25	3.46	0.0748
Treat2	2	25	24.13	<.0001
Treat1*Treat2	2	25	7.96	0.0021

Least Squares Means

Effect	Treat1	Treat2	Estimate	Standard Error	DF	t Value	Pr > |t|
Treat1*Treat2	b	c	259.83	21.0816	25	12.33	<.0001
Treat1*Treat2	b	d	288.84	21.1683	25	13.64	<.0001
Treat1*Treat2	b	t	329.49	23.2247	25	14.19	<.0001
Treat1*Treat2	n	c	229.69	21.0649	25	10.90	<.0001
Treat1*Treat2	n	d	281.26	25.9339	25	10.85	<.0001
Treat1*Treat2	n	t	472.67	25.8628	25	18.28	<.0001

Tests of Effect Slices

Effect	Treat1	Treat2	Num DF	Den DF	F Value	Pr > F
Treat1*Treat2	b		2	25	2.47	0.1050
Treat1*Treat2	n		2	25	27.63	<.0001
Treat1*Treat2		c	1	25	1.02	0.3215
Treat1*Treat2		d	1	25	0.05	0.8228
Treat1*Treat2		t	1	25	16.97	0.0004

Statistical analysis of the arrest SERR for samples bonded with PF-film adhesive

The SAS System
The Mixed Procedure
Model Information

Data Set	WORK.JESSICA
Dependent Variable	G_arr
Covariance Structure	Variance Components
Estimation Method	REML
Residual Variance Method	Profile
Fixed Effects SE Method	Model-Based
Degrees of Freedom Method	Containment

Class Level Information

Class	Levels	Values
Specimen	6	1 2 3 4 5 6
Treat1	2	b n
Treat2	3	c d t

Dimensions

Covariance Parameters	2
Columns in X	12
Columns in Z	31
Subjects	1
Max Obs Per Subject	303
Observations Used	303
Observations Not Used	0
Total Observations	303

Iteration History

Iteration	Evaluations	-2 Res Log Like	Criterion
0	1	3173.64681451	
1	2	2874.75516547	0.00027842
2	1	2874.38293750	0.00002052
3	1	2874.35779648	0.00000014
4	1	2874.35762824	0.00000000

Convergence criteria met.

Covariance Parameter Estimates

Cov Parm	Estimate
Speci(Treat1*Treat2)	2289.06
Residual	640.23

Fit Statistics

-2 Res Log Likelihood	2874.4
AIC (smaller is better)	2878.4
AICC (smaller is better)	2878.4
BIC (smaller is better)	2881.2

PARMS Model Likelihood Ratio Test

DF	Chi-Square	Pr > ChiSq
1	299.29	<.0001

Type 3 Tests of Fixed Effects

Effect	Num DF	Den DF	F Value	Pr > F
Treat1	1	25	3.83	0.0616
Treat2	2	25	26.45	<.0001
Treat1*Treat2	2	25	8.22	0.0018

Least Squares Means

Effect	Treat1	Treat2	Estimate	Standard Error	DF	t Value	Pr > |t|
Treat1*Treat2	b	c	233.53	19.7729	25	11.81	<.0001
Treat1*Treat2	b	d	262.49	19.8593	25	13.22	<.0001
Treat1*Treat2	b	t	303.68	21.7906	25	13.94	<.0001
Treat1*Treat2	n	c	200.28	19.7562	25	10.14	<.0001
Treat1*Treat2	n	d	264.07	24.3306	25	10.85	<.0001
Treat1*Treat2	n	t	439.48	24.2598	25	18.12	<.0001

Tests of Effect Slices

Effect	Treat1	Treat2	Num DF	Den DF	F Value	Pr >
Treat1*Treat2	b		2	25	2.85	0.0768
Treat1*Treat2	n		2	25	29.83	<.0001
Treat1*Treat2		c	1	25	1.41	0.2454
Treat1*Treat2		d	1	25	0.00	0.9601
Treat1*Treat2		t	1	25	17.34	0.0003

Statistical analysis of the arrest SERR for samples bonded with pMDI adhesive

The SAS System
The Mixed Procedure
Model Information

Data Set	WORK.JESSICA
Dependent Variable	G_arr
Covariance Structure	Variance Components
Estimation Method	REML
Residual Variance Method	Profile
Fixed Effects SE Method	Model-Based
Degrees of Freedom Method	Containment

Class Level Information

Class	Levels	Values
Specimen	6	1 2 3 4 5 6
Treat1	2	b n
Treat2	3	c d t

Dimensions

Covariance Parameters	2
Columns in X	12
Columns in Z	29
Subjects	1
Max Obs Per Subject	270
Observations Used	270
Observations Not Used	0
Total Observations	270

Iteration History

Iteration	Evaluations	-2 Res Log Like	Criterion
0	1	2677.28761020	
1	2	2455.24347682	0.00350932
2	1	2450.85174142	0.00127070
3	1	2449.32446506	0.00026774
4	1	2449.02420611	0.00001780
5	1	2449.00590771	0.00000010
6	1	2449.00580895	0.00000000

Convergence criteria met.

Covariance Parameter Estimates

Cov Parm	Estimate
Speci(Treat1*Treat2)	1592.84
Residual	422.91

Fit Statistics

-2 Res Log Likelihood	2449.0
AIC (smaller is better)	2453.0
AICC (smaller is better)	2453.1
BIC (smaller is better)	2455.7

PARMS Model Likelihood Ratio Test

DF	Chi-Square	Pr > ChiSq
1	228.28	<.0001

Type 3 Tests of Fixed Effects

Effect	Num DF	Den DF	F Value	Pr > F
Treat1	1	23	10.83	0.0032
Treat2	2	23	36.52	<.0001
Treat1*Treat2	2	23	4.55	0.0216

Least Squares Means

Effect	Treat1	Treat2	Estimate	Standard Error	DF	t Value	Pr > |t|
Treat1*Treat2	b	c	145.69	16.4903	23	8.84	<.0001
Treat1*Treat2	b	d	260.23	23.5621	23	11.04	<.000
Treat1*Treat2	b	t	40.4265	20.5942	23	1.96	0.0619
Treat1*Treat2	n	c	162.33	16.4734	23	9.85	<.0001
Treat1*Treat2	n	d	282.14	20.2497	23	13.93	<.0001
Treat1*Treat2	n	t	156.39	16.5145	23	9.47	<.0001

Tests of Effect Slices

Effect	Treat1	Treat2	Num DF	Den DF	F Value	Pr >
Treat1*Treat2	b		2	23	24.77	<.0001
Treat1*Treat2	n		2	23	13.83	0.0001
Treat1*Treat2		c	1	23	0.51	0.4826
Treat1*Treat2		d	1	23	0.50	0.4876
Treat1*Treat2		t	1	23	19.30	0.0002

Statistical analysis of the arrest SERR for samples bonded with pMDI adhesive

The SAS System
The Mixed Procedure
Model Information

Data Set	WORK.JESSICA
Dependent Variable	G_max
Covariance Structure	Variance Components
Estimation Method	REML
Residual Variance Method	Profile
Fixed Effects SE Method	Model-Based
Degrees of Freedom Method	Containment

Class Level Information

Class	Levels	Values
Specimen	6	1 2 3 4 5 6
Treat1	2	b n
Treat2	3	c d t

Dimensions

Covariance Parameters	2
Columns in X	12
Columns in Z	29
Subjects	1
Max Obs Per Subject	270
Observations Used	270
Observations Not Used	0
Total Observations	270

Iteration History

Iteration	Evaluations	-2 Res Log Like	Criterion
0	1	2724.69569470	
1	2	2511.52912267	0.00275973
2	1	2508.00163970	0.00090785
3	1	2506.89348319	0.00015650
4	1	2506.71656042	0.00000675
5	1	2506.70953129	0.00000002
6	1	2506.70951582	0.00000000

Convergence criteria met.

Covariance Parameter Estimates

Cov Parm	Estimate
Speci(Treat1*Treat2)	1818.69
Residual	530.41

Fit Statistics

-2 Res Log Likelihood	2506.7
AIC (smaller is better)	2510.7
AICC (smaller is better)	2510.8
BIC (smaller is better)	2513.4

PARMS Model Likelihood Ratio Test

DF	Chi-Square	Pr > ChiSq
1	217.99	<.0001

Type 3 Tests of Fixed Effects

Effect	Num DF	Den DF	F Value	Pr > F
Treat1	1	23	10.42	0.0037
Treat2	2	23	37.32	<.0001
Treat1*Treat2	2	23	4.53	0.0219

Least Squares Means

Effect	Treat1	Treat2	Estimate	Standard Error	DF	t Value	Pr > |t|
Treat1*Treat2	b	c	163.29	17.6412	23	9.26	<.0001
Treat1*Treat2	b	d	289.45	25.2310	23	11.47	<.0001
Treat1*Treat2	b	t	46.3863	22.0718	23	2.10	0.0467
Treat1*Treat2	n	c	187.35	17.6215	23	10.63	<.0001
Treat1*Treat2	n	d	303.41	21.6685	23	14.00	<.0001
Treat1*Treat2	n	t	170.67	17.6696	23	9.66	<.0001

Tests of Effect Slices

Effect	Treat1	Treat2	Num DF	Den DF	F Value	Pr > F
Treat1*Treat2	b		2	23	26.40	<.0001
Treat1*Treat2	n		2	23	12.59	0.0002
Treat1*Treat2		c	1	23	0.93	0.3445
Treat1*Treat2		d	1	23	0.18	0.6786
Treat1*Treat2		t	1	23	19.32	0.0002

Appendix F
Failed PF-film Fracture Surface Photos
(Reflected Light Microscope)

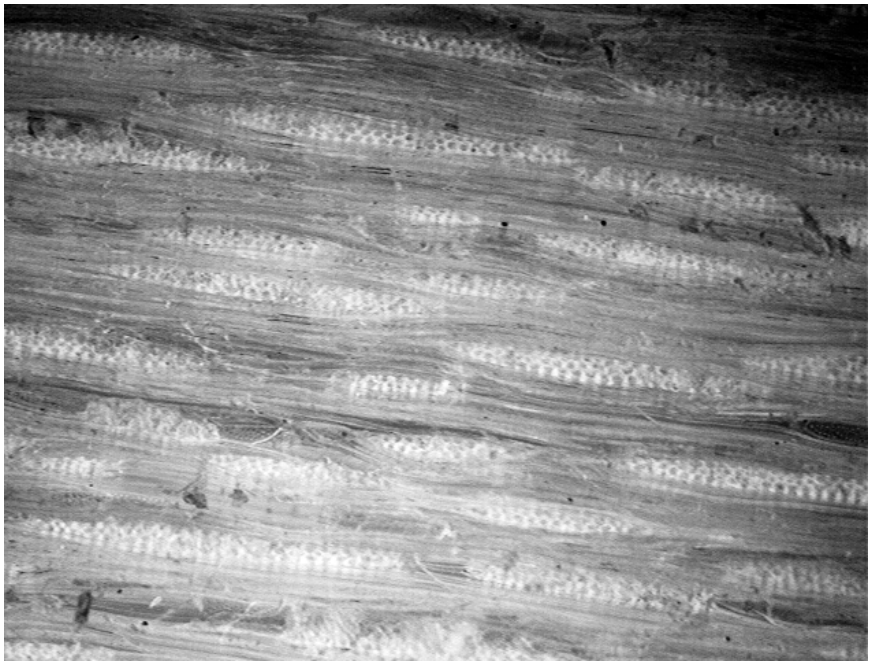

Figure F.1: Image 1 of non-bonded control yellow-poplar (taken @ 5x, 1626 x 1235 μm field of view).

Figure F.2: Image 2 of non-bonded control yellow-poplar (taken @ 5x, 1626 x 1235 μm field of view).

Figure F.3: Image 1 of non-bonded hygro-thermally treated yellow-poplar (taken @ 5x, 1626 x 1235 μm field of view).

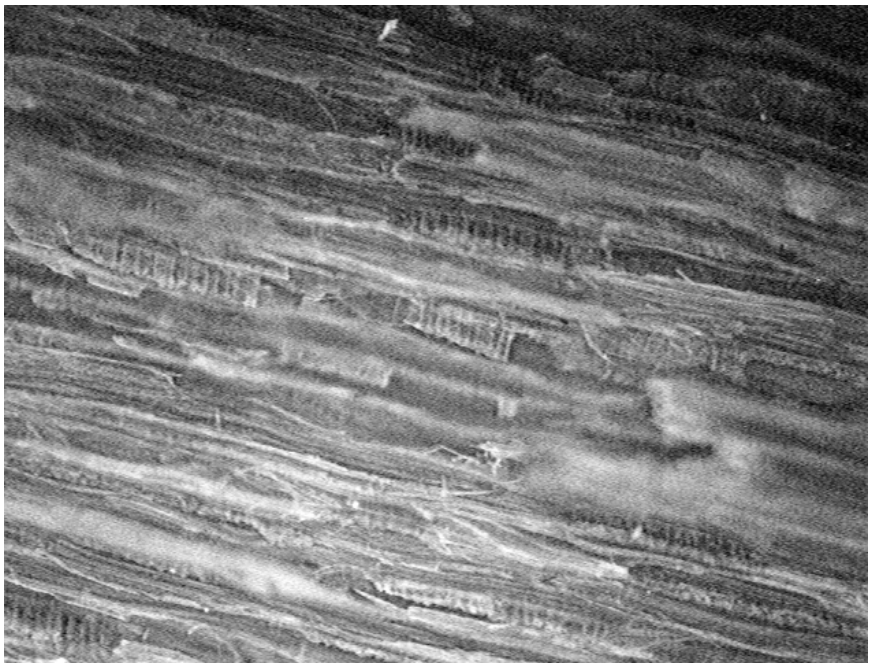

Figure F.4: Image 2 of non-bonded hygro-thermally treated yellow-poplar (taken @ 5x, 1626 x 1235 μm field of view).

Figure F.5: Image 1 of non-bonded densified yellow-poplar (taken @ 5x, 1626 x 1235 μm field of view).

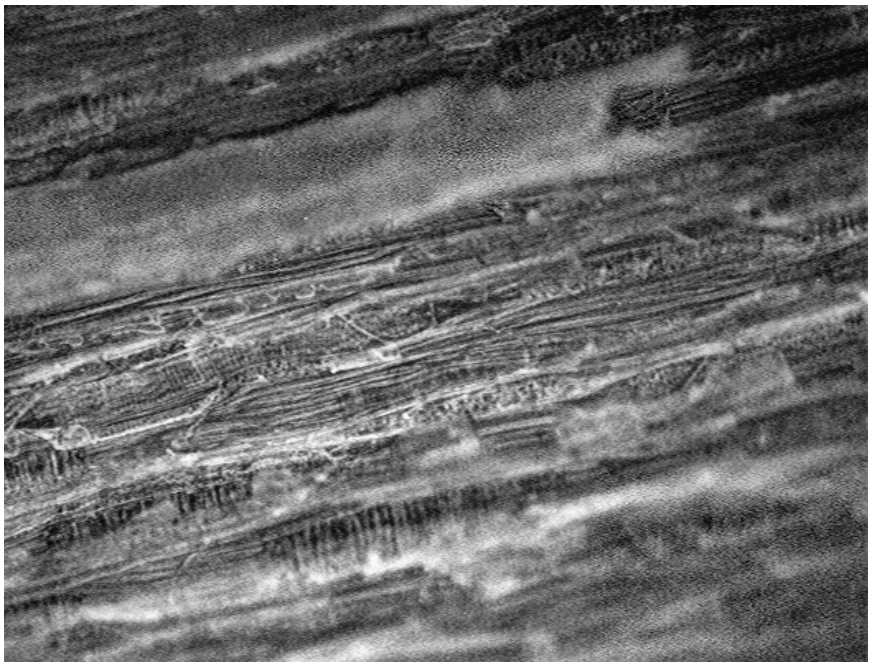

Figure F.6: Image 2 of non-bonded densified yellow-poplar (taken @ 5x, 1626 x 1235 μm field of view).

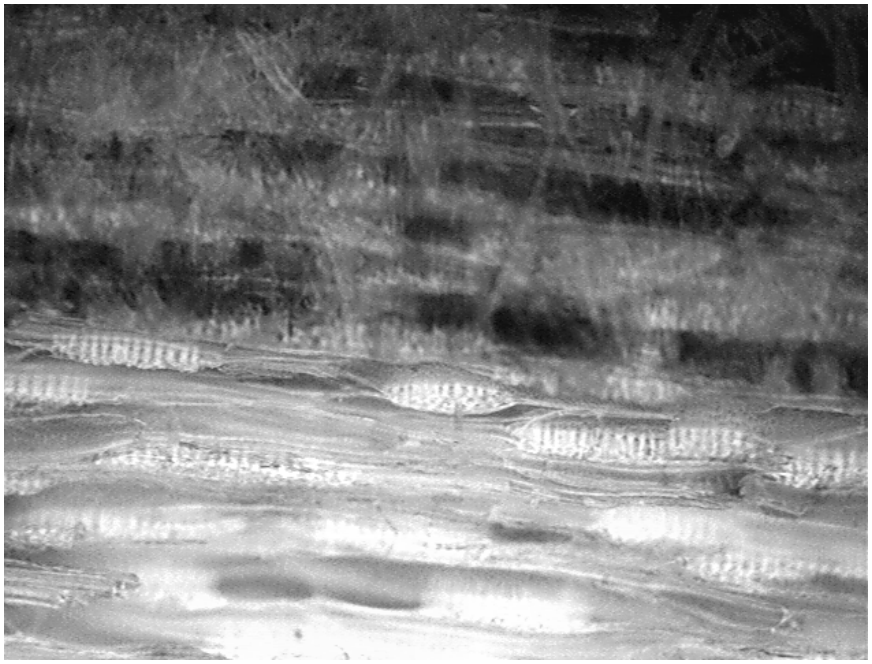

Figure F.7: Image 1 of a PF-film bonded control sample (taken @ 5x, 1626 x 1235 μm field of view).

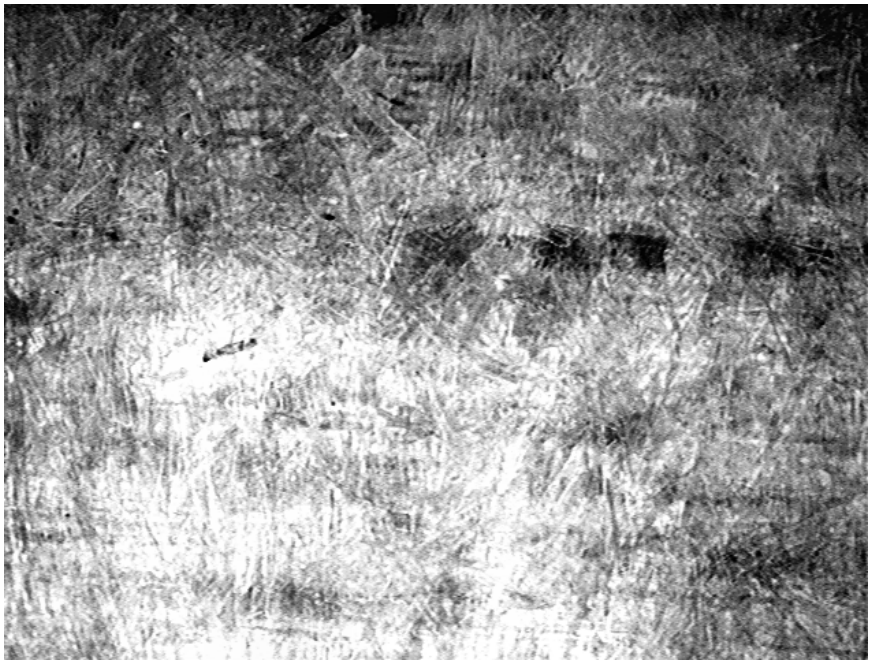

Figure F.8: Image 2 of a PF-film bonded control sample (taken @ 5x, 1626 x 1235 μm field of view).

Figure F.9: Image 1 of a PF-film bonded hygro-thermal treated sample (taken @ 5x, 1626 x 1235 μm field of view).

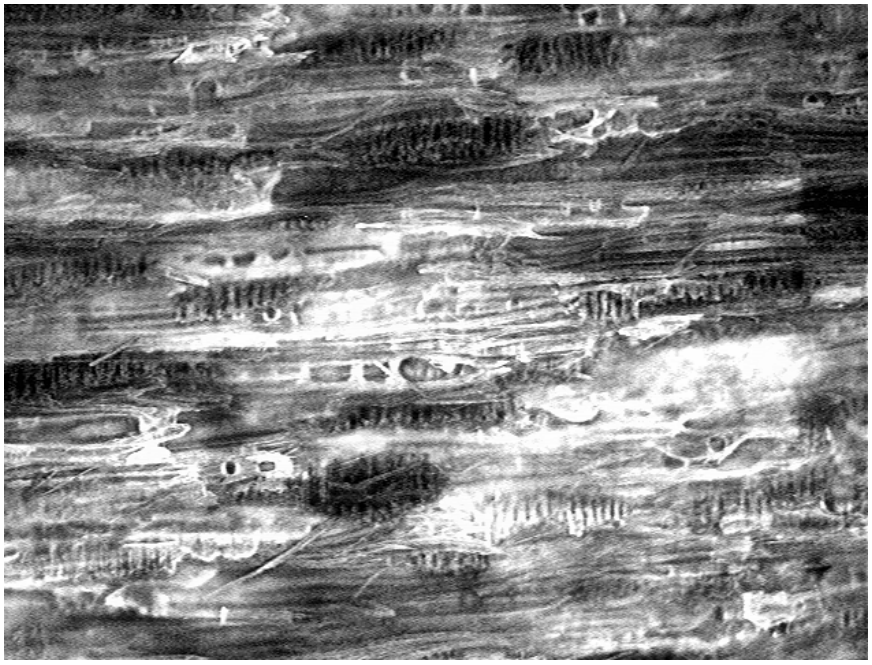

Figure F.10: Image 2 of a PF-film bonded hygro-thermal treated sample (taken @ 5x, 1626 x 1235 μm field of view).

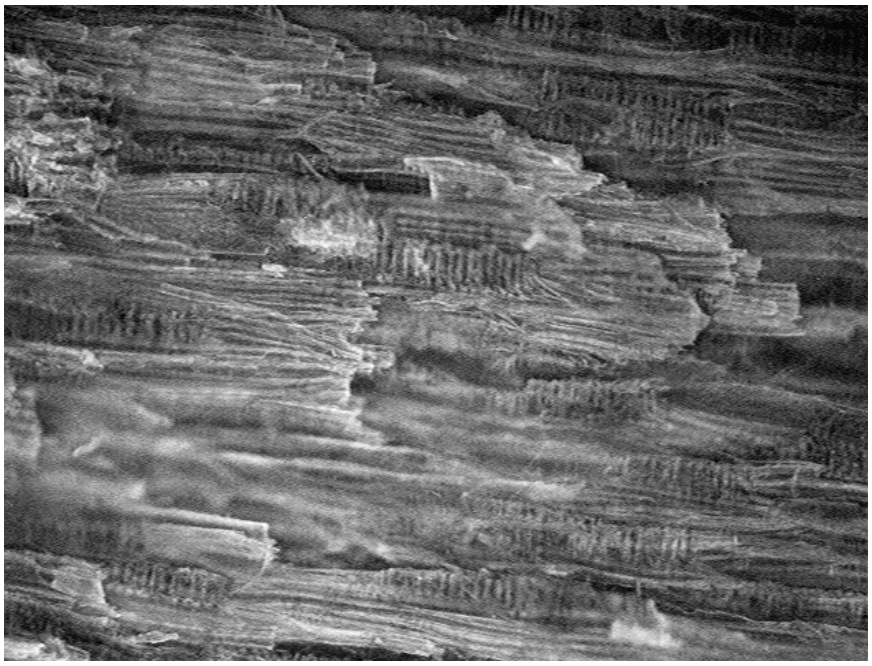

Figure F.11: Image 3 of a PF-film bonded hygro-thermal treated sample (taken @ 5x, 1626 x 1235 μm field of view).

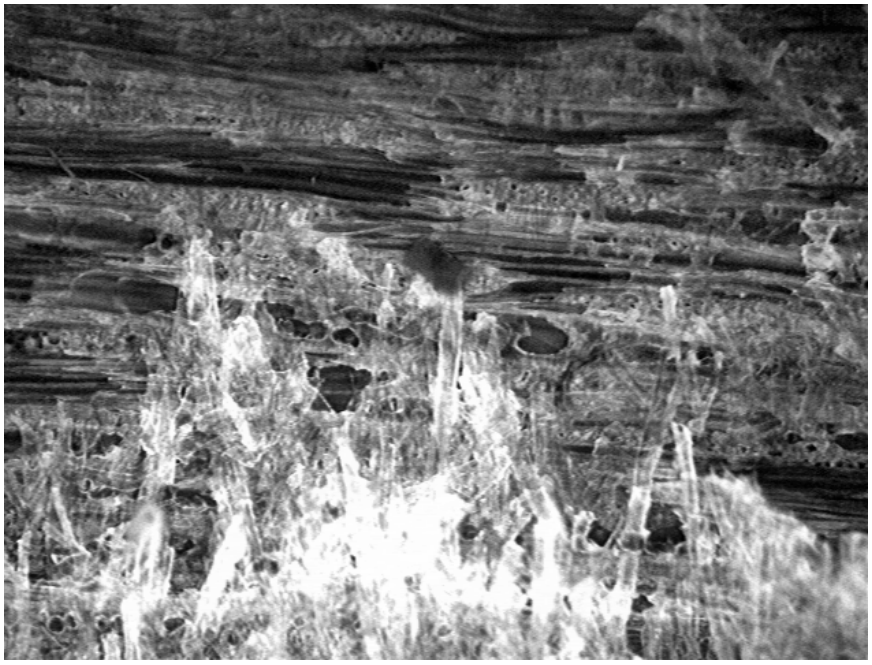

Figure F.12: Image 4 of a PF-film bonded hygro-thermal treated sample (taken @ 5x, 1626 x 1235 μm field of view).

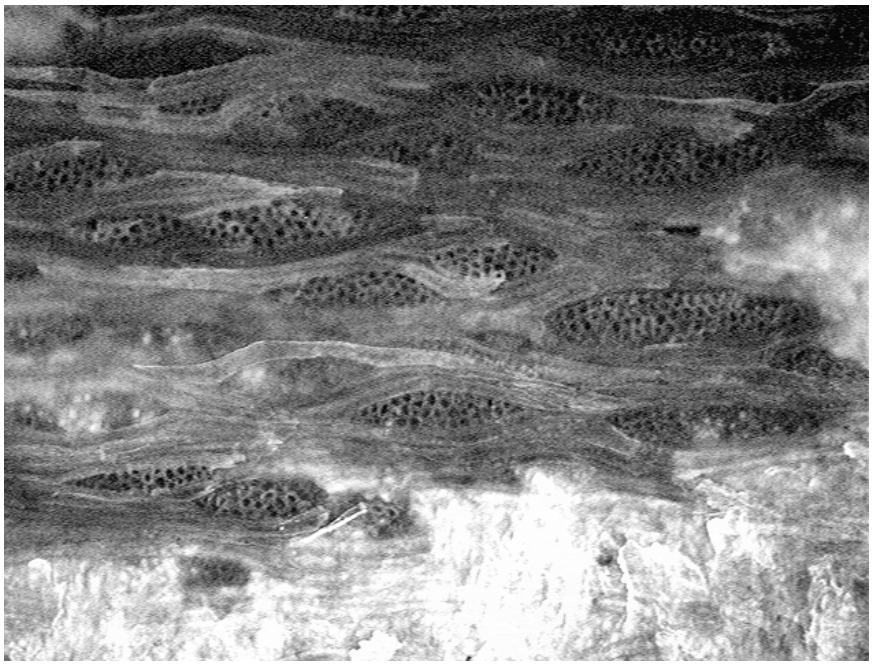

Figure F.13: Image 1 of a PF-film bonded densified sample (taken @ 5x, 1626 x 1235 μm field of view).

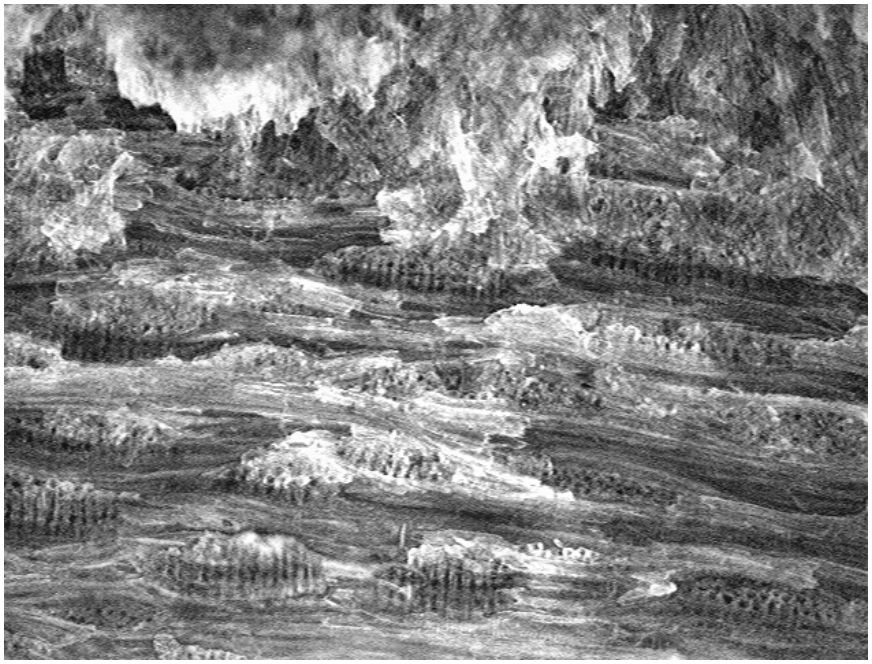

Figure F.14: : Image 2 of a PF-film bonded densified sample (taken @ 5x, 1626 x 1235 μm field of view).

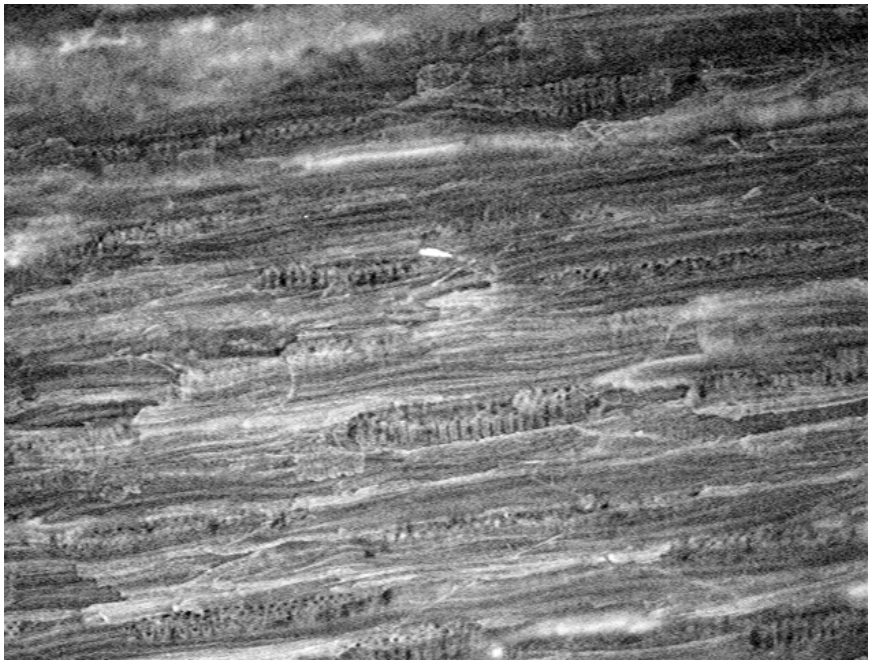

Figure F.15: : Image 3 of a PF-film bonded densified sample (taken @ 5x, 1626 x 1235 μm field of view).

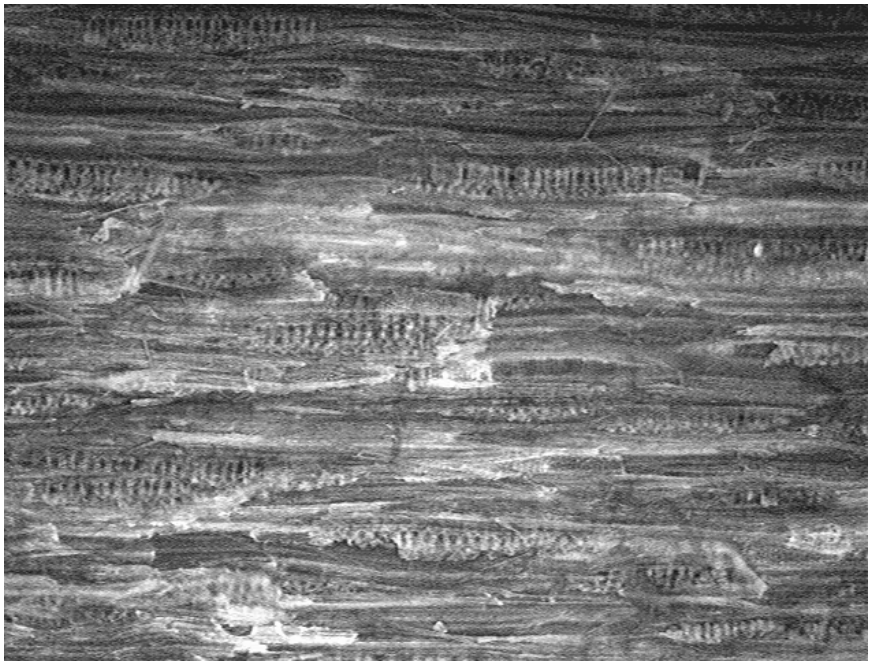

Figure F.16: : Image 4 of a PF-film bonded densified sample (taken @ 5x, 1626 x 1235 μm field of view).

Figure F.17: : Image 5 of a PF-film bonded densified sample (taken @ 5x, 1626 x 1235 μm field of view).

Figure F.18: : Image 6 of a PF-film bonded densified sample (taken @ 5x, 1626 x 1235 μm field of view).

Appendix G
Failed pMDI Fracture Surface Photos
(Reflected Light Microscope)

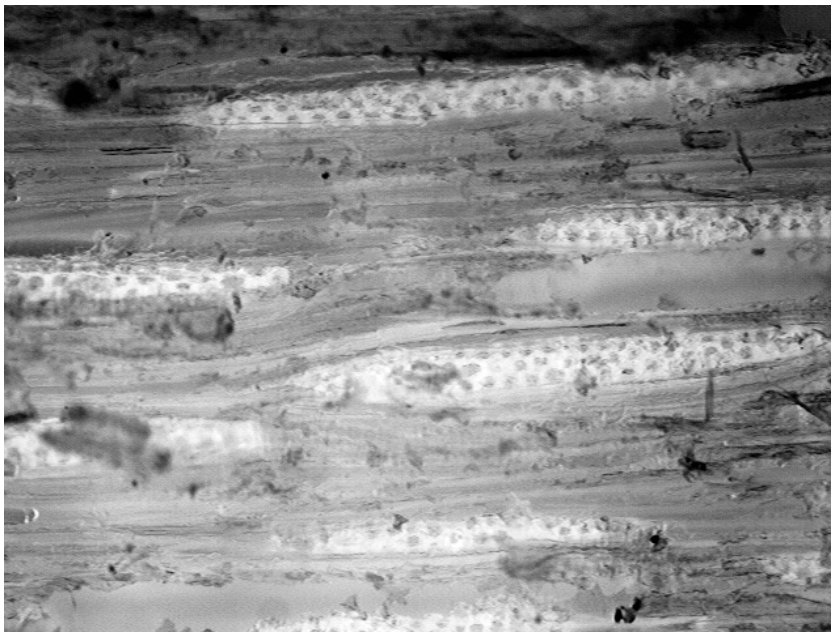

Figure G.1: Image 1 of a pMDI bonded control sample (taken @ 10x, 827 x 628 μm field of view).

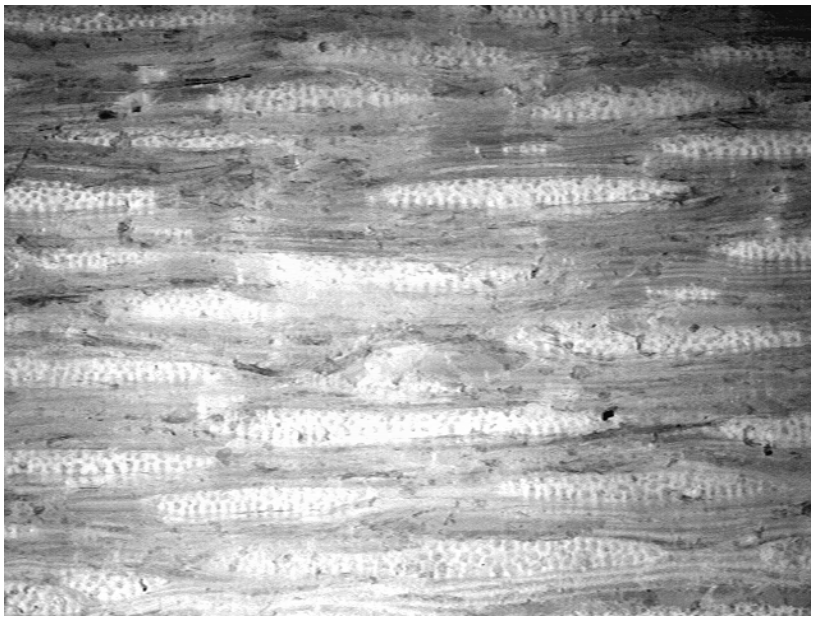

Figure G.2: Image 2 of a pMDI bonded control sample (taken @ 5x, 1626 x 1235 μm field of view).

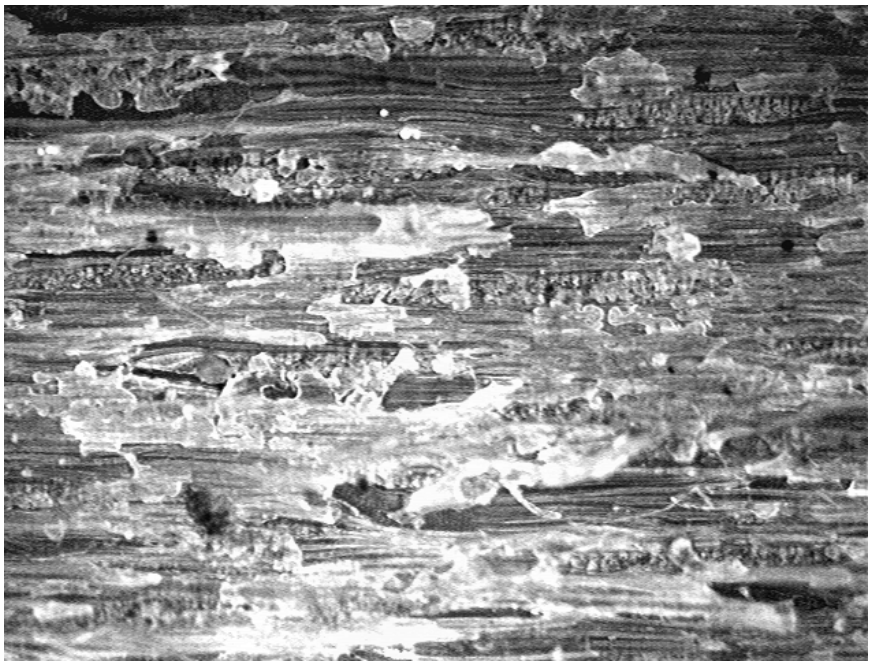

Figure G.3: Image 1 of a pMDI bonded hygro-thermal treated sample (taken @ 5x, 1626 x 1235 μm field of view).

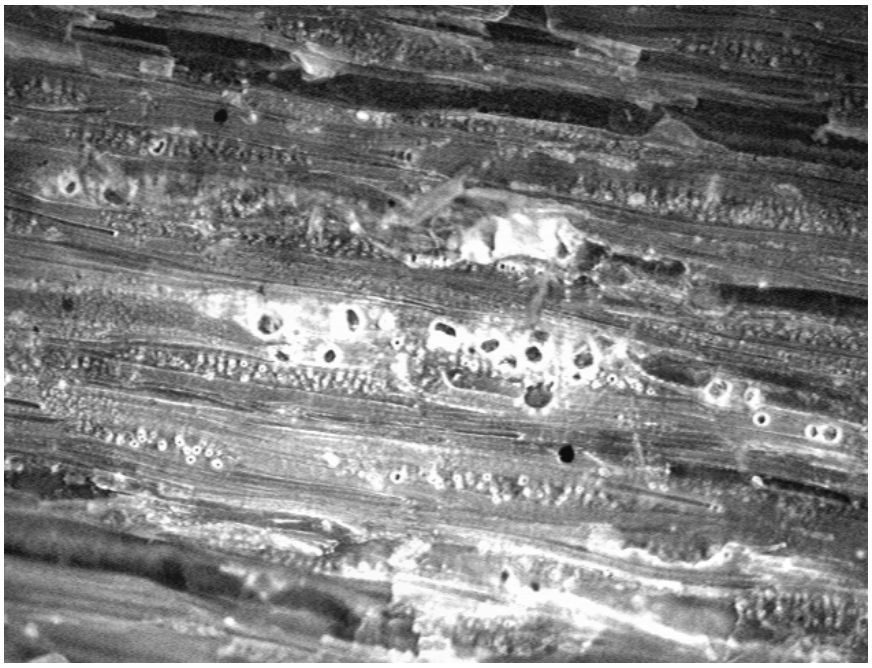

Figure G.4: Image 2 of a pMDI bonded hygro-thermal treated sample (taken @ 5x, 1626 x 1235 μm field of view).

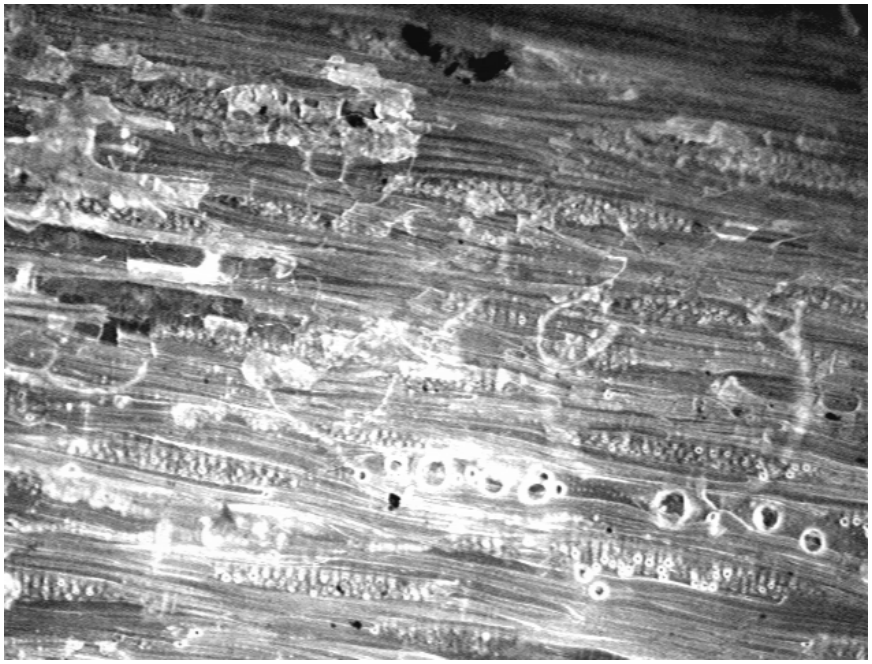

Figure G.5: Image 3 of a pMDI bonded hygro-thermal treated sample (taken @ 5x, 1626 x 1235 μm field of view).

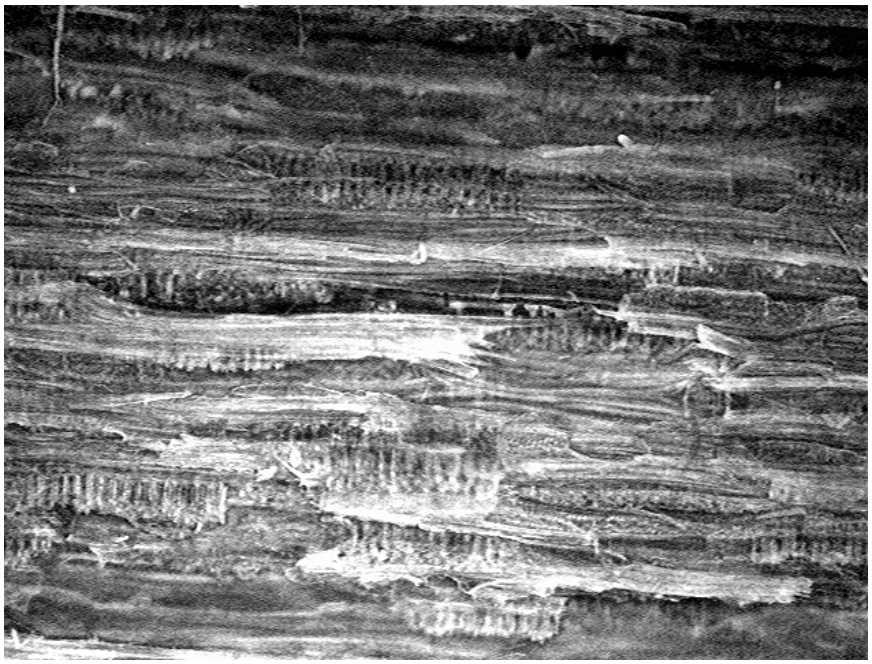

Figure G.6: Image 1 of a pMDI bonded densified sample (taken @ 5x, 1626 x 1235 μm field of view).

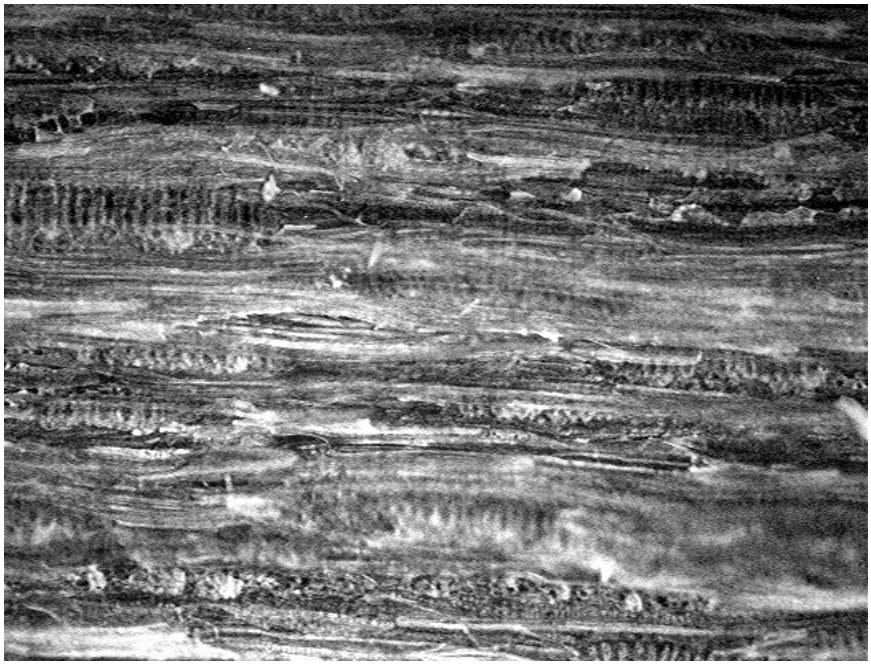

Figure G.7: Image 2 of a pMDI bonded densified sample (taken @ 5x, 1626 x 1235 μm field of view).

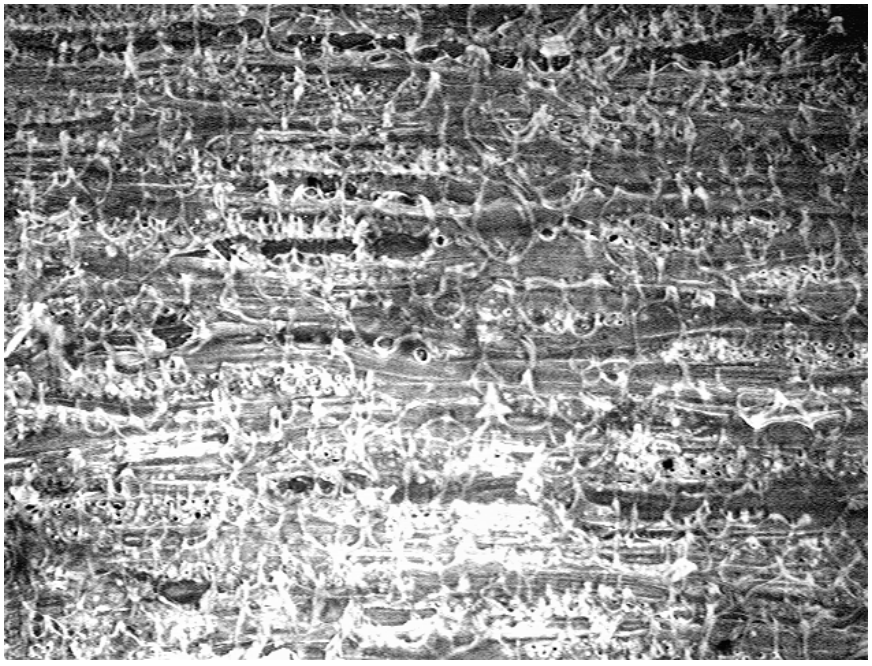

Figure G.8: Image 3 of a pMDI bonded densified sample (taken @ 5x, 1626 x 1235 μm field of view).

Appendix H
Boiled Fracture Sample Dimensions Data

Table H.1: Dimension data for boiled fracture samples bonded with PF-film and pMDI adhesives before and after boiling.

Sample Type	Sample #	Av. Thickness		Av. Width		Length	
		before	after	before	after	before	after
Control bonded with PF-Film	1	18.0	17.5	20	20	188	187
	2	18.0	17.6	20	20	188	187
	3	18.0	17.6	20	20	188	187
	4	18.0	17.7	20	20	188	187
	5	18.0	17.6	20	20	190	189
	6	18.0	17.6	20	20	188	188
Control bonded with pMDI	1	18.0	17.5	20	20	188	188
	2	17.5	17.4	20	19	188	188
	3	18.0	17.5	20	19	188	187
	4	17.5	17.4	20	20	188	188
	5	17.5	17.4	20	20	189	190
	6	18.0	17.5	20	20	188	187
Hygro-thermal bonded with PF-Film	1	12.0	13.0	21	20	183	182
	2	12.0	13.4	20	20	183	182
	3	12.0	13.0	20	19	183	182
	4	12.0	13.0	20	20	183	181
	5	12.0	13.1	20	19	183	181
	6	12.0	12.7	20	19	183	182
Hygro-thermal bonded with pMDI	1	12.5	14.7	20	19	183	182
	2	12.5	14.2	20	19	183	183
	3	13.0	15.1	20	19	183	182
	4	13.0	15.3	21	19	182	181
	5	12.0	14.3	20	19	183	182
	6	13.0	14.3	20	19	183	182
Densified bonded with PF-Film	1	7.0	7.2	20	20	180	180
	2	7.0	7.4	20	19	183	182
	3	7.0	7.4	20	19	178	178
	4	7.0	7.4	20	20	178	178
	5	7.0	7.5	20	20	180	179
	6	7.0	7.4	20	19	180	179
Densified bonded with pMDI	1	7.0	7.7	20	19	181	179
	2	7.0	8.4	20	19	176	175
	3	7.0	8.1	20	19	183	182
	4	7.0	7.4	17	16	184	184
	5	8.5	8.8	20	19	178	176
	6	9.0	8.3	20	19	183	182

Appendix I
Failed PF-film Durability Fracture Surface Photos (Reflected Light Microscope)

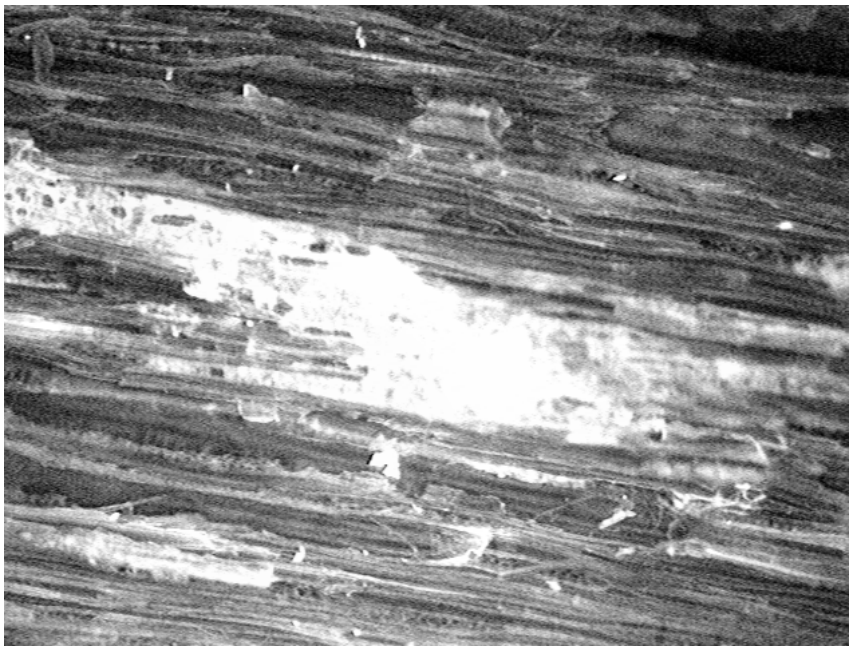

Figure I.1: Image 1 of a boiled PF-film bonded hygro-thermal treated sample (taken @ 5x, 1626 x 1235 μm field of view).

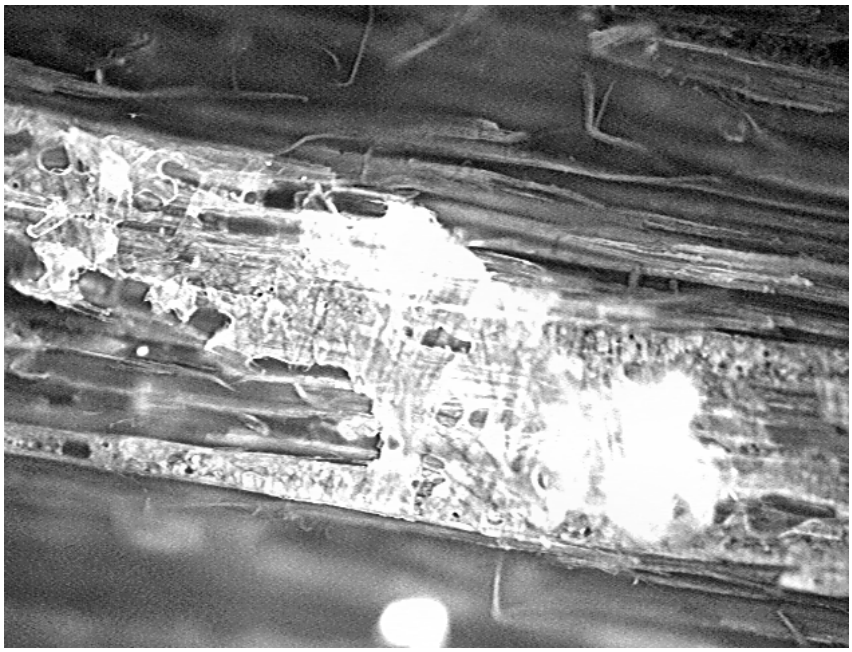

Figure I.2: Image 2 of a boiled PF-film bonded hygro-thermal treated sample (taken @ 10x, 827 x 628 μm field of view).

Figure I.3: Image 3 of a boiled PF-film bonded hygro-thermal treated sample (taken @ 10x, 827 x 628 μm field of view).

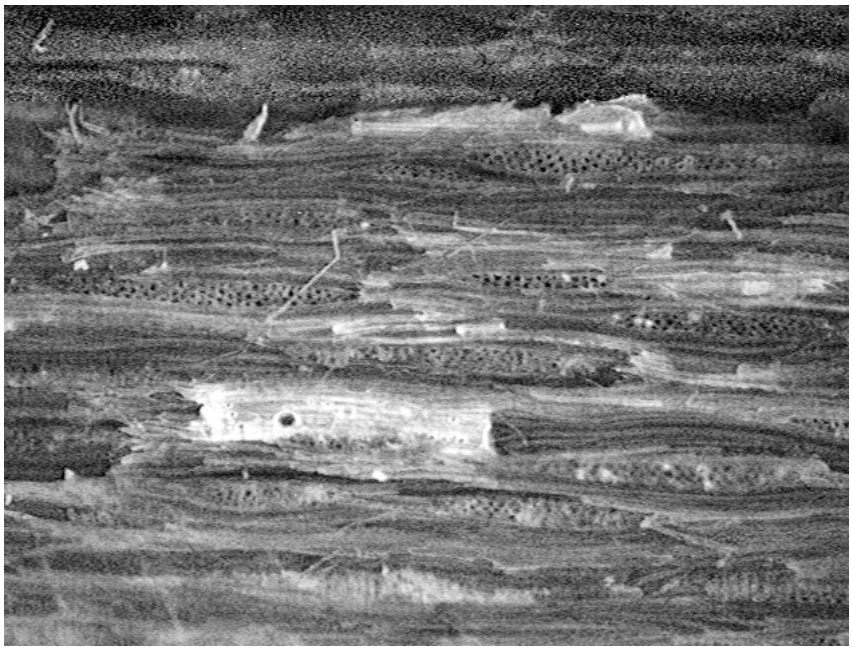

Figure I.4: Image 1 of a boiled PF-film bonded densified sample (taken @ 5x, 1626 x 1235 μm field of view).

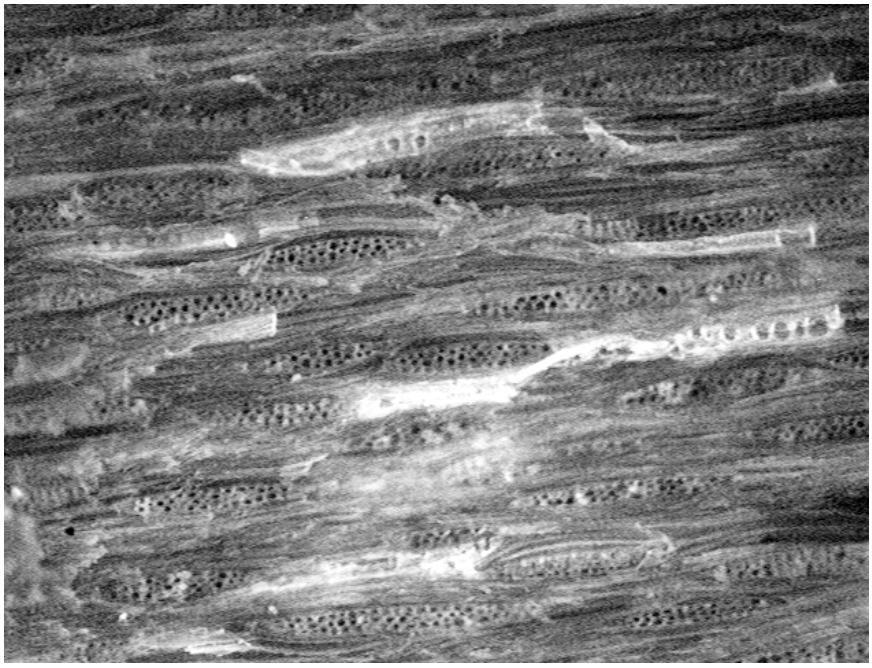

Figure I.5: Image 2 of a boiled PF-film bonded densified sample (taken @ 5x, 1626 x 1235 μm field of view).

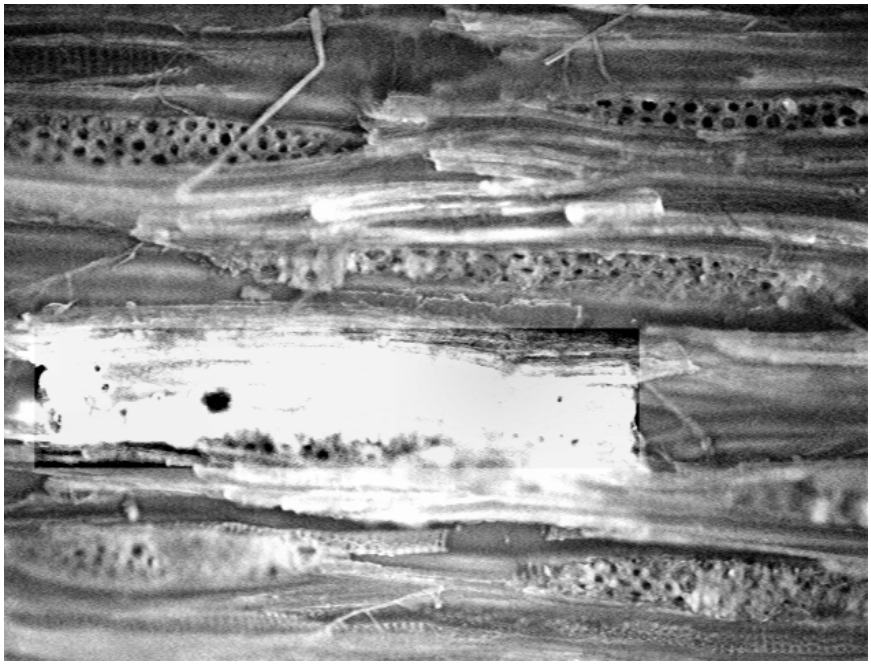

Figure I.6: *Image 3 of a boiled PF-film bonded densified sample (taken @ 10x, 827 x 628 μm field of view).*

Appendix J
Failed pMDI Durability Fracture Surface Photos (Reflected Light Microscope)

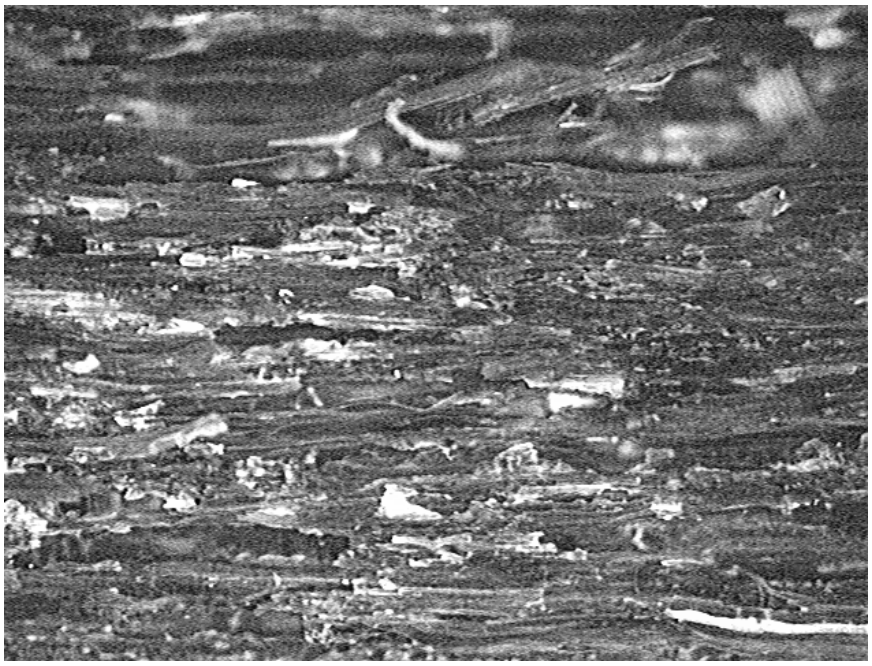

Figure J.1: Image 1 of a boiled pMDI bonded hygro-thermal treated sample (taken @ 5x, 1626 x 1235 μm field of view).

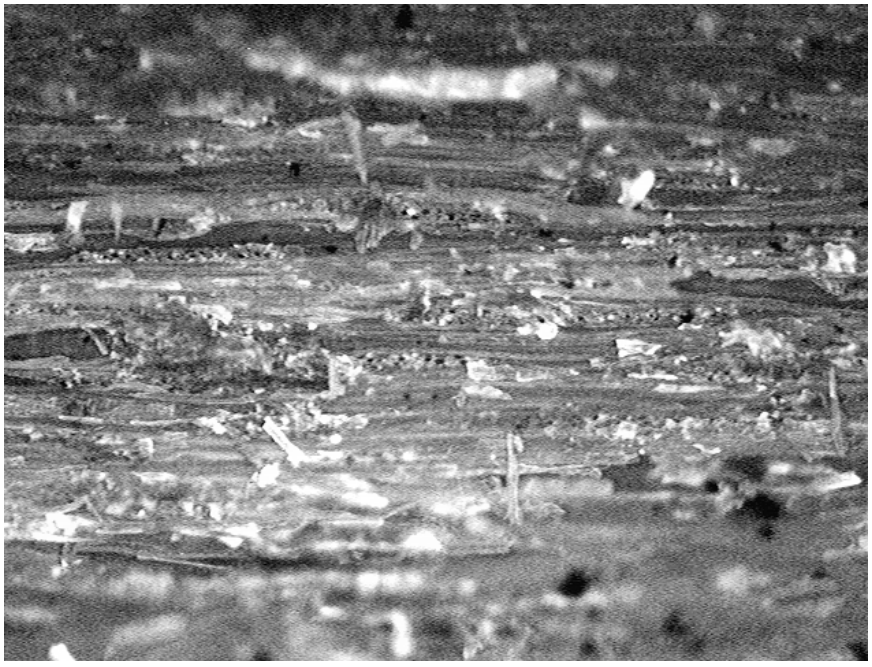

Figure J.2: Image 2 of a boiled pMDI bonded hygro-thermal treated sample (taken @ 5x, 1626 x 1235 μm field of view).

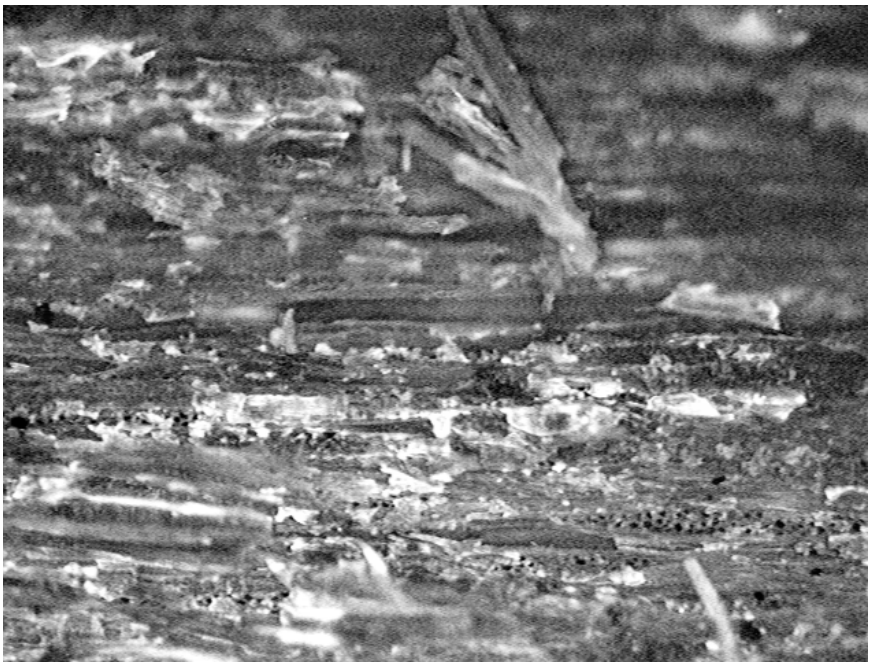

Figure J.3: Image 3 of a boiled pMDI bonded hygro-thermal treated sample (taken @ 5x, 1626 x 1235 μm field of view).

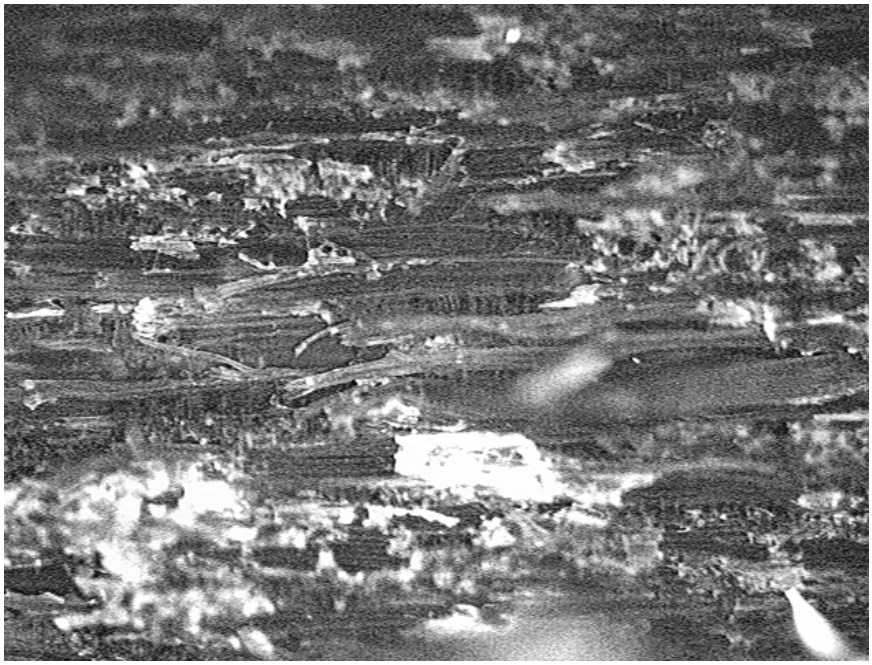

Figure J.4: Image 4 of a boiled pMDI bonded hygro-thermal treated sample (taken @ 5x, 1626 x 1235 μm field of view).

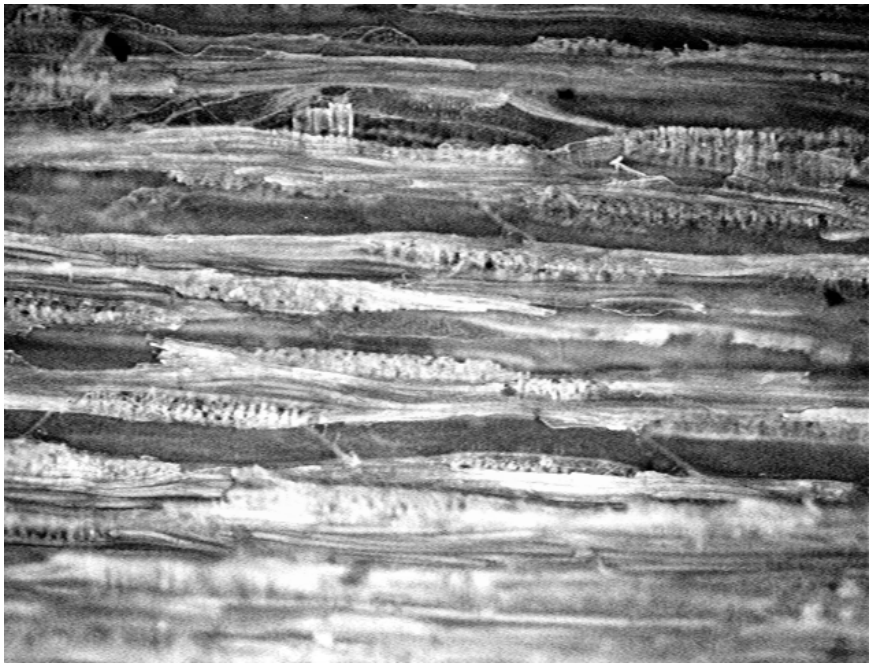

Figure J.5: Image 1 of a boiled pMDI bonded densified sample (taken @ 5x, 1626 x 1235 μm field of view).

Figure J.6: Image 2 of a boiled pMDI bonded densified sample (taken @ 5x, 1626 x 1235 μm field of view).

Figure J.7: Image 3 of a boiled pMDI bonded densified sample (taken @ 10x, 827 x 628 μm field of view).

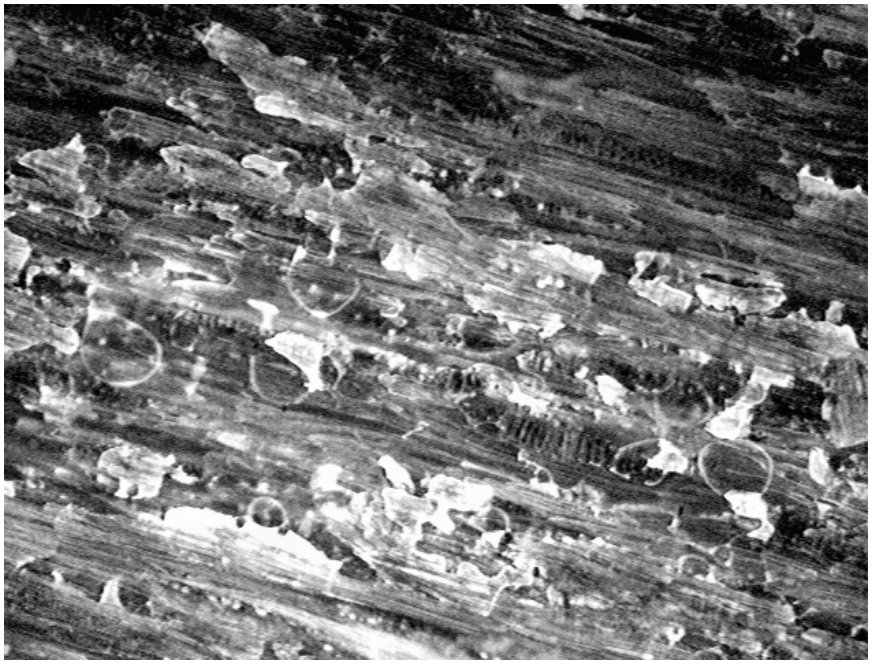

Figure J.8: Image 4 of a boiled pMDI bonded densified sample (taken @ 5x, 1626 x 1235 μm field of view).

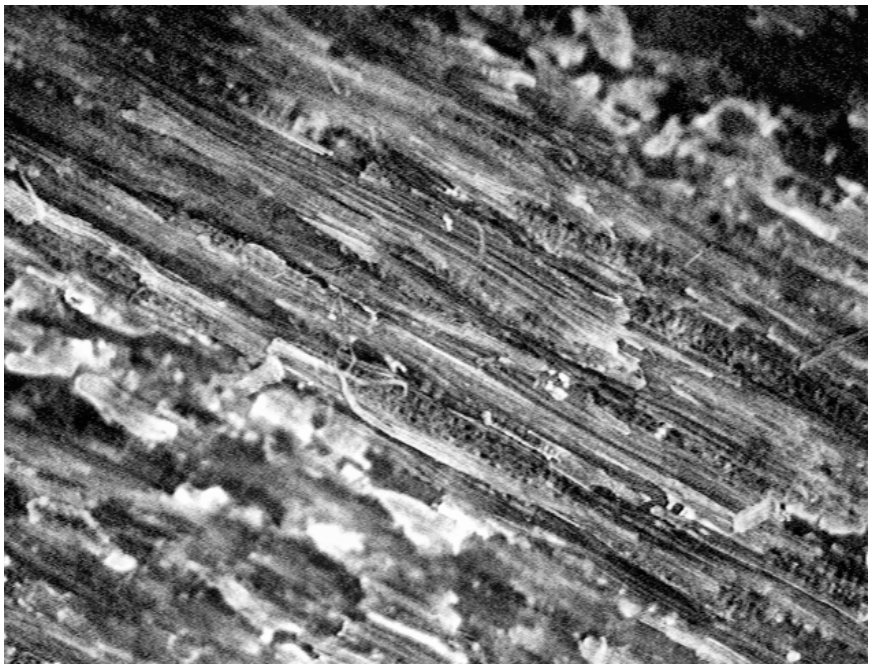

Figure J.9: Image 5 of a boiled pMDI bonded densified sample (taken @ 5x, 1626 x 1235 μm field of view).

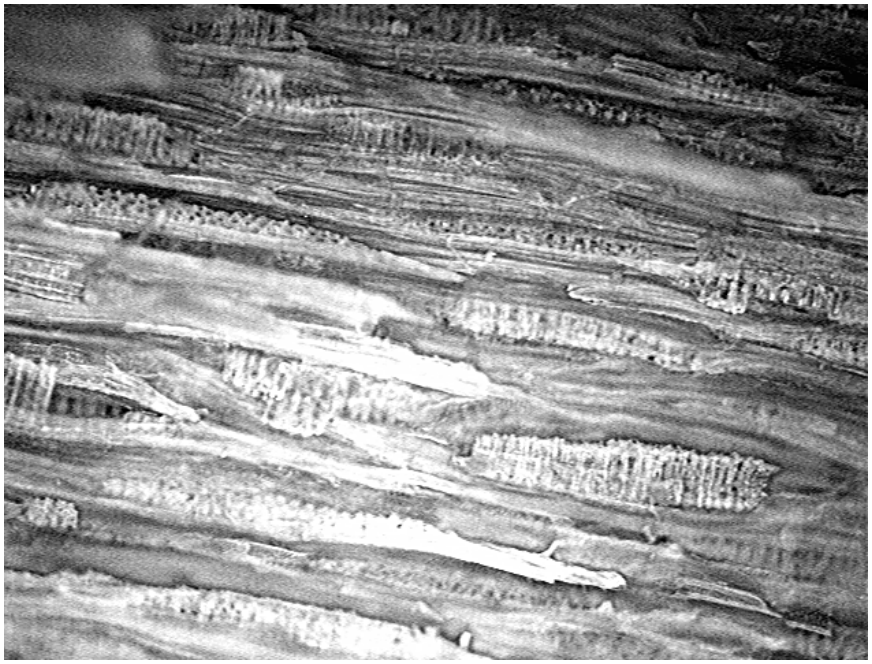

Figure J.10: Image 6 of a boiled pMDI bonded densified sample (taken @ 5x, 1626 x 1235 μm field of view).

Appendix K
Contact Angle Data

Table K.1: Contact angle data, measured in degrees, collected from control yellow-poplar samples.

Yellow Poplar Control						
Sample #	**Replication**	**Water**	**glycerol**	**ethylene glycol**	**formamide**	**a-Bromonapthalene**
1	1	50.964	57.444	38.333	23.069	13.069
	2	40.815	49.223	28.564	28.982	10.535
	3	35.909	51.071	25.619	25.04	8.971
2	1	51.555	67.714	29.239	31.654	16.133
	2	44.433	60.489	25.133	34.305	15.506
	3	43.833	60.848	26.871	17.028	13.379
3	1	42.245	61.125	28.626	14.967	14.327
	2	42.877	63.669	27.76	25.589	13.626
	3	44.802	64.119	29.36	18.977	7.864
4	1	43.212	43.219	20.448	18.048	11.95
	2	37.774	57.702	23.856	18.544	15.968
	3	39.522	74.548	24.811	19.671	12.816
5	1	40.439	56.895	27.239	21.759	14.505
	2	41.173	54.279	24.047	21.448	12.245
	3	34.232	69.261	25.053	29.566	11.914
6	1	34.308	51.368	21.231	15.457	9.529
	2	40.141	55.257	21.799	21.888	10.768
	3	35.949	54.887	24.716	13.206	9.044
7	1	45.612	57.686	24.295	20.685	10.928
	2	34.497	59.124	23.423	20.649	10.094
	3	39.401	53.584	24.523	20.481	11.075
8	1	38.541	76.059	31.163	27.451	12.697
	2	51.346	77.144	27.217	25.907	18.123
	3	49.662	77.159	34.972	19.717	12.477
9	1	39.286	66.178	29.295	20.095	17.625
	2	36.873	66.727	19.283	20.136	15.605
	3	40.377	67.478	32.521	22.182	13.992
10	1	40.236	68.102	30.727	23.962	19.463
	2	54.934	78.704	31.952	17.945	15.409
	3	33.811	64.536	24.619	21.662	20.236

Table K.2: Contact angle data, measured in degrees, collected from hygro-thermally treated yellow-poplar.

Hygro-thermally Treated Yellow-poplar						
Sample #	**Replication**	**Water**	**glycerol**	**ethylene glycol**	**formamide**	**a-Bromonapthalene**
1	1	70.169	90.939	57.388	30.606	5.436
	2	67.773	83.028	58.158	42.327	19.948
	3	76.792	85.374	39.088	*51.004*	23.485
2	1	83.218	95.633	48.451	46.159	25.738
	2	91.396	91.929	55.735	59.479	19.046
	3	84.943	94.799	47.626	51.009	*28.522*
3	1	93.485	99.649	75.986	50.576	22.814
	2	85.836	106.858	46.845	22.74	14.695
	3	84.463	101.117	57.055	61.424	22.126
4	1	80.092	93.028	53.437	59.249	21.356
	2	83.446	82.309	40.756	40.606	33.171
	3	86.027	80.428	37.768	39.386	27.413
5	1	50.605	90.966	60.094	62.241	34.716
	2	82.926	99.469	57.618	46.119	30.248
	3	79.682	98.448	66.124	46.115	31.812
6	1	74.771	99.697	63.455	64.797	32.872
	2	71.901	112.242	68.276	57.109	28.544
	3	84.191	112.322	59.278	57.635	23.718
7	1	85.081	106.102	60.795	59.638	24.277
	2	83.937	102.901	59.973	52.329	39.284
	3	97.029	96.709	57.148	47.194	23.344
8	1	80.782	106.999	70.11	57.171	19.495
	2	81.379	108.914	72.897	62.823	29.785
	3	77.885	116.091	71.016	68.019	22.476
9	1	87.859	101.598	51.774	44.639	23.727
	2	80.745	104.771	58.7	59.845	23.344
	3	73.381	98.18	55.466	59.454	37.186
10	1	92.974	97.343	58.213	53.988	31.127
	2	94.716	103.725	57.802	68.305	30.759
	3	92.892	103.452	61.915	57.838	25.682

Table K.3: Contact angle data, measured in degrees, collected from densified yellow-poplar.

Densified Yellow-poplar						
Sample #	**Replication**	**Water**	**glycerol**	**ethylene glycol**	**formamide**	**a-Bromonapthalene**
1	1	81.297	94.279	48.949	47.533	33.539
	2	94.209	78.454	53.879	46.126	33.866
	3	87.062	87.957	68.603	45.969	18.199
2	1	92.891	88.705	44.578	47.887	19.624
	2	90.278	87.725	53.335	53.724	26.807
	3	86.678	83.48	46.848	52.815	22.421
3	1	73.407	104.654	59.452	57.841	24.586
	2	76.286	93.548	56.469	58.545	27.081
	3	79.507	103.536	58.985	53.671	26.495
4	1	88.934	103.835	54.371	54.02	25.848
	2	84.539	94.619	53.019	47.102	25.566
	3	85.577	104.534	56.846	52.012	35.222
5	1	65.331	95.937	50.378	52.352	19.695
	2	66.582	94.022	44.094	48.27	22.166
	3	65.98	93.848	51.005	44.787	18.836
6	1	93.943	104.044	61.175	54.219	22.989
	2	87.99	101.627	64.182	52.095	26.229
	3	91.863	102.266	58.299	42.809	25.716
7	1	98.077	93.824	55.074	54.482	30.418
	2	99.187	103.649	60.563	59.921	35.331
	3	94.476	113.441	63.581	56.092	24.934
8	1	84.779	93.405	48.908	62.128	23.137
	2	89.792	102.912	51.465	58.125	25.036
	3	84.519	100.247	48.397	60.439	20.056
9	1	89.719	92.316	65.471	48.991	28.124
	2	97.829	94.373	56.095	43.652	33.018
	3	88.14	99.284	60.139	60.654	34.049
10	1	83.678	100.418	62.241	52.593	26.685
	2	85.996	92.227	55.99	54.172	28.935
	3	89.723	104.5	66.958	61.419	31.801

Appendix L
Statistics for Contact Angles

The SAS System
The Mixed Procedure
Model Information

Data Set	WORK.JESS
Dependent Variable	y
Covariance Structure	Variance Components
Estimation Method	REML
Residual Variance Method	Profile
Fixed Effects SE Method	Model-Based
Degrees of Freedom Method	Satterthwaite

Class Level Information

Class	Levels	Values
Rep	10	1 2 3 4 5 6 7 8 9 10
Treat1	3	C D T
Treat2	5	a b c d e

Dimensions

Covariance Parameters	2
Columns in X	24
Columns in Z	30
Subjects	1
Max Obs Per Subject	450
Observations Used	450
Observations Not Used	0
Total Observations	450

Iteration History

Iteration	Evaluations	-2 Res Log Like	Criterion
0	1	3025.62372814	
1	1	2951.89970411	0.00000000

Convergence criteria met.

Covariance Parametes Estimates

Cov Parm	Estimate
Rep(Treat1)	14.4823
Residual	41.1308

Fit Statistics

-2 Res Log Likelihood	2951.9
AIC (smaller is better)	2955.9
AICC (smaller is better)	2955.9
BIC (smaller is better)	2958.7

PARMS Model Likelihood Ratio Test

DF	Chi-Square	Pr > ChiSq
1	73.72	<.0001

Type 3 Tests of Fixed Effects

Effect	Num DF	Den DF	F Value	Pr > F
Treat1	2	27	177.85	<.0001
Treat2	4	408	1359.82	<.0001
Treat1*Treat2	8	408	30.06	<.0001

Least Squares Means

Effect	Treat1	Treat2	Estimate	Standard Error	DF	t Value	Pr > |t|
Treat1*Treat2	C	a	41.6253	1.6791	70.4	24.79	<.0001
Treat1*Treat2	C	b	62.1866	1.6791	70.4	37.04	<.0001
Treat1*Treat2	C	c	26.8898	1.6791	70.4	16.01	<.0001
Treat1*Treat2	C	d	22.0023	1.6791	70.4	13.10	<.0001
Treat1*Treat2	C	e	13.3291	1.6791	70.4	7.94	<.0001
Treat1*Treat2	D	a	85.9423	1.6791	70.4	51.18	<.0001
Treat1*Treat2	D	b	96.9222	1.6791	70.4	57.72	<.0001
Treat1*Treat2	D	c	55.9783	1.6791	70.4	33.34	<.0001
Treat1*Treat2	D	d	52.8148	1.6791	70.4	31.45	<.0001
Treat1*Treat2	D	e	26.5470	1.6791	70.4	15.81	<.0001
Treat1*Treat2	T	a	82.0125	1.6791	70.4	48.84	<.0001
Treat1*Treat2	T	b	98.8340	1.6791	70.4	58.86	<.0001
Treat1*Treat2	T	c	57.6316	1.6791	70.4	34.32	<.0001
Treat1*Treat2	T	d	52.6608	1.6791	70.4	31.36	<.0001
Treat1*Treat2	T	e	25.8715	1.6791	70.4	15.41	<.0001

Tests of Effect Slices

Effect	Treat1	Treat2	Num DF	Den DF	F Value	Pr > F
Treat1*Treat2	C		4	408	268.28	<.0001
Treat1*Treat2	D		4	408	575.64	<.000
Treat1*Treat2	T		4	408	576.03	<.0001
Treat1*Treat2		a	2	70.4	213.45	<.0001
Treat1*Treat2		b	2	70.4	150.94	<.0001
Treat1*Treat2		c	2	70.4	106.05	<.0001
Treat1*Treat2		d	2	70.4	111.69	<.0001
Treat1*Treat2		e	2	70.4	19.66	<.0001

Appendix M
Contact Angle Result Graphs

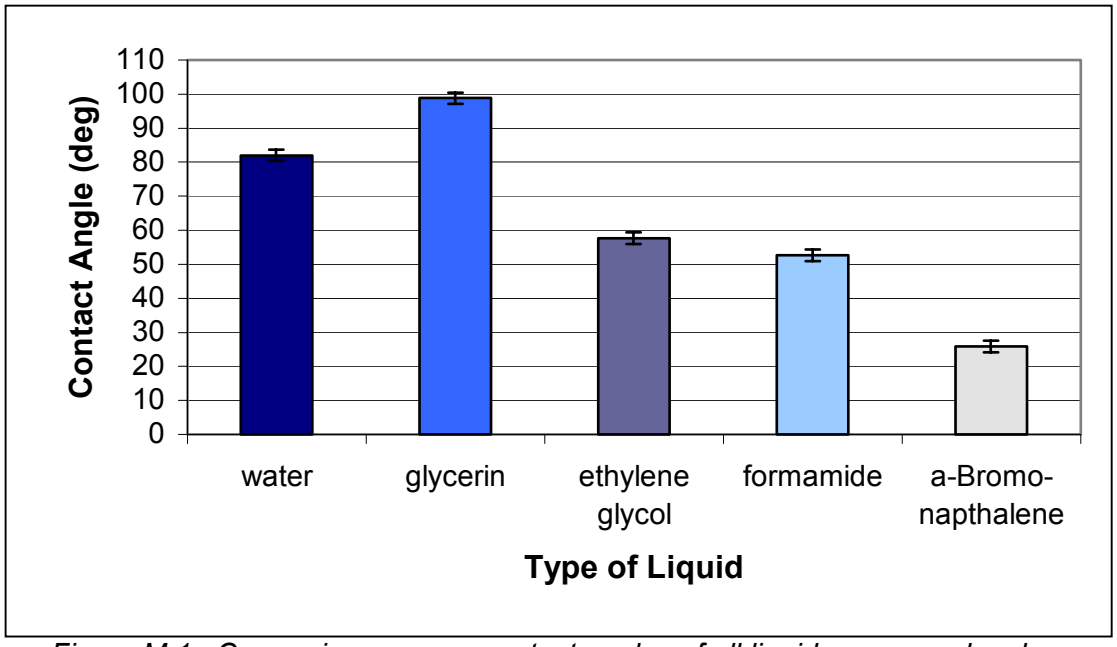

Figure M.1: Comparing average contact angles of all liquids measured on hygo-thermally treated samples.

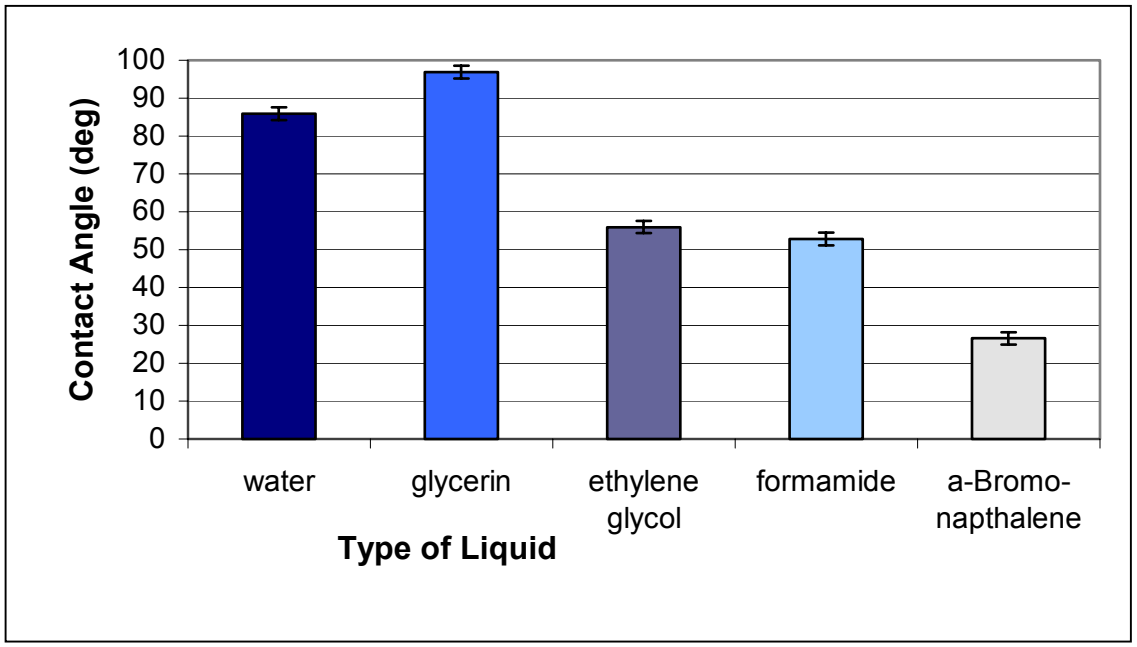

Figure M.2: Comparing average contact angles of all liquids measured on densified samples.

Vita
Jessica D. Jennings

Jessica Diane-McLaughlin Jennings, the daughter of William J. and Georgene B. McLaughlin, was born on February 28, 1977. She graduate from Oldtown High School in 1995. She then attended Virginia Polytechnic Institute and State University, where she graduated from the College of Natural Resources in 2000. She received a B.Sc. in Wood Science and a B.Sc. in Wildlife Science. Prior to beginning her graduate studies, she completed a summer internship with Borden Chemical. This thesis completes her M.Sc. degree in Wood Science from Virginia Tech.